

CONTRIBUTION OF BORON COMPOUNDS AND NANOCCLAYS ON THE  
FLAME RETARDANCY OF ALUMINIUM DIETHYLPHOSPHINATE IN NEAT  
AND FIBER REINFORCED POLYAMIDE-6

A THESIS SUBMITTED TO  
THE GRADUATE SCHOOL OF NATURAL AND APPLIED SCIENCES  
OF  
MIDDLE EAST TECHNICAL UNIVERSITY

BY

OSMAN POLAT

IN PARTIAL FULFILMENT OF THE REQUIREMENTS  
FOR  
THE DEGREE OF DOCTOR OF PHILOSOPHY  
IN  
POLYMER SCIENCE AND TECHNOLOGY

DECEMBER 2014



Approval of the thesis:

**CONTRIBUTION OF BORON COMPOUNDS AND NANOCCLAYS ON THE  
FLAME RETARDANCY OF ALUMINIUM DIETHYLPHOSPHINATE IN  
NEAT AND FIBER REINFORCED POLYAMIDE-6**

submitted by **OSMAN POLAT** in partial fulfillment of the requirements for the degree of **Doctor of Philosophy in Polymer Science and Technology Department, Middle East Technical University** by,

Prof. Dr. M. Gülbin Dural Ünver  
Dean, Graduate School of **Natural and Applied Sciences**

\_\_\_\_\_

Prof. Dr. Necati Özkan  
Head of Department, **Polymer Science and Technology**

\_\_\_\_\_

Prof. Dr. Cevdet Kaynak  
Supervisor, **Metalurgical and Materials Eng. Dept., METU**

\_\_\_\_\_

**Examining Committee Members**

Prof. Dr. Teoman Tinçer  
Chemistry Dept., METU

\_\_\_\_\_

Prof. Dr. Cevdet Kaynak  
Metalurgical and Materials Eng. Dept., METU

\_\_\_\_\_

Prof. Dr. Necati Özkan  
Polymer Science and Technology Dept., METU

\_\_\_\_\_

Assoc. Prof. Dr. H. Emrah Ünalan  
Metalurgical and Materials Eng. Dept., METU

\_\_\_\_\_

Assist. Prof. Dr. Seha Tirkeş  
Chemical Eng. and Applied Chem. Dept., Atılım Univ.

\_\_\_\_\_

**Date :**

**I hereby declare that all information in this document has been obtained and presented in accordance with academic rules and ethical conduct. I also declare that, as required by these rules and conduct, I have fully cited and referenced all material and results that are not original to this work.**

Name, Last name : Osman Polat

Signature :

## **ABSTRACT**

### **CONTRIBUTION OF BORON COMPOUNDS AND NANOCCLAYS ON THE FLAME RETARDANCY OF ALUMINIUM DIETHYLPHOSPHINATE IN NEAT AND FIBER REINFORCED POLYAMIDE-6**

Polat, Osman  
Ph.D., Department of Polymer Science and Technology  
Supervisor : Prof. Dr. Cevdet Kaynak

December 2014, 133 pages

The main objective of this dissertation was to investigate contribution of three different boron compounds and nanoclays to the flame retardancy of polyamide-6 and its 15 wt% short glass fiber reinforced composite with and without an organophosphorus flame retardant aluminum diethylphosphinate. All material combinations and nanocomposites were compounded by melt mixing method via twin-screw extruder and the specimens for testing and analyses were shaped by injection and compression molding.

In the first part of the thesis, effects of zinc borate (ZB) were investigated. UL-94 vertical burning, limiting oxygen index (LOI) and mass loss cone calorimetry (MLC) analyses indicated that replacement of certain amount of aluminum diethylphosphinate (ADP) with ZB could lead to significant improvements in many flame retardancy parameters. For instance, the suppression in peak heat release rate (PHRR) value of polyamide-6 could be as much as 82%, while it was only 32% when ADP was used alone. Char microscopy, thermogravimetric analyses, X-ray diffraction and evolved gas analyses revealed that the main contribution of ZB to the

barrier mechanism of ADP was the formation of additional boron phosphate layers together with aluminum phosphate layers.

In the second part of the thesis, effects of both boron oxide (BO) and boric acid (BA) were investigated. In this case, there were no improvements in the values of UL-94 and LOI, but significant improvements in many MLC flame retardancy parameters of especially the neat polyamide-6 specimens. For example, replacement of certain amount of ADP with BO or BA resulted in PHRR suppression of polyamide-6 as much as 84% or 86% respectively, which was only 32% when ADP was used alone. Various analyses indicated that the main contribution of BO and BA to the barrier mechanism of ADP was the formation of additional glassy boron oxide layers and boron phosphate layers.

In the third part of the thesis, effects of organically modified montmorillonite type nanoclays (NC) were investigated. Transmission electron microscopy and X-ray diffraction analyses indicated that NC layers had intercalated/exfoliated morphology in the polyamide-6 matrix. UL-94, LOI and MLC analyses revealed that use of only 5 wt% NC could improve many flammability parameters. Contributions of NC silicate layers were much more significant when 5 wt% NC were used together with 15 wt% ADP. Various analyses clarified that the basic flame retardancy mechanism of NC was the formation of insulative barrier via tortuous pathway of silicate layers preventing the underlying polymer from heat and mass transfer during fire. It was also found that, all the mechanical properties lost due to the use of ADP could be compensated when its 5 wt% was replaced with NC.

**Keywords:** zinc borate, boron oxide, boric acid, aluminum diethylphosphinate, nanoclays, flame retardancy, polyamide-6.

## ÖZ

### ALÜMİNYUM DİETİLFOSFİNATIN SAF VE ELYAF TAKVİYELİ POLİAMİD-6'DAKİ ALEVLENME DAYANIMINA BOR BİLEŞİKLERİ VE NANOKİLİN KATKILARI

Polat, Osman  
Doktora, Polimer Bilimi ve Teknolojisi Bölümü  
Tez Yöneticisi : Prof. Dr. Cevdet Kaynak

Aralık 2014, 133 sayfa

Bu tezin ana amacı üç farklı bor bileşiği ve nanokilin, poliamid-6 ve onun ağırlıça %15 kısa cam elyaf takviyeli kompozitinin alevlenme dayanımına katkılarını, alev geciktirici bir organofosfor olan alüminyum dietilfosfinatın varlığında ve yokluğunda incelemektir. Tüm malzeme kombinasyonları ve nanokompozitler çift vidalı ekstrüder ile eriyik halde karıştırma yöntemi ile hazırlanmış, testler ve analizler için gereken numuneler ise enjeksiyon ve basınçlı kalıplama yöntemleri ile şekillendirilmiştir.

Tezin ilk bölümünde çinko boratın (ZB) etkileri araştırılmıştır. UL-94 dikey yanma, oksijen limiti indeksi (LOI) ve kütle kaybı konik kalorimetre (MLC) analizleri belirli miktarda alüminyum dietilfosfinatın (ADP) yerine ZB kullanımının pek çok alevlenme dayanımı parametrelerini önemli ölçüde iyileştirdiğini göstermiştir. Örneğin, poliamid-6'nın ısı açığa çıkma hızı tavan (PHRR) değerindeki azalma tek başına ADP kullanıldığı zaman sadece %32 iken, ZB eklentisi ile %82'ye kadar yükselmiştir. Küllerin morfolojik analizleri, termogravimetrik analiz (TGA), X-ışını kırınımı (XRD) ve çıkan gaz analizleri (EGA), ZB'nin ana katkısının ADP'nin

alüminyum fosfinat tabakaları ile oluşan bariyer mekanizmasına bor fosfat tabakalarının eklenmesi yoluyla olduğunu açığa çıkarmıştır.

Tezin ikinci bölümünde bor oksit (BO) ve borik asitin (BA) etkileri araştırılmıştır. Bu bölümde, UL-94 ve LOI değerlerinde iyileşmeler görülmemiştir, ancak özellikle poliamid-6 numunelerinin pek çok MLC alevlenme dayanımı parametrelerinde önemli iyileşmeler kaydedilmiştir. Örneğin belirli bir miktar ADP'nin BO veya BA ile yer değiştirmesi poliamid-6 numunelerinin PHRR değerini sırası ile %84 ve %86 bastırmıştır, oysa bu değer tek başına ADP kullanıldığı durumda yalnızca %32'dir. Çeşitli analizler BO ve BA'nın ana katkılarının ADP'nin bariyer mekanizmasına ek olarak oluşan camsı bor oksit tabakaları ve bor fosfat tabakaları ile olduğunu, göstermiştir.

Tezin üçüncü bölümünde ise organik olarak modifiye edilmiş montmorillonit türü nanokilin (NC) etkileri araştırılmıştır. Geçirimli electron mikroskopu ve x-ışını kırınımı analizleri NC tabakalarının polyamide-6 matrisi içerisinde interkale/exfoliye morfolojiye sahip olduklarını göstermiştir. UL-94, LOI ve MLC analizleri yalnızca ağ. %5 NC kullanımının pek çok alevlenme dayanımı parametrelerini iyileştirdiğini açığa çıkarmıştır. NC silikat tabakalarının katkıları ağ. %5 NC ile ağ. %15 ADP birlikte kullanıldığında çok daha önemli olmaktadır. Yapılan çeşitli analizler NC'nin temel alevlenme dayanımı mekanizmasının silika tabakalarının oluşturduğu dolambaçlı yalıtkan yollar içeren bariyer olduğunu böylece yangın sırasında alttaki polimer tabakasını ısı ve kütle transferinden koruduğunu göstermiştir. Ayrıca, ADP kullanımı ile düşen tüm mekanik özelliklerin ağ. %5'nin NC ile yer değiştirmesi ile tamamen telafi edildiği gözlemlenmiştir.

**Anahtar sözcükler:** çinko borat, bor oksit, borik asit, alüminyum dietilfosfinat, nanokil, alevlenme dayanımı, poliamid-6.

*to my mother, brother and sister  
to the memory of my father*

## ACKNOWLEDGMENTS

I express my sincere appreciation to Prof. Dr. Cevdet Kaynak for his guidance, support and encouragement throughout this study.

I would also like to express my gratitude to my thesis supervising committee members Prof. Dr. Necati Özkan and Assoc. Prof. Dr. H. Emrah Ünalan for their valuable discussions and contributions to this thesis.

I would like to thank BOREN National Boron Research Institute for the grant with the project number 2009-Ç-0236, and Eti Mine Works Inc. for providing boron compounds.

I would like to thank all the technical staff and administrative board of the Metallurgical and Materials Engineering Department for supplying all the research facilities required in this thesis. I would also like to thank to METU Central Laboratory for TEM analyses and METU Wind Energy Center for supplying TGA-FTIR coupled system.

I specially thank to my laboratory mates, N. Ali Işıtman, A. Çağıl Özkaraca, B. Melike Sipahioğlu, Esin İbibikcan, Seçil Şankal, İlker Kaygusuz, Yelda Meyva and A. Rıza Erdoğan for their kindly friendship and helps.

And my deep thanks are to my mother Nursabah Polat, my younger brother Ahmet Polat and my sister Özlem Polat for their understanding, encouragement and patience.

## TABLE OF CONTENTS

<b>ABSTRACT</b> .....	<b>v</b>
<b>ÖZ</b> .....	<b>vii</b>
<b>ACKNOWLEDGMENTS</b> .....	<b>x</b>
<b>TABLE OF CONTENTS</b> .....	<b>xi</b>
<b>LIST OF TABLES</b> .....	<b>xiv</b>
<b>LIST OF FIGURES</b> .....	<b>xvi</b>
<b>NOMENCLATURE</b> .....	<b>xx</b>
<b>CHAPTERS</b>	
<b>1. INTRODUCTION</b> .....	<b>1</b>
<b>1.1 POLYAMIDE-6, ITS FIBER-REINFORCED AND NANOCCLAY COMPOSITES</b> .....	<b>1</b>
1.1.1 Polyamide-6 (PA) and Short Glass Fiber Reinforced Composites (PA/GF) .....	1
1.1.2 Polyamide-6/Nanoclay Composites (PA/NC).....	4
<b>1.2 FIRE BEHAVIOR OF POLYMERIC MATERIALS</b> .....	<b>7</b>
1.2.1 Methods for Measuring Flammability of Polymeric Materials.....	10
1.2.2 Mechanisms of Flame Retardancy .....	16
1.2.3 Traditional Flame Retardants and Boron Compounds.....	18
<b>1.3 LITERATURE SURVEY</b> .....	<b>20</b>
1.3.1 Studies on the Effects of Zinc Borate .....	20
1.3.2 Studies on the Effects of Boron Oxide and Boric Acid .....	21
1.3.3 Studies on the Effects of Nanoclays.....	23

1.4 AIM OF THE STUDY .....	25
<b>2. EXPERIMENTAL WORK .....</b>	<b>27</b>
2.1 MATERIALS USED .....	27
2.1.1 Polyamide-6 (PA) and Short Glass Fibers (GF).....	27
2.1.2 Organophosphorus Flame Retardant (ADP) .....	27
2.1.3 Boron Compounds (ZB, BO, BA).....	29
2.1.4 Montmorillonite Type Nanoclay (NC).....	29
<b>2.2 PRODUCTION OF THE SPECIMENS .....</b>	<b>30</b>
<b>2.3 FLAMMABILITY TESTS .....</b>	<b>33</b>
2.3.1 UL-94 Vertical Burning .....	33
2.3.2 Limiting Oxygen Index .....	34
2.3.3 Mass Loss Cone Calorimetry .....	34
<b>2.4 OTHER TESTS AND ANALYSIS .....</b>	<b>34</b>
2.4.1 Thermogravimetric Analysis .....	34
2.4.2 X-ray Diffraction Analysis .....	35
2.4.3 Scanning Electron Microscopy .....	35
2.4.4 Transmission Electron Microscopy.....	35
2.4.5 Evolved Gas Analysis .....	35
2.4.6 Tensile Testing .....	36
<b>3. RESULTS AND DISCUSSION.....</b>	<b>37</b>
<b>3.1 EFFECTS OF ZINC BORATE.....</b>	<b>37</b>
3.1.1 UL-94 and LOI Flammability Tests .....	37
3.1.2 SEM Analysis of LOI Chars .....	41
3.1.3 Mass Loss Cone Calorimetry Analysis .....	43
3.1.4 Flame Retardancy Mechanisms.....	49

3.1.5 Thermogravimetric Analysis.....	50
3.1.6 XRD Analysis of MLC Residues .....	54
3.1.7 Evolved Gas Analysis .....	56
3.1.8 Tensile Testing for Mechanical Properties .....	58
<b>3.2 EFFECTS OF BORON OXIDE AND BORIC ACID .....</b>	<b>63</b>
3.2.1 UL-94 and LOI Flammability Tests.....	63
3.2.2 SEM Analysis of LOI Chars .....	66
3.2.3 Mass Loss Cone Calorimetry Analysis .....	69
3.2.4 Flame Retardancy Mechanisms .....	77
3.2.5 Thermogravimetric Analysis.....	78
3.2.6 XRD Analysis of MLC Residues .....	82
3.2.7 Evolved Gas Analysis .....	84
3.2.8 Tensile Testing for Mechanical Properties .....	86
<b>3.3 EFFECTS OF NANOCCLAYS.....</b>	<b>91</b>
3.3.1 Nanocomposite Structure .....	91
3.3.2 UL-94 and LOI Flammability Tests.....	94
3.3.3 SEM Analysis of LOI Chars .....	97
3.3.4 Mass Loss Cone Calorimetry Analysis .....	100
3.3.5 Flame Retardancy Mechanisms .....	107
3.3.6 Thermogravimetric Analysis.....	108
3.3.7 XRD Analysis of MLC Residues.....	111
3.3.8 Tensile Testing for Mechanical Properties .....	113
<b>4. CONCLUSIONS .....</b>	<b>119</b>
<b>REFERENCES.....</b>	<b>123</b>
<b>CURRICULUM VITAE.....</b>	<b>131</b>

## LIST OF TABLES

### TABLES

<b>Table 1.1</b> Rating Classes of UL-94 Vertical Burning Test.....	12
<b>Table 2.1</b> Chemical Structure of the Materials Used.....	28, 29
<b>Table 2.2</b> Designations and Compositions (wt%) of the Specimens Produced for the First Part of This Thesis.....	31
<b>Table 2.3</b> Designations and Compositions (wt%) of the Specimens Produced for the Second Part of This Thesis.....	32
<b>Table 2.4</b> Designations and Compositions (wt%) of the Specimens Produced for the Third Part of This Thesis.....	33
<b>Table 3.1</b> Results of UL-94 and LOI Flammability Tests.....	38
<b>Table 3.2</b> Mass Loss Cone Calorimeter Parameters of the Specimens.....	48
<b>Table 3.3</b> Thermal Degradation Parameters of the Representative Specimens Determined from TG and DTG Curves.....	53
<b>Table 3.4</b> Tensile Mechanical Properties of the Specimens.....	59
<b>Table 3.5</b> Results of UL-94 and LOI Flammability Tests.....	66
<b>Table 3.6</b> Mass Loss Cone Calorimeter Parameters of the Specimens.....	75, 76
<b>Table 3.7</b> Thermal Degradation Parameters of the Representative Specimens Determined from TG and DTG Curves.....	81
<b>Table 3.8</b> Tensile Mechanical Properties of the Specimens.....	87
<b>Table 3.9</b> Results of UL-94 and LOI Flammability Tests.....	97
<b>Table 3.10</b> Mass Loss Cone Calorimeter Parameters of the Specimens.....	106

<b>Table 3.11</b> Thermal Degradation Parameters of the Specimens Determined from TG and DTG Curves.....	110
<b>Table 3.12</b> Tensile Mechanical Properties of the Specimens.....	114

## LIST OF FIGURES

### FIGURES

<b>Figure 1.1</b> Synthesis of Polyamide-6 by Hydrolytic Polymerization.....	2
<b>Figure 1.2</b> Synthesis of Polyamide-6 by Anionic Polymerization.....	3
<b>Figure 1.3</b> Two Different Thermal Degradation Mechanisms of Polyamide-6.....	4
<b>Figure 1.4</b> Layered Structure of Montmorillonite Clays.....	5
<b>Figure 1.5</b> Formation of Micro- and Nanocomposite Structures.....	7
<b>Figure 1.6</b> Three Ingredients of Polymer Combustion.....	8
<b>Figure 1.7</b> Stages of Polymer Combustion.....	10
<b>Figure 1.8</b> UL-94 Vertical Burning Test Setup.....	11
<b>Figure 1.9</b> Limiting Oxygen Index Test Setup.....	13
<b>Figure 1.10</b> Mass Loss Cone Calorimetry Test Setup.....	14
<b>Figure 1.11</b> Structure of Some Organophosphorus Flame Retardants.....	19
<b>Figure 3.1</b> Photographs of the Representative Specimens after UL-94 Test.....	39
<b>Figure 3.2</b> Photographs of the Representative Specimens after LOI Test.....	40
<b>Figure 3.3</b> SEM Images Showing Surface Char Barriers of the Representative PA Based Materials.....	41
<b>Figure 3.4</b> SEM Images Showing Surface Char Barriers of the Representative PA/GF Based Materials.....	42
<b>Figure 3.5</b> Photographs of the Remaining Char Structure of MLC Specimens of the Representative PA Based Materials.....	44

<b>Figure 3.6</b> Photographs of the Remaining Char Structure of MLC Specimens of the Representative PA/GF Based Materials.....	45
<b>Figure 3.7</b> Heat Release Rate and Mass Loss Rate Curves for the PA Based Materials.....	46
<b>Figure 3.8</b> Heat Release Rate and Mass Loss Rate Curves for the PA/GF Based Materials.....	47
<b>Figure 3.9</b> Thermogravimetric (TG) and Differential Thermogravimetric (DTG) Curves for the Representative PA Based Materials.....	52
<b>Figure 3.10</b> XRD Patterns of the MLC Residues of the Representative PA Based Materials.....	55
<b>Figure 3.11</b> Evolved Gas Analysis Spectra of the Representative PA Based Materials.....	57
<b>Figure 3.12</b> Tensile Stress-Strain Curves of the (a) PA and (b) PA/GF Based Materials.....	60
<b>Figure 3.13</b> SEM Fractographs of the Representative PA Based Materials.....	61
<b>Figure 3.14</b> SEM Fractographs of the Representative PA/GF Based Materials.....	62
<b>Figure 3.15</b> Photographs of the Representative Specimens after UL-94 Test.....	64
<b>Figure 3.16</b> Photographs of the Representative Specimens after LOI Test.....	65
<b>Figure 3.17</b> SEM Images Showing Surface Char Barriers of the Representative PA Based Materials.....	67
<b>Figure 3.18</b> SEM Images Showing Surface Char Barriers of the Representative PA/GF Based Materials.....	68
<b>Figure 3.19</b> Photographs of the Remaining Char Structure of MLC Specimens of the Representative PA Based Materials.....	71
<b>Figure 3.20</b> Photographs of the Remaining Char Structure of MLC Specimens of the Representative PA/GF Based Materials.....	72
<b>Figure 3.21</b> Heat Release Rate and Mass Loss Rate Curves for the PA Based Materials.....	73

<b>Figure 3.22</b> Heat Release Rate and Mass Loss Rate Curves for the PA/GF Based Materials.....	74
<b>Figure 3.23</b> Thermogravimetric (TG) and Differential Thermogravimetric (DTG) Curves for the Representative PA Based Materials.....	80
<b>Figure 3.24</b> XRD Patterns of the MLC Residues of the Representative PA Based Materials.....	83
<b>Figure 3.25</b> Evolved Gas Analysis Spectra of the Representative PA Based Materials.....	85
<b>Figure 3.26</b> Tensile Stress-Strain Curves of the (a) PA and (b) PA/GF Based Materials.....	88
<b>Figure 3.27</b> SEM Fractographs of the Representative PA Based Materials.....	89
<b>Figure 3.28</b> SEM Fractographs of the Representative PA/GF Based Materials.....	90
<b>Figure 3.29</b> XRD Patterns of the Nanoclay and Nanocomposite Specimens.....	92
<b>Figure 3.30</b> TEM Images Showing (i) and (ii) Uniform Distribution, (iii) and (iv) Intercalated and Partly Exfoliated Structure of NC Silicate Layers in PA Matrix.....	93
<b>Figure 3.31</b> Photographs of the Specimens after UL-94 Test.....	95
<b>Figure 3.32</b> Photographs of the Specimens after LOI Test.....	96
<b>Figure 3.33</b> SEM Images Showing Surface Char Barriers of the PA Based Materials.....	98
<b>Figure 3.34</b> SEM Images Showing Surface Char Barriers of the PA/GF Based Materials.....	99
<b>Figure 3.35</b> Photographs of the Remaining Char Structure of MLC Specimens of the PA Based Materials.....	102
<b>Figure 3.36</b> Photographs of the Remaining Char Structure of MLC Specimens of the PA/GF Based Materials.....	103
<b>Figure 3.37</b> Heat Release Rate and Mass Loss Rate Curves for the PA Based Materials.....	104

<b>Figure 3.38</b> Heat Release Rate and Mass Loss Rate Curves for the PA/GF Based Materials.....	105
<b>Figure 3.39</b> Thermogravimetric (TG) and Differential Thermogravimetric (DTG) Curves for the PA Based Materials.....	109
<b>Figure 3.40</b> XRD Patterns of the MLC Residues of the PA Based Materials.....	112
<b>Figure 3.41</b> Tensile Stress-Strain Curves of the (a) PA and (b) PA/GF Based Materials.....	115
<b>Figure 3.42</b> SEM Fractographs of the PA Based Materials.....	116
<b>Figure 3.43</b> SEM Fractographs of the PA/GF Based Materials.....	117

## NOMENCLATURE

ADP	aluminum diethylphosphinate
BA	boric acid
BO	boron oxide
DTG	differential thermogravimetry
FGI	fire growth index
FIGRA	fire growth rate
FTIR	Fourier-transform infrared spectroscopy
GF	glass fiber
HRR	heat release rate
LOI	limiting oxygen index
MLR	mass loss rate
NC	nanoclays
OP	organophosphorus compounds
PA	polyamide-6
PHRR	peak heat release rate
SEM	scanning electron microscopy
TBT	total burning time
TEM	transmission electron microscopy
THE	total heat evolved
TGA	thermogravimetric analysis
TML	total mass loss
TPHRR	time to peak heat release rate
TTI	time to ignition
XRD	X-ray diffraction
ZB	zinc borate

# CHAPTER 1

## INTRODUCTION

### 1.1 POLYAMIDE-6, ITS FIBER-REINFORCED AND NANOCLAY COMPOSITES

#### 1.1.1 Polyamide-6 (PA) and Short Glass Fiber Reinforced Composites (PA/GF)

Polyamide-6 (PA) is a member of large polyamide family which is characterized with  $-(C=ONH)-$  structure in the backbone of the chain. It is a widely used engineering polymer with sufficient performance in terms of melting point, physical properties, resistance to chemicals and solvents, electrical insulation and dimensional stability. Moreover, PA can be reinforced with short glass fibers and other additives to produce its composites for those applications requiring higher engineering performance. Therefore, PA and its composites are used in many sectors including electrical-electronics, automotive and textile industry.

PA can be synthesized from lactams (cyclic monomer e.g.  $\epsilon$ -caprolactam) via ring-opening polymerization. This polymerization can be achieved by several ways such as hydrolytic and anionic polymerization, where the second one is especially preferred in industry. The mechanisms of hydrolytic and anionic polymerization are shown in Figures 1.1 and 1.2, respectively [1].

In the hydrolytic polymerization, lactams containing six or more carbons in the ring are heated in the presence of water above the melting point of polyamide. The reaction begins with the hydrolytic ring opening of the lactam (the reaction can be

catalyzed by an acid or base, an amino acid, or an amine carboxylate). The resulting amino acid then condenses in a stepwise manner to form a growing polymer chain. As in direct polymerization, cyclic oligomers are also formed; hence  $\epsilon$ -caprolactam can be formed in the reverse of the reaction.

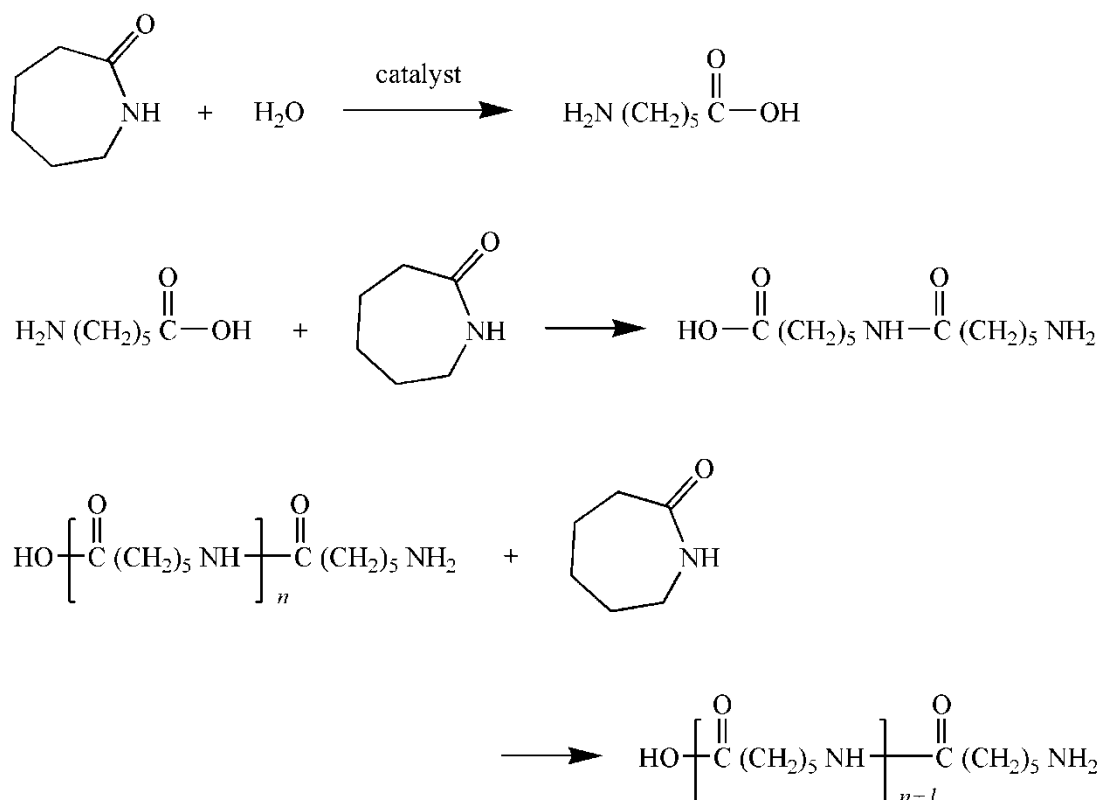


**Figure 1.1** Synthesis of Polyamide-6 by Hydrolytic Polymerization [1]

In anionic polymerization, the reaction is initiated by a strong base such as metal hydrides, alkali metal alkoxides, organometallic compounds, or hydroxides to form a lactamate. The lactamate then initiates a two-step reaction which adds a molecule of lactam to polymer chain.

Lactam can also be polymerized under anhydrous conditions by a cationic mechanism initiated by strong protic acids, their salts, and Lewis acids, as well as

amines and ammonia. The complete mechanism is complex and has some difficulties to be used in industry.

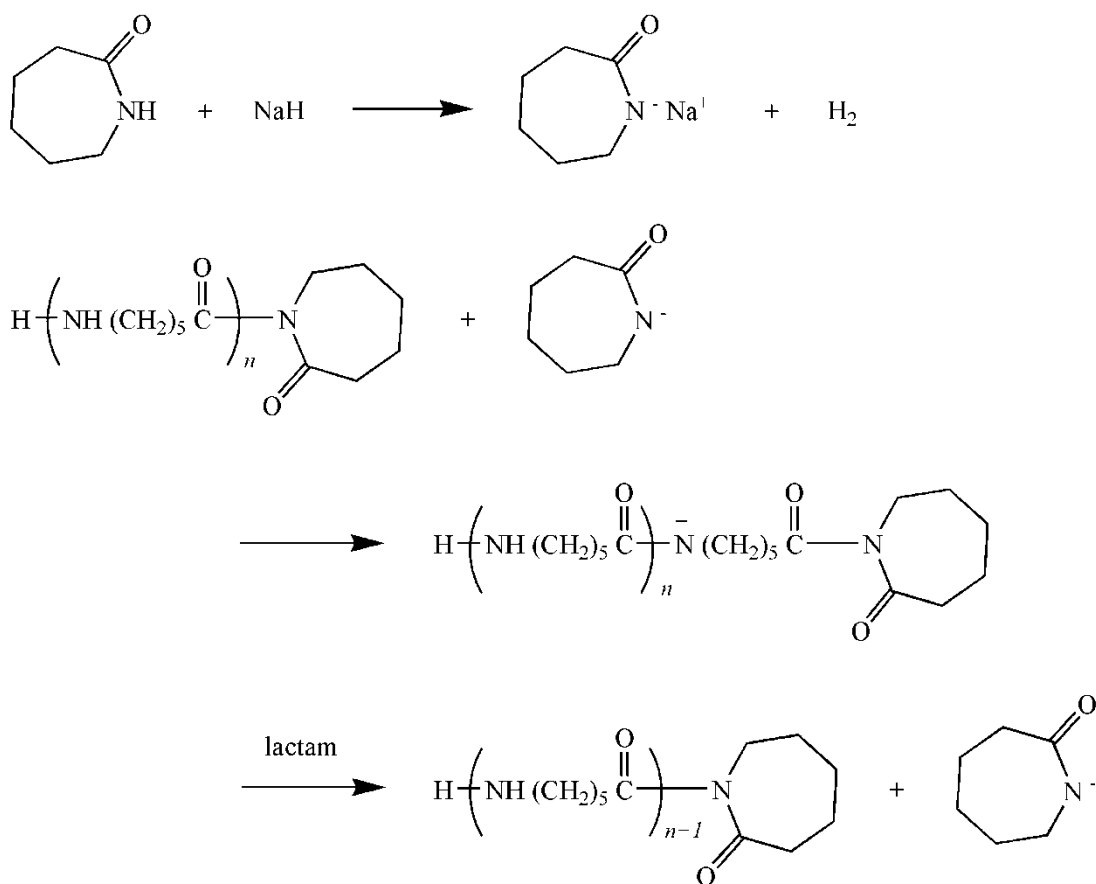


**Figure 1.2** Synthesis of Polyamide-6 by Anionic Polymerization [1]

The hydrolytic process is preferred in industry because of its easier control and better adaptation for large-scale production. Polymerization process of polyamide-6 with hydrolytic mechanism can be both batch or continuous. Continuous polymerization contains steps of addition of caprolactam and additives, hydrolysis, addition, condensation, pelletizing for remelt processing, leaching/extraction of monomers, drying and packaging.

Compared to other polymers, although PA has good thermal stability, it starts to thermally decompose around 300°C. It has been reported that [2] the predominant volatile pyrolysis product of PA is  $\epsilon$ -caprolactam. Cyclic oligomers and products with nitrile end-groups have also been reported. Two degradation processes are involved, an intramolecular back-biting process (a) and a hydrogen transfer reaction leading to scission of the C-N bond  $\beta$  to the amide group (b) as shown in Figure 1.3 [2].

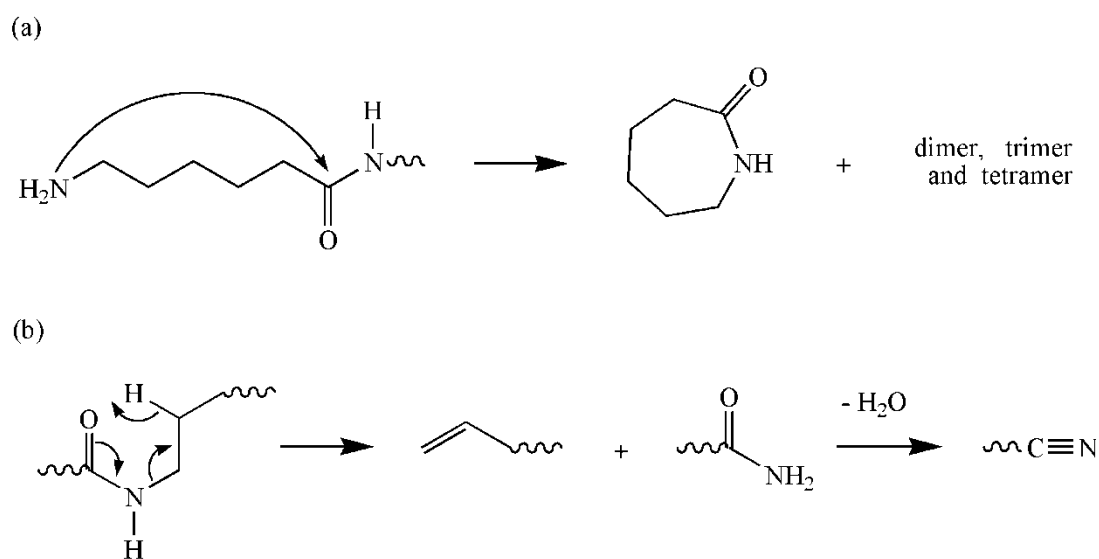


**Figure 1.3** Two Different Thermal Degradation Mechanisms of Polyamide-6 [2]

### 1.1.2 Polyamide-6/Nanoclay Composites (PA/NC)

Recently, novel composites reinforced with nano scale materials are becoming important because of much higher enhancements in physical, mechanical, optical, electrical, thermal, and fire resistance properties. The degree of enhancement depends on many factors such as aspect ratio of the fillers, degree of dispersion, orientation in the matrix and the interfacial strength between the matrix and the nano-filler [3].

Montmorillonite clays (in the form of two tetrahedral silicate layers sandwiching one octahedral alumina layer) are the most studied and commercially available nanomaterials also for PA matrices. Layered structure of montmorillonite is given in Figure 1.4 [4]. The thickness of one montmorillonite clay sheet formed by these three layers is around 1 nm. Stacking of the layers leads to a regular van der Waals gap called “interlayer” or “gallery”. The sum of the single layer thickness and the interlayer is called “d-spacing” or “basal spacing”. In the natural state, Na<sup>+</sup> cations (or other cations such as K<sup>+</sup>) reside in these galleries.

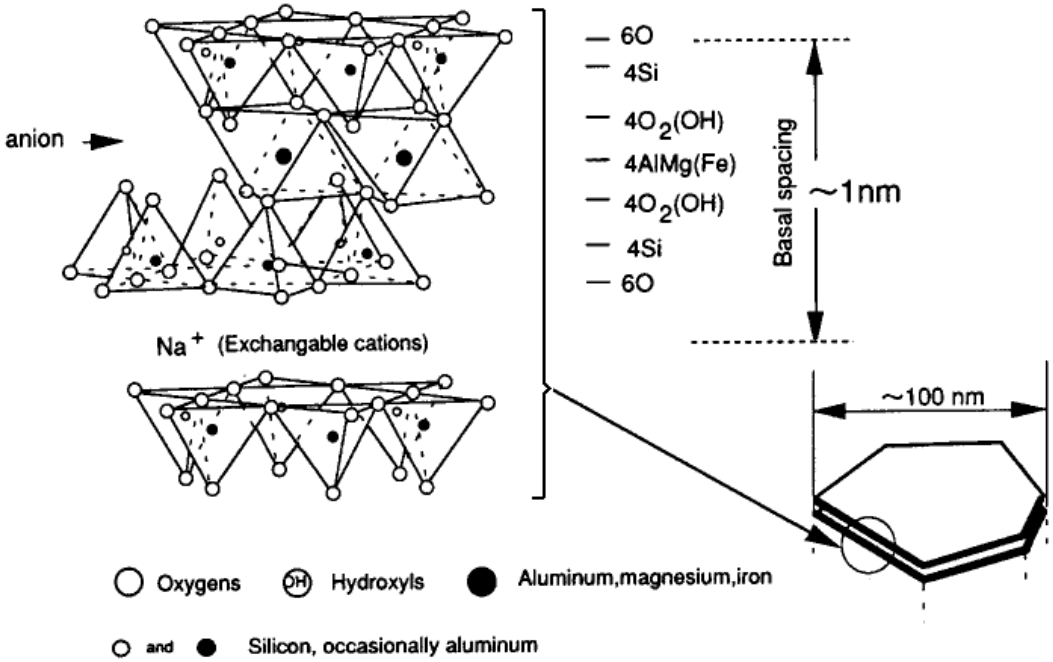


**Figure 1.4** Layered Structure of Montmorillonite Clays [4]

Since the montmorillonite layers consist of mostly silica and alumina, it has “hydrophilic” nature with a tendency of stack formation. Therefore, it is necessary to organically modify and make it “organophilic” in order to incorporate into polymer matrices. This modification eases the transportation of polymer chains through the “galleries” and result in wider interlayer gap, which is called “intercalation”.

Organic modification of layered silicates is generally done by cation exchange reaction. That is, inorganic cations (typically sodium) on the surface of the montmorillonite to balance the negative charge of aluminum/magnesium silicate layer, are replaced with the organic cations (typically alkyl ammonium ions) so that the clay become organophilic.

Three methods (solution mixing, in-situ polymerization and melt mixing) can be used to produce nanocomposites. In solution mixing; nanoclays dispersed and exfoliated into single layers in solvent, then polymer is added to this mixture. Polymer chains transfer into galleries and delaminate the sheets. After removal of the solvent, sheets reassemble in which the polymer chain in, and multilayer structure is performed. In in-situ polymerization; nanoclay is swollen in liquid monomer or monomer solution. Polymerization occurs in between the intercalated clay layers, resulting in a structure that is kinetically trapped in a well dispersed structure. In melt mixing; polymers and nanoclays are mixed and heated just above the melting point of the polymer used. In this process, polymer chains move into clay galleries and increase the interlayer distance forming intercalated and/or exfoliated structure.

When clay particles are incorporated into polymer matrix, depending on the preparation methods used and strength of interfacial interactions between polymer and nanoclays, three forms of nanocomposites can be obtained (Figure 1.5).

When polymer chains are unable to transfer through clay galleries due to poor polymer and clay interaction “phase separated (micro) composite” is obtained (Figure 1.5 (a)). In this case, no further enhancement is achieved in the performance compared to conventional composites.

“Intercalated nanocomposite” structure (Figure 1.5 (b)) is obtained when one or more polymer chains diffuse between clay layers, leading to a well ordered multilayer structure of alternating polymeric and inorganic layers. Repeating distance of these

layers is found to be in the range of a few nanometers. Intercalated structure causes significant improvements in the performance of polymers.

In “exfoliated nanocomposite” structures (Figure 1.5 (c)), uniform and complete dispersion of individual clay layers is attained in a continuous polymer matrix. Polymer-clay interactions are maximized in exfoliated nanocomposites, leading to outstanding improvements in the performance of polymers.

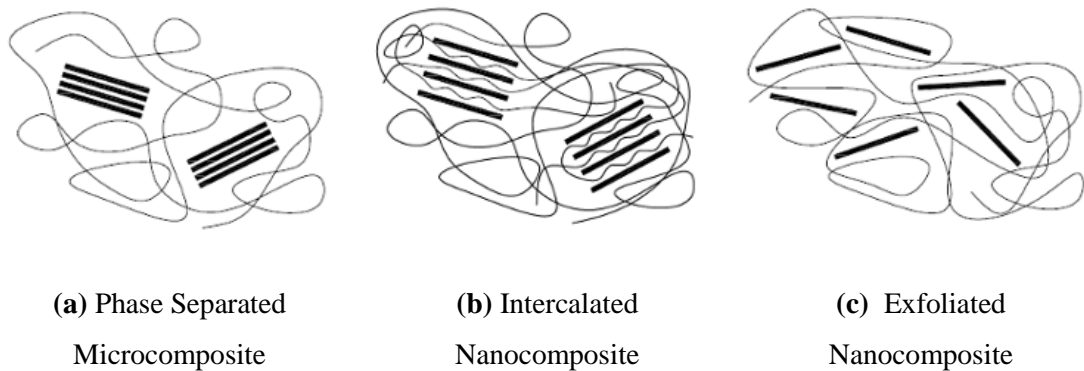


**Figure 1.5** Formation of Micro- and Nanocomposite Structures

## 1.2 FIRE BEHAVIOR OF POLYMERIC MATERIALS

For the combustion of polymers and polymeric composites there are three ingredients required; *fuel (polymer)*, *oxygen* and *heat* as represented in Figure 1.6.

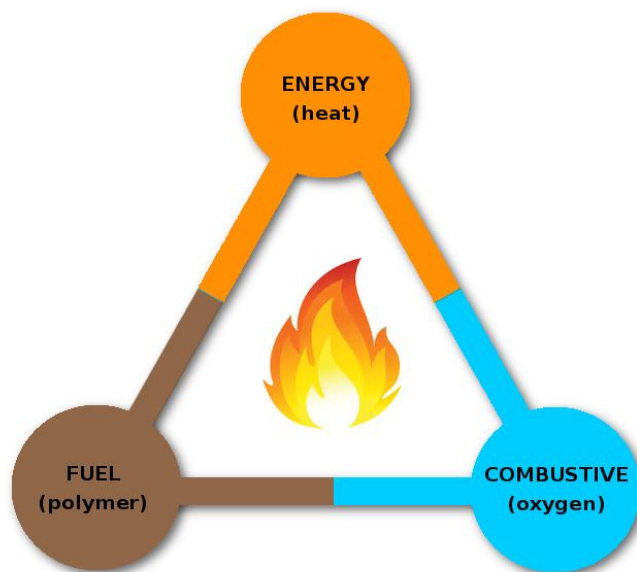


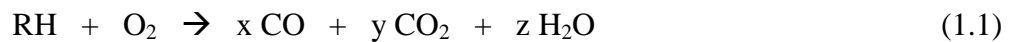
**Figure 1.6** Three Ingredients of Polymer Combustion

Polymeric materials can provide a rich supply of hydrocarbon fuel that drives the growth of a fire. When a polymer is heated to a sufficiently high temperature, it will thermally decompose. Most polymers decompose over the temperature range of 350° to 600°C with the production of flammable gases. Decomposition occurs by a series of reactions that breaks down the polymer chains into low molecular weight volatiles that diffuse into the flame.

Depending on the chemical composition and molecular structure of the polymer, the thermal degradation reactions may proceed by various paths. The majority of polymers degrade thermally by a random chain scission process. This basically involves the break-down of the long organic chains at the lowest-energy bond sites into small fragments. Polymers can also decompose by other processes, including depolymerisation (that involves the breakdown of the chain into monomers) and chain-end initiated scission (that involves the process starting from the chain ends and propagating along the chain length until it is completely degraded). Regardless of the decomposition process, when the vapor pressure and molecular weight of the

fragments from the polymer chain become sufficiently small they diffuse into the flame and become fuel to sustain the fire [5].

Combustion of the gases occurs in the solid and (to a lesser extent) intermittent zones of the flame with the formation of highly active H• radicals when polymer chain starts to degrade under high temperature. This radical combines with oxygen in the flame (or air) to produce hydroxyl radicals (OH•) according to reactions below [5].



The H• radicals produced in the reactions feed back into the reactions, and thereby the combustion process becomes a self-sustaining process when sufficient oxygen is available. This is known as the combustion cycle of organic polymers. The cycle stops only when the fuel source has been exhausted, which is usually when the organic components in a composite have been completely degraded [5].

The combustion process can be divided into certain stages as shown in Figure 1.7 [5]. Ignition is the point when the fuel source ignites and undergoes sustained flaming combustion. The initial growth of a fire is dependent mainly on the fuel itself. The fire will grow and the temperature will continue to rise (350°-500°C) if sufficient fuel and oxygen are available. Flashover occurs when all combustible items are involved in the fire and average upper gas temperature exceeds 600°C. Fully developed fire occurs when the heat release rate and temperature of a fire are at their greatest. The peak temperature of a typical post-flashover is 900°-1000°C, although it can reach as high as 1200°C. The final decay stage occurs as the fuel and combustible materials become consumed (or by active fire suppression systems), causing the temperature to fall [5].

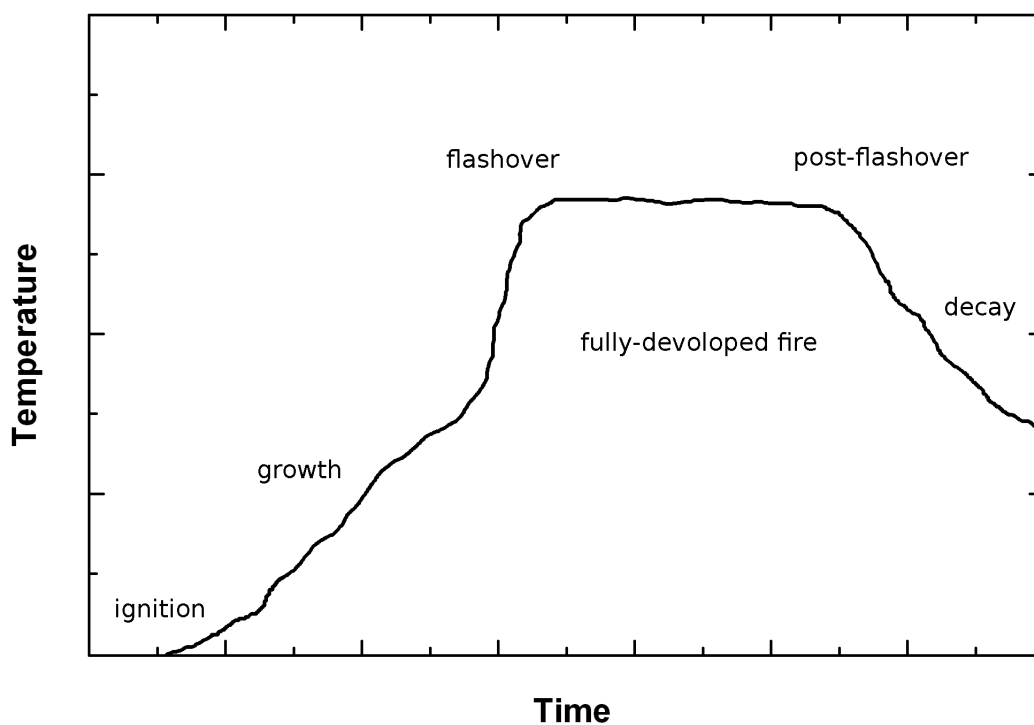


**Figure 1.7** Stages of Polymer Combustion [5]

### 1.2.1 Methods for Measuring Flammability of Polymeric Materials

In order to evaluate the fire performance of polymeric materials many test methods have been developed and standardized. These tests can be divided into two groups as specific tests for the end products and general laboratory scale tests. Most accepted and commonly used laboratory scale tests are UL-94, LOI (Limiting Oxygen Index) and MLC (Mass Loss Cone Calorimetry).

**UL-94 Vertical Burning Tests:** *UL-94 Tests for Flammability of Plastic Materials for Parts in Devices and Appliances*, a standard developed by Underwriters Laboratories (USA), is one of the simplest and most widely used flammability test method employed in polymer industry in order to determine the acceptability of

a polymeric material in terms of flammability. Most common configuration for the UL-94 test is “vertical burning”, its schematic representation is given in Figure 1.8.

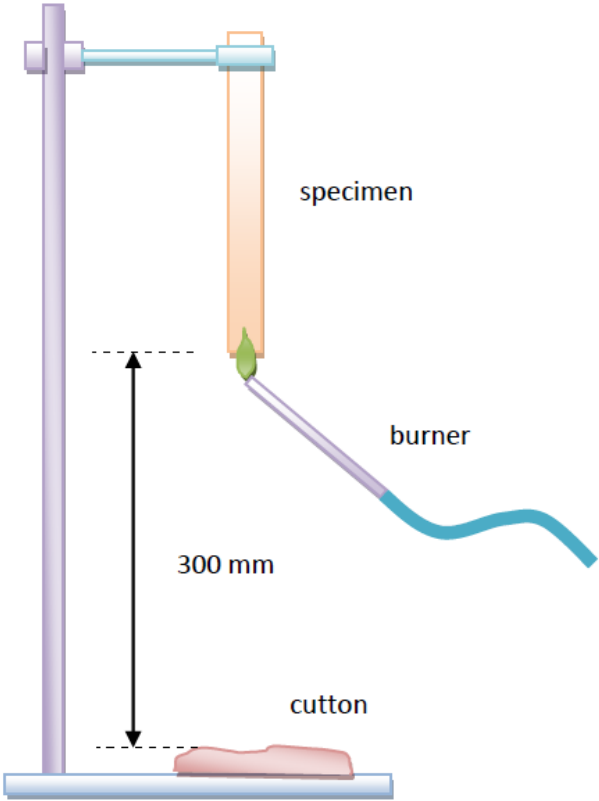


**Figure 1.8** UL-94 Vertical Burning Test Setup

In this test, a small calibrated flame is applied from the bottom of the bar shaped specimen for 10 seconds, twice. Time to extinguishment after each flame application is measured together with the observation of ignition of the cotton by the drips of burning polymer. There are four ratings in the UL-94 vertical burning test as tabulated in Table 1.1.

**Table 1.1** Rating Classes of UL-94 Vertical Burning Test

Criteria	Ratings			
	V-0	V-1	V-2	Fail
Afterflame time of each individual specimen ( $t_1$ or $t_2$ ) in seconds	$\leq 10$	$\leq 30$	$\leq 30$	$> 30$
Total afterflame time for 5 specimens ( $t_1 + t_2$ ) in seconds	$\leq 50$	$\leq 250$	$\leq 250$	
Afterflame plus afterglow time for each individual specimen after the second flame application ( $t_2 + t_3$ )	$\leq 30$	$\leq 60$	$\leq 60$	
Afterflame or afterglow of any specimen up to the holding clamp	No	No	No	
Cotton indicator ignited by flaming particle or drops	No	No	Yes	

**Limiting Oxygen Index (LOI) Tests:** This test is described in *ISO 4589 Determination of Burning Behavior by Oxygen Index* standard and it is one of the most important flammability tests. A schematic representation of the test apparatus is given in Figure 1.9.

In this test, bar shaped specimen oriented vertically inside a glass chimney is ignited by a propane flame from the top. Then, minimum oxygen concentration in a mixture of oxygen/nitrogen flowing through a glass chimney at ambient temperature which will sustain the burning of the specimen for 3 minutes or consume a length of 5 cm of the sample is determined by varying the oxygen concentration, and named as the Limiting Oxygen Index (LOI) value.

Higher LOI values indicate better flame retardancy. A LOI value below 21% may be classified as “combustible” whereas those with a LOI value above 27% may be

classified as “self-extinguishing”. It should be noted that the test is carried out at ambient temperature and obtained values are very sensitive to the temperature.

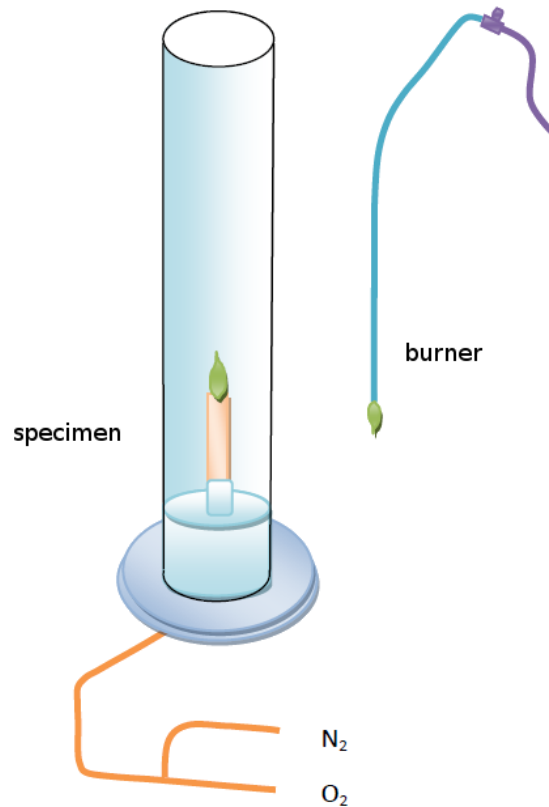


**Figure 1.9** Limiting Oxygen Index Test Setup

**Mass Loss Cone Calorimeter (MLC) Tests:** Today, heat release rate calorimetry is accepted as the most scientific way for the flame retardancy measurements. A schematic drawing of the mass loss calorimeter is shown in Figure 1.10 and the corresponding standard for measuring the heat release rate by this method is *ISO 13927 Simple Heat Release Test Using a Conical Radiant Heater and a Thermopile Detector*.

In MLC tests, heat release is determined from the outputs of the thermopiles located in the chimney above the burning specimen which is subjected to a specified radiant

heat flux from the cone heaters. The output from the thermopiles, which in the unit of millivolts (mV), is converted to the heat release rate, in the units of  $\text{kW/m}^2$ , by using the calibration graph which is obtained by burning propane with a known calorific value, in the same apparatus. Besides this, the mass of the specimen is continuously recorded by the load cell.

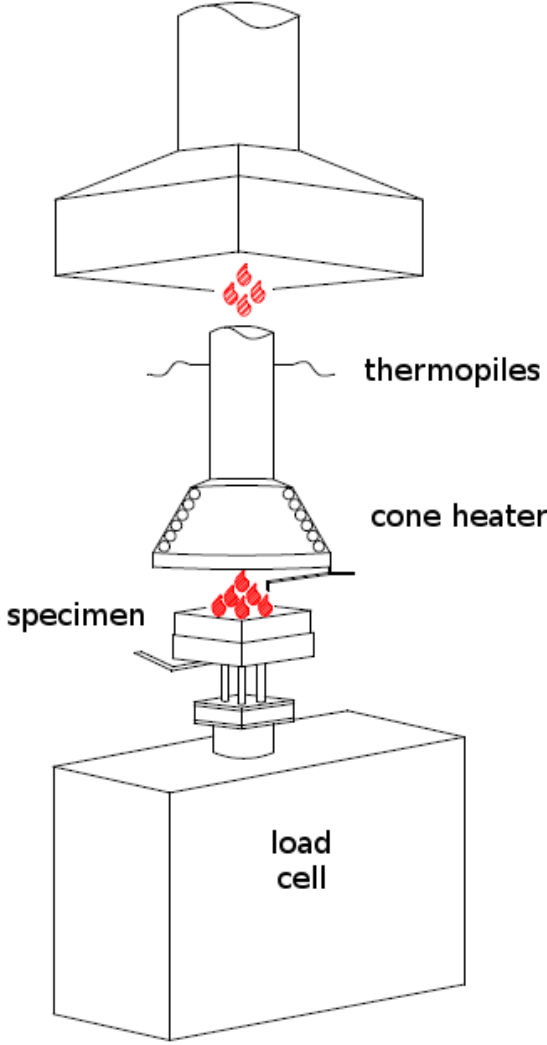


**Figure 1.10** Mass Loss Cone Calorimetry Test Setup

A rigid specimen with a smooth surface (with 100x100x4 mm<sup>3</sup> dimensions) is placed in the holder above the load cell in order to measure the evaluation of mass loss during the experiment. Conic Heaters, set to the corresponding temperature for the preferred external heat flux, continuously radiates the sample from above. The combustion is triggered by an electric spark.

There are several parameters that can be obtained from the curves of MLC test which give information about flammability of the materials such as:

**Peak Heat Release Rate (PHRR) (kW/m<sup>2</sup>):** the maximum quantity of heat released from the specimen.

**Total Heat Evolved (THE) (MJ/m<sup>2</sup>):** the area under the Heat Release Rate vs. Time curve.

**Time to Ignition (TTI) (s):** the time between sparking and ignition of a material under external irradiation.

**Time to Peak Heat Release Rate (TPHRR) (s):** the time elapsed up to peak heat release rate.

**FGI (Fire Growth Index):** contribution of a material to fire propagation; ratio of PHRR to TTI.

**FIGRA (Fire Growth Rate Index):** contribution of a material to fire propagation rate; ratio of PHRR to TPHRR.

**Char yield (wt%):** weight percent of solid fire residue of a material measured at flame-out.

### 1.2.2 Mechanisms of Flame Retardancy

Although the mechanisms of flame retardancy are not totally well understood, some classification may be done. There are two main classes of mechanisms available (condensed phase action and gas phase action) and can be further subdivided.

#### *(i) Condensed Phase Actions*

The “condensed phase” refers to the polymer, whether in the solid or molten state. Condensed phase activity includes several flame retardancy mechanisms as given below:

**Insulative Barrier Formation:** By addition of certain compounds (especially phosphorous and nitrogen containing), insulative barrier layers (generally carbonaceous char or glassy vitreous) form just over the polymer surface, and they prevent or reduce transfer of heat, oxygen and combustible gases which are mandatory to sustain fire.

**Endothermic Heat Sink:** Reducing the temperature by the addition of filler (generally metal hydroxides like aluminum hydroxide and magnesium hydroxide) that acts as a heat sink while decompose endothermically to yield water or other non-combustible products (the reactions given below) with a high specific heat capacity. Those products also absorb large amount of heat while changing their state like evaporation.



**Polymer Dilution:** Diluting the amount of combustible organic material by the addition of inert filler particles to the polymer.

*(ii) Gas Phase Actions*

The “gas phase” refers to the mixture of gas just above the condensed phase. Gas phase activity includes several flame retardancy mechanisms as given below:

**Flame Inhibition:** Halogens like bromine or phosphorus based radicals terminate the exothermic combustion reactions by removing H• and OH• radicals from the flame. As a result, both flame propagation and the amount of heat returned from the fire to the material are reducing.

The termination of the exothermic combustion reactions can be summarized as follows. The H• radicals produced in the combustion reactions (Reactions 1.3 and 1.4) react with bromine and form hydrogen bromide (HBr) product. HBr combines with oxygen and hydroxyl radicals and forms bromine radicals which react with hydrocarbon radicals and terminate it.



**Fuel Gas Dilution:** Another common mechanism is the release of noncombustible vapors to dilute the concentration of oxygen or H• and OH• radicals in the flame, which also lowers the temperature.

**Insulative Gas Barrier Formation:** If the concentration of noncombustible gases is high enough, it forms a gas blanket over condensed phase and reduces the transfer of heat, oxygen and fuel.

### 1.2.3 Traditional Flame Retardants and Boron Compounds

**Halogen Containing Additives:** Generally they are Cl and Br containing compounds, but recently the use of all Cl and some Br compounds are restricted or banned in many countries. They can be used in combination with synergistic metal oxides, metal salts, and phosphorus containing products. The main advantage of halogen-based flame retardants are their very high level of effectiveness in polymers.

Three basic mechanisms suggested for these compounds are: (i) Generation of free-radical chain-terminating agents. (ii) Promotion of char formation through dehydrogenation reactions. (iii) Formation of a blanket of hydrogen halides which acts as a gas barrier between the fuel gas and condensed phases.

**Metal Hydroxides:** In this group especially aluminum hydroxide “Al(OH)<sub>3</sub>” and magnesium hydroxide “Mg(OH)<sub>2</sub>” are used. In order to be effective they need to be used in large quantities leading to some mixing problems and decreases in mechanical properties.

Basic mechanisms suggested were: (i) They decompose endothermically and absorb heat. (ii) Formed H<sub>2</sub>O during decomposition dilutes the flame with vapors. (iii) Formed ceramic layer “Al<sub>2</sub>O<sub>3</sub> or MgO” over the polymer acts as a barrier preventing the heat and mass transfer.

**Nitrogen-containing Additives:** These are melamine, melamine derivatives and related heterocyclic compounds. They have a simple structure and compatible with many polymers.

Basic mechanisms suggested were: (i) They promote dripping of the polymer. (ii) They sublime endothermically, dilute the flame with vapor and can dissociate endothermically in the flame, even further to cyanamide. (iii) In the condensed phase melamine undergoes endothermic self-condensation with release of ammonia and formation of highly thermostable solid residues.

**Phosphorus-containing Additives:** Generally red phosphorus, phosphorus containing organic products (organophosphorus), phosphoric acids, phosphine oxides and inorganic phosphates (such as ammonium polyphosphate) are used. The main groups of organophosphorus compounds are phosphate esters, phosphonates and phosphinates as shown in Figure 1.11 [6].

Basic mechanisms suggested were: (i) They may act as dehydrating agents and promote char formation in the condensed phase. The presence of an isolative layer (thin glassy or liquid protective coating) will result in lower heat, mass (fuel) and oxygen transfer between the gas and the condensed phases, which slows down the heating and decomposition process. (ii) Formed phosphoric and related acids may act as a heat sink because they retard oxidation of carbon monoxide to carbon dioxide. (iii) Most phosphorus-containing additives decrease the pyrolysis temperature of the polymer.

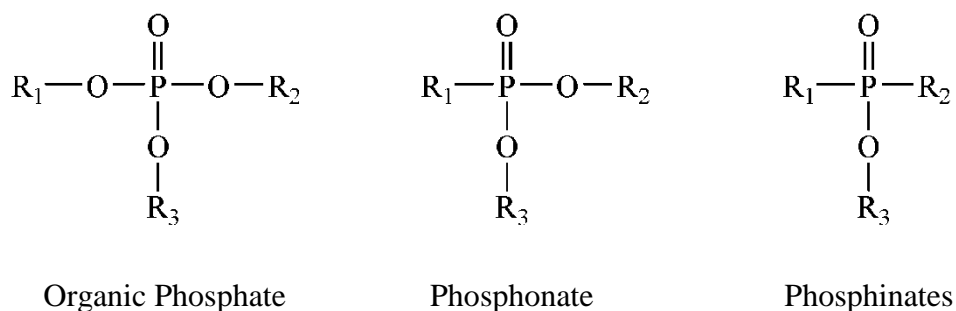


**Figure 1.11** Structure of Some Organophosphorus Flame Retardants

**Boron Compounds:** According to the very limited number of literature [7,8], *zinc borate* and *boric acid* additives appear to retard processes occurring primarily in the condensed phase. Basic mechanisms suggested were: (i) They dehydrate endothermically, and the hydrate water vaporizes, absorbs heat, and dilutes oxygen and gaseous flammable components. (ii) At a sufficiently high temperature they can melt to produce a glassy layer insulating the flammable surface.

## 1.3 LITERATURE SURVEY

### 1.3.1 Studies on the Effects of Zinc Borate

In the literature, there are several studies revealing the effects of halogenated compounds [6,9-12], metal hydroxides [6,11,13-15], nitrogen-containing [16-21] and phosphorus-containing [11,22-28] compounds. Recent studies are concerned on the non-halogenated novel type “organophosphorus compounds” especially “aluminum phosphinate” based compounds. Limited number of these studies [29-34] investigating the use of aluminum phosphinate based organocompounds for neat and fiber reinforced polyamides can be summarized as follows;

The first comprehensive work on the use of aluminum phosphinate based organophosphorus compound for polyamide-6,6 reinforced with 30 wt% short glass fibers was conducted by Braun, Scharrel and their coworkers [29]. They revealed that using 18 wt% aluminum diethylphosphinate has no improvements in the “fail” grade of UL-94, while limiting oxygen index (LOI) value increased from 21.5 to 37.9 O<sub>2</sub>%, and peak heat release rate (PHRR) value (under irradiation of 35 kW/m<sup>2</sup>) suppressed from 323 down to 157 kW/m<sup>2</sup>. They also indicated that the main flame retardancy mechanism of aluminum diethylphosphinate was flame inhibition.

In their next study [30], Braun, Bahr and Scharrel again used 18 wt% aluminum diethylphosphinate, this time for polyamide-6 with 30 wt% short glass fibers. Again, there was no improvement in the UL-94 fail grade, but LOI increased from 22.8 to 34.8 O<sub>2</sub>%, while PHRR (under irradiation of 50 kW/m<sup>2</sup>) suppressed from 478 to 326 kW/m<sup>2</sup>.

Apart from aluminum diethylphosphinate, other forms of aluminum phosphinate were investigated. For example, Hu et.al. [31] used 30 wt% aluminum phenylphosphinate to improve flame retardancy of polyamide-6 composites with 30 wt% glass fibers. They indicated that there is no improvement in UL-94 fail rating, but

PHRR value (under a heat flux of  $50 \text{ kW/m}^2$ ) can be suppressed from 461 to  $301 \text{ kW/m}^2$ .

Zhao et.al. [32] studied effects of three different amounts (15, 20, 25 wt%) of aluminum isobutylphosphinate on the flammability behavior of neat polyamide-6. They found that using 25 wt% aluminum isobutylphosphinate can lead to UL-94 V-0 rating, and also a suppression of PHRR from 789 to  $218 \text{ kW/m}^2$  under  $50 \text{ kW/m}^2$  heat flux.

Braun et.al. [29] also indicated that replacement of certain amount of aluminum diethylphosphinate with melamine polyphosphate and zinc borate may lead to more significant flame retardancy due to their additional mechanisms. For instance, they revealed that using these three compounds together lead to UL-94 V-0 rating which was not possible when aluminum diethylphosphinate was used alone.

Similarly, Isitman et.al. [33] studied effects of using aluminum diethylphosphinate in combination with melamine polyphosphate and zinc borate. They used a total of 15 wt% commercial compound containing these three ingredients in certain amount for polyamide-6 reinforced with 15 wt% short glass fibers. They revealed that UL-94 V-2 rating could be upgraded to V-0 rating, while LOI values can increase from 22.4 to 29.3 % $\text{O}_2$ , and PHRR value can be suppress from 611 down to  $228 \text{ kW/m}^2$  under external heat flux of  $35 \text{ kW/m}^2$ .

### **1.3.2 Studies on the Effects of Boron Oxide and Boric Acid**

One of the first study conducted by Gao et.al. [35] was not for a polymeric material, but it was for wood. Wood specimens were impregnated with aqueous solutions of gucinyl urea phosphate (GUP) and boric acid (BA). Their cone calorimetry studies under  $35 \text{ kW/m}^2$  heat flux indicated that, peak heat release rate (PHRR) of wood

can be suppressed from 135 kW/m<sup>2</sup> to 81 kW/m<sup>2</sup> when GUP was used alone, but the suppression was down to 50 kW/m<sup>2</sup> when GUP was mixed with BA.

A comprehensive work by Nyambo, Kandare, Wilkie [36] revealed effects of boric acid (BA) together with layered double hydroxide (LDH) and melamine polyphosphate (MP) in the copolymeric matrix material of ethylene vinyl acetate (EVA). Cone calorimetry measurements indicated that incorporation of BA resulted in significant reductions in time to ignition (TTI) and PHRR values. For instance, PHRR of EVA decreases from 1680 to 715 kW/m<sup>2</sup> when only 10 wt% traditional MP was used, while the reduction was to 671 kW/m<sup>2</sup> when 6 wt% MP was replaced by BA and LDH.

Demirel et.al. [37] studied effects of boric acid amount on the flammability behavior of unsaturated polyester by conducting only limiting oxygen index (LOI) tests. They showed that when used together with 5 wt% short glass fibers, increasing the BA amount increases the LOI value from 19.5 O<sub>2</sub>% to 25.3, 27.5 and 34.5 O<sub>2</sub>% for the 15, 20 and 30 wt% BA contents, respectively.

Xie et.al. [38] investigated use of boric acid and a nitrogen containing compounds as a finishing material for cotton fabrics. They impregnated cotton fabrics with the aqueous solutions of boric acid (BA) and 2,4,6-tri[(2-hydroxy-3-trimethylammonium)propyl]-1,3,5-triazine chloride (Tri-HTAC) having different concentrations. Their LOI measurements revealed that when the cotton fabrics were treated with only Tri-HTAC solution, LOI value of cotton fabrics increases from 17.5 to 22 O<sub>2</sub>%, on the other hand, when BA was added with a concentrations of 40 g/l, the LOI value increases further to 27.5 O<sub>2</sub>%.

Use of boron oxide (BO) was studied by Mulazim et.al. [39] for a high performance polymeric material polyimide (PI). Aminosilane treated BO particles were incorporated in PI matrix with various amounts. Due to the inherent high temperature stability LOI value of PI was 33 O<sub>2</sub>%, much higher compared to many other

polymeric materials. They showed that when only 5 wt% BO was added, LOI value increases up to 46 O<sub>2</sub>%.

Recently, Ibibikcan and Kaynak [40] revealed usability of boron oxide (BO) and boric acid (BA) for the flame retardancy enhancements of polyethylene-based cable insulation materials LDPE and LDPE/EVA. It is known that for the production of halogen-free cable insulation materials, very high amounts of traditional metal hydroxide flame retardants such as 65 wt% aluminum hydroxide (ATH) are required to fulfill cable directives. They indicated that when only 10 wt% of ATH was replaced with BO or BA, many flammability parameters could be improved. For instance with 10 wt% BO replacement, the best rating of UL-94 standard which is V-0 can be obtained, LOI values can be increased from 30 to 36 O<sub>2</sub>%, PHRR can be suppressed from 82 down to 51 kW/m<sup>2</sup>. They claimed that these improvements were basically due to further contribution of BO or BA to the physical barrier mechanism of ATH in both gas and condensed phases.

### **1.3.3 Studies on the Effects of Nanoclays**

Investigations on the effects of organically modified montmorillonite type nanoclays on the flammability behavior of many polymeric materials [41-50] including engineering thermoplastic polyamide-6 [51-54] revealed that nanoclays could improve certain flame retardancy parameters. These studies for instance indicated that peak heat release rate (PHRR) values of polymers could be significantly suppressed by the addition of only 1-5 wt% nanoclays.

The main flame retardancy mechanism ascribed for nanoclays in the literature [41,42,44,45,47-50,55] is the formation of effective physical barrier of silicate layers preventing mass and heat transfer.

On the other hand, although there are certain levels of improvements in some of the flame retardancy parameters of cone calorimetry analysis such as PHRR values, improvements via nanoclays alone are far from the required levels of industrial standards such as limiting oxygen index (LOI) values and UL-94 ratings.

Therefore, studies especially try to reach synergistic improvements by replacing certain amount of traditional flame retardants with very low amount of nanoclays, rather than using nanoclays alone.

In this respect, for many polymeric materials, there are various investigations revealing synergistic effect of nanoclays when used together with traditional flame retardants such as metal hydroxides [56-58], brominated compounds [59,60], phosphorous and nitrogen containing compounds [61-63], etc.

Polyamide-6 (PA) and its short-glass-fibers-reinforced composites (PA/GF) find a wide range of engineering applications in various industrial sectors including electrical-electronic equipment, automotive parts, etc., where high level of flame retardancy is required. The most effective flame retardants used for PA and PA/GF today especially belongs to phosphorous based compounds.

In the literature for PA and/or PA/GF based matrices, there seems to be very limited number of studies [64-66] investigating the synergistic contribution of nanoclays when used together with traditional phosphorous based flame retardants. In these studies, contribution of nanoclays (NC) when used together with red phosphorus (RP) and melamine polyphosphate (MPP) were reported indicating the improved flammability parameters (LOI, UL-94, PHRR, etc.) of PA and PA/GF.

In industry for PA and PA/GF based materials, recently use of non-halogenated novel type “organophosphorus” flame retardants, particularly “aluminum diethylphosphinate” (ADP) type compounds are on the rise. On the other hand, to the

best of our knowledge, only four works [67-70] were reported investigating the contribution of NC to ADP based compounds.

For the matrix of PA, Bourbigot et.al. [67] and Dahiya et.al. [69] indicated that using 5 wt% NC alone results in significant suppressions in PHRR values, but almost no improvements in LOI values and UL-94 rating. They revealed that, when 5 wt% NC was used together with ADP, both LOI values and UL-94 ratings were also improved. Isitman et.al. [68] also indicated that all these synergistic contribution of 5 wt% NC was valid not only for PA matrix, but also for PA/GF based materials. Later on, Dogan et.al. [70] reported that, for the matrix of PA, these synergistic contributions could be obtained even with only 1 wt% NC.

#### **1.4 AIM OF THE STUDY**

Polyamide-6 (PA6) is today one of the most widely used engineering thermoplastic in many industrial applications including electrical and electronic equipment parts mainly due to its good strength and toughness, high glass transition temperature, good electrical insulating property, ease of processability and excellent resistance to solvents and abrasion. Additionally, for the structural applications such as automotive components, higher mechanical properties and dimensional stability are required; then, PA6 is usually reinforced with 15-30 wt% short glass fibers. However, in many of these industrial applications especially for the certain parts of electrical and electronic equipment, high levels of flame retardancy is mandatory. In the academia and industry, there are various investigations on the use of traditional flame retardants to sustain required levels of fire resistance for neat polyamide-6 and its composites with short fiber reinforcements.

On the other hand, to the best of our knowledge there is no work reported on the effects of using zinc borate and metal phosphinate organocompounds together for any polymeric material. Therefore, the first purpose of this thesis was to explore

flame retardancy of aluminum diethylphosphinate when its certain amount was replaced by different levels of zinc borate in neat and 15 wt% short fiber reinforced polyamide-6.

Today, researchers are trying to improve flame retardancy performance of traditional flame retardants by adding certain synergistic materials. In the literature, there are numerous publications investigating the synergistic flame retardancy enhancements by the incorporation of zinc borate, antimony oxide, nanoclays, and many other materials.

However, to the best of our knowledge, there is no work reported on the effects of using boron oxide or boric acid together with any metal phosphinate organocompounds for PA and/or PA/GF based materials. In fact, there is no publication studying the flammability behavior of any polymeric material when any organophosphorus compound was used together with BO or BA, yet. Therefore, the second aim of this thesis was to investigate flame retardancy of aluminum diethylphosphinate type organophosphorus compound when its certain amount was replaced by different levels of boron oxide or boric acid in neat and 15 wt% short glass fiber reinforced polyamide-6.

After the discovery of polymer/clay nanocomposites at Toyota research center almost two decades ago, numerous studies were conducted in academia and industry on the effects of nanoclays to improve mechanical, thermal, barrier and flame retardancy properties of polymers.

However, there are extremely limited number of literature studying the effects of nanoclays (NC) on the flammability of the material systems used in this research. Therefore, the third purpose of this thesis was, for both PA and PA/GF based materials, to investigate flame retardancy contribution of NC, first of all when NC was used alone, then when certain amount of ADP was replaced with NC, and then the effects of replacement with NC-ZB (nanoclay - zinc borate) couple.

## CHAPTER 2

### EXPERIMENTAL WORK

#### 2.1 MATERIALS USED

Chemical structures of the materials used in this study are given in Table 2.1, while other properties are given below.

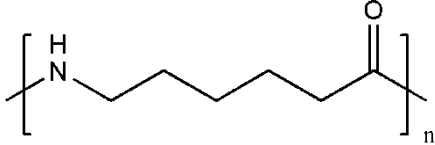
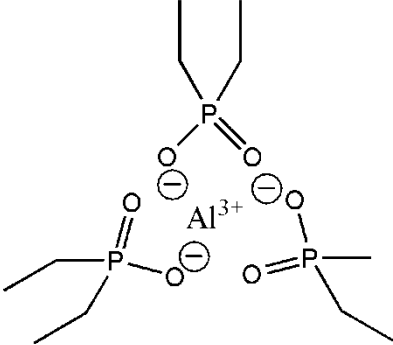
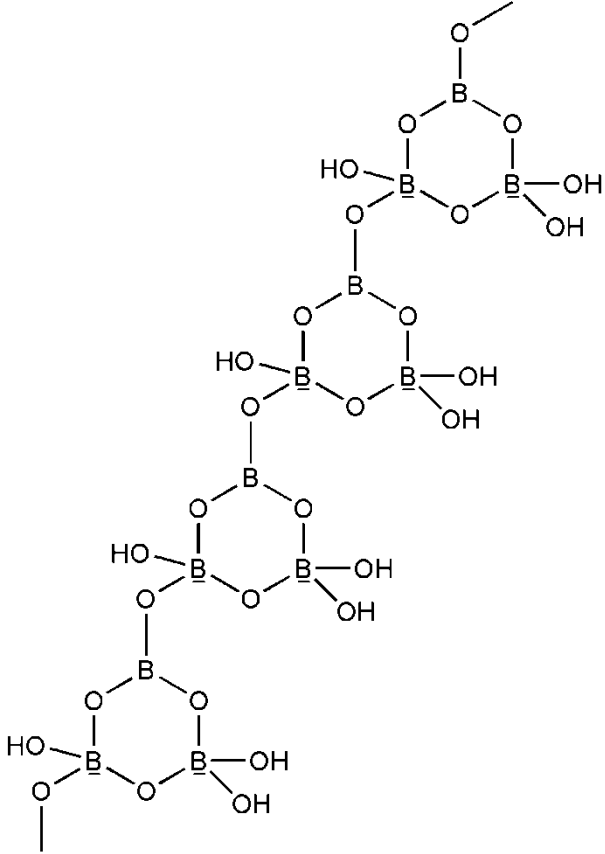
##### 2.1.1 Polyamide-6 (PA) and Short Glass Fibers (GF)

Polyamide-6 (PA) (Biesterfeld, Orbimid® B27) used as a matrix material had a density of  $1.14 \text{ g/cm}^3$ , mold shrinkage of 1.1-1.6%, and water absorption of 10% (w/w). Silane treated short glass fibers (GF) (Camelyaf, PA-2) used had initial length of 3 mm and diameter of  $10.5 \text{ }\mu\text{m}$ . Aminosilane sizing was applied with  $\gamma$ -aminopropyltrimethoxysilane (APS).

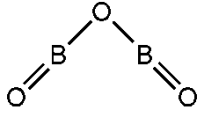
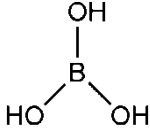
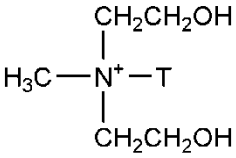
##### 2.1.2 Organophosphorus Flame Retardant (ADP)

Organophosphorus type novel flame retardant used was aluminum diethylphosphinate (ADP) (Clariant, Exolit OP 1230) with the chemical formula of  $\text{Al}[\text{OP}(\text{O})(\text{C}_2\text{H}_5)_2]_3$ , density of  $1.35 \text{ g/cm}^3$ , decomposition temperature of  $350^\circ\text{C}$  (TGA 2% weight loss), and average particle size of  $42.3 \text{ }\mu\text{m}$  (D[4,3]) and its phosphorous content was approximately 23-24% (w/w).

**Table 2.1** Chemical Structure of the Materials Used

Materials	Chemical Structure
Polyamide-6 (PA)	 $\left[ \text{NH} \text{---} \text{CH}_2 \text{---} \text{CH}_2 \text{---} \text{CH}_2 \text{---} \text{CH}_2 \text{---} \text{CH}_2 \text{---} \text{CH}_2 \text{---} \text{C}(=\text{O}) \right]_n$
Aluminum Diethylphosphinate (ADP)	
Zinc Borate (ZB)	 <p>(zinc atoms that complex with oxygen atoms are not displayed)</p>

**Table 2.1** Chemical Structure of the Materials Used Continued

Materials	Chemical Structure
Boron Oxide (BO)	
Boric Acid (BA)	
Methyltallow Bis-2-hydroxyethyl Quaternary Ammonium (MT2EtOH) (Organic Modifier of the Nanoclay)	 <p data-bbox="794 1003 1353 1034">Where T is Tallow (~65 % C18; ~30 % C16; ~5 % C14)</p>

### 2.1.3 Boron Compounds (ZB, BO, BA)

Three different boron compounds; zinc borate (ZB) with a formula of  $2\text{ZnO} \cdot 3\text{B}_2\text{O}_3 \cdot 3.5\text{H}_2\text{O}$ , boron oxide (BO) with a formula of  $\text{B}_2\text{O}_3$  and boric acid (BA) with a formula of  $\text{H}_3\text{BO}_3$  were kindly provided by ETI Mine Works Inc (Turkey). ZB, BO and BA had average particle sizes of 12.4, 12.8, 33.7  $\mu\text{m}$  (D[4,3]), and purities of 97, 91, 99%, respectively.

### 2.1.4 Montmorillonite Type Nanoclay (NC)

The nanoclay (Southern Clay Products, Cloisite 30B) used had a specific gravity of 1.98, dry particle size range 10% < 2  $\mu\text{m}$ , 50% < 6  $\mu\text{m}$ , 90% < 13  $\mu\text{m}$ , d-spacing of

18.5 Å, organic content of 30% (w/w), and modifier concentration of 90 meq/100 g clay.

It is a montmorillonite type organoclay produced by the cation exchange reaction of sodium with methyl, tallow, bis-2-hydroxyethyl quaternary ammonium (MT2EtOH). The chemical structure of this organic modifier is given in Table 2.1. (T stands for hydrogenated tallow; long organic molecules having ~65% C<sup>18</sup>; ~30% C<sup>16</sup>; ~5% C<sup>14</sup>).

## 2.2 PRODUCTION OF THE SPECIMENS

In this thesis compounding was done for two groups of materials; the first group was based on neat PA and the second one was based on PA reinforced with 15 wt% short glass fibers (PA/GF). In order to evaluate effects of boron compounds (ZB, BO, BA) and nanoclays (NC), the control sample material was chosen as PA or PA/GF with 20 wt% ADP type organophosphorus compound.

After pre-drying of PA granules in a vacuum oven at 80°C for 24 h; PA, GF, ADP, ZB, BO, BA and NC were compounded by melt mixing method in a laboratory size twin-screw extruder (Rondol Microlab 10 mm, L/D=20). Although there were slight changes for each compound composition, in general, the temperature profile during extrusion for the PA based compounds was 180°-200°-225°-230°-196°C with 70 rpm screw speed, while for the PA/GF based compounds it was 180°-205°-225°-230°-195°C with 75 rpm screw speed.

After drying operation of compounds, specimens were shaped by two methods; compression and injection molding. Square plates for cone calorimeter tests were compression molded at 240°C with 4 minutes preheating followed by 100 bar pressure for 1 minute. Injection Molding (DSM Xplore Micro) for the flammability

and mechanical test specimens were done with barrel and mold temperatures of 240°C and 70°C, respectively, under three step pressure of 13 bar for 4-5 minutes.

Since this thesis has three main parts, the specimens were produced in three groups. Designations and compositions of the specimens produced for each group are given in Tables 2.2, 2.3 and 2.4.

**Table 2.2** Designations and Compositions (wt%) of the Specimens Produced for the First Part of This Thesis

<b>Specimens</b>	<b>PA</b>	<b>GF</b>	<b>ADP</b>	<b>ZB</b>
PA	100	-	-	-
PA-ZB 20	80	-	-	20
PA-ADP 20	80	-	20	-
PA-ADP 19-ZB 1	80	-	19	1
PA-ADP 17-ZB 3	80	-	17	3
PA-ADP 15-ZB 5	80	-	15	5
PA-ADP 13-ZB 7	80	-	13	7
PA/GF	85	15	-	-
PA/GF-ZB 20	65	15	-	20
PA/GF-ADP 20	65	15	20	-
PA/GF-ADP 19-ZB 1	65	15	19	1
PA/GF-ADP 17-ZB 3	65	15	17	3
PA/GF-ADP 15-ZB 5	65	15	15	5
PA/GF-ADP 13-ZB 7	65	15	13	7

**PA:** Polyamide-6, **GF:** Short Glass Fibers, **ADP:** Aluminum Diethylphosphinate, **ZB:** Zinc Borate

**Table 2.3** Designations and Compositions (wt%) of the Specimens Produced for the Second Part of This Thesis

<b>Specimens</b>	<b>PA</b>	<b>GF</b>	<b>ADP</b>	<b>BO</b>	<b>BA</b>
PA	100	-	-	-	-
PA-BO 10	90	-	-	10	-
PA-BA 10	90	-	-	-	10
PA-ADP 20	80	-	20	-	-
PA-ADP 19-BO 1	80	-	19	1	-
PA-ADP 17-BO 3	80	-	17	3	-
PA-ADP 15-BO 5	80	-	15	5	-
PA-ADP 19-BA 1	80	-	19	-	1
PA-ADP 17-BA 3	80	-	17	-	3
PA-ADP 15-BA 5	80	-	15	-	5
PA/GF	85	15	-	-	-
PA/GF-BO 10	75	15	-	10	-
PA/GF-BA 10	75	15	-	-	10
PA/GF-ADP 20	65	15	20	-	-
PA/GF-ADP 17-BO 3	65	15	17	3	-
PA/GF-ADP 15-BO 5	65	15	15	5	-
PA/GF-ADP 17-BA 3	65	15	17	-	3
PA/GF-ADP 15-BA 5	65	15	15	-	5

**PA:** Polyamide-6, **GF:** Short Glass Fibers, **ADP:** Aluminum Diethylphosphate, **BO:** Boron Oxide, **BA:** Boric Acid

**Table 2.4** Designations and Compositions (wt%) of the Specimens Produced for the Third Part of This Thesis

<b>Specimens</b>	<b>PA</b>	<b>GF</b>	<b>ADP</b>	<b>NC</b>	<b>ZB</b>
PA	100	-	-	-	-
PA-NC	95	-	-	5	-
PA-ADP 20	80	-	20	-	-
PA-ADP 15-NC	80	-	15	5	-
PA-ADP 10-ZB-NC	80	-	10	5	5
PA/GF	85	15	-	-	-
PA/GF-NC	80	15	-	5	-
PA/GF-ADP 20	65	15	20	-	-
PA/GF-ADP 15-NC	65	15	15	5	-
PA/GF-ADP 10-ZB-NC	65	15	10	5	5

**PA:** Polyamide-6, **GF:** Short Glass Fibers, **ADP:** Aluminum Diethylphosphinate, **NC:** Nanoclay, **ZB:** Zinc Borate,

## 2.3 FLAMMABILITY TESTS

Limiting Oxygen Index (LOI) measurements, UL-94 vertical burning and Mass Loss Cone Calorimeter (MLC) tests were utilized to investigate flame retardancy properties of the specimens. The procedure and the parameters obtained from these particular tests were discussed in Section 1.2.1 in detail.

### 2.3.1 UL-94 Vertical Burning

UL-94 vertical burning tests were assessed as the procedure explained in the standard *UL-94 Tests for Flammability of Plastic Materials for Parts in Devices and*

*Appliances* developed by Underwriters Laboratories. Tests were performed for the 3.2 mm thick specimens.

### **2.3.2 Limiting Oxygen Index**

Limiting Oxygen Index (LOI) measurements were conducted by an oxygen index apparatus (Fire Testing Technology Inc.) having a paramagnetic oxygen analyzer according to the standard of *ISO 4589 Determination of Burning Behavior by Oxygen Index*.

### **2.3.3 Mass Loss Cone Calorimetry**

Mass Loss Cone Calorimeter (Fire Testing Technology Inc.) was utilized to measure heat release rates and mass loss rates of the burning specimens having the dimensions of 100x100x4 mm<sup>3</sup> according to the procedure given in the standard *ISO 13927 Simple Heat Release Test Using a Conical Radiant Heater and a Thermopile Detector*. During the test, external heat flux was kept as 35 kW/m<sup>2</sup>. Data were recorded using a data-acquisition system and the outcomes of the test indicated that measured heat release rates are reproducible with  $\pm 10\%$  deviation.

## **2.4 OTHER TESTS AND ANALYSIS**

### **2.4.1 Thermogravimetric Analysis**

In order to investigate thermal degradation of the specimens, thermogravimetric analysis (TGA) (Netzsch STA 449 F3 Jupiter) was carried out under nitrogen at a flow rate of 20 ml/min and a heating rate of 10°C/min.

#### **2.4.2 X-ray Diffraction Analysis**

Wide angle X-ray diffraction analysis (XRD) (Rigaku D-Max 2200) with Cu K $\alpha$  radiation (40 kV, 40 mA) was first utilized for MLC chars over a scanning range of 5°-80°. Then, it was also conducted in order to evaluate dispersibility and intercalation/exfoliation state of NC silicate layers in PA and PA/GF matrices over the continuous range of 1°-10°.

#### **2.4.3 Scanning Electron Microscopy**

Morphological studies of the LOI specimen chars and fracture surfaces of tensile test specimens were conducted under scanning electron microscopy (SEM) (FEI Nova Nano 430). Sample surfaces were coated with a thin layer of gold to avoid electrostatic charging and provide conductive surfaces.

#### **2.4.4 Transmission Electron Microscopy**

For the visual evidence of intercalation/exfoliation of nanoclay layers in the matrix, transmission electron microscopy (TEM) (FEI Tecnai G2 Spirit Bio TWIN) was conducted at an acceleration voltage of 80 kV. To prepare samples for TEM, an ultra-microtome (Leica EM UC6) with a diamond knife was utilized. Sections having less than 100 nm thicknesses were sliced and transferred to 400 mesh copper grids.

#### **2.4.5 Evolved Gas Analysis**

In order to support flame retardancy mechanism of the compounds, evolved gas analysis (EGA) was also conducted by a TGA-FTIR coupled system (Perkin Elmer TGA 4000- Spectrum Two). TGA was run from 20° to 900°C under nitrogen flow (20 ml/min) with a heating rate of 10°C/min, while FTIR scanning was from 4000 to 400 cm<sup>-1</sup> with a resolution of 4 cm<sup>-1</sup>.

#### **2.4.6 Tensile Testing**

Mechanical behavior of the specimens were evaluated by tensile tests on at least five *ISO 527 Type IA* samples using a universal testing machine (Instron 5565A, 5 kN). Tests were conducted at least for five specimens of each formulation, and the data were evaluated as the average values with standard deviations.

## **CHAPTER 3**

### **RESULTS AND DISCUSSION**

As stated before, since this dissertation has three main purposes and consequently three basic experimental stages, their results are presented and discussed successively in the following three subsections.

#### **3.1 EFFECTS OF ZINC BORATE**

In order to evaluate flame retardancy enhancement of ZB, the control sample material was chosen as PA or PA/GF with 20 wt% ADP type organophosphorus compound. Then, for each compound group, the amount of ADP was replaced with 1, 3, 5, and 7 wt% ZB. In order to observe effects of ZB alone, specimens having only 20 wt% ZB were also produced. Designations and compositions of the specimens produced for this first part of the thesis are given in Table 2.2 and the results are discussed below.

##### **3.1.1 UL-94 and LOI Flammability Tests**

Results of UL-94 and LOI flammability tests are tabulated in Table 3.1, while appearances of the representative specimens after these two tests are given in Figure 3.1 and 3.2 respectively. It is seen that both PA and PA/GF specimens have V-2 rating from UL-94 tests, and LOI values of 26.1 and 23.3 O<sub>2</sub>%, respectively. When 20 wt% ZB was added alone, there was almost no enhancement in the flammability values, except a slight increase of LOI (from 23.3 to 25.1) in the specimen of PA/GF-ZB 20, which should be due to formation of certain level of charring as shown in Figure 3.2(b)(ii).

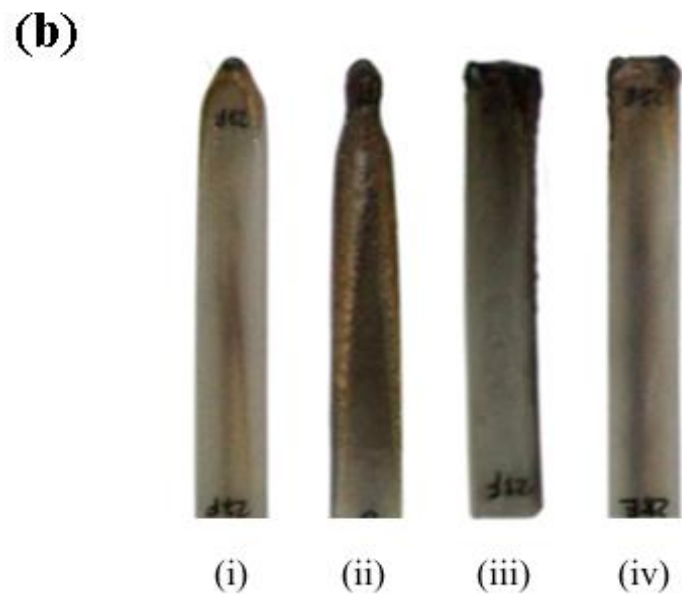
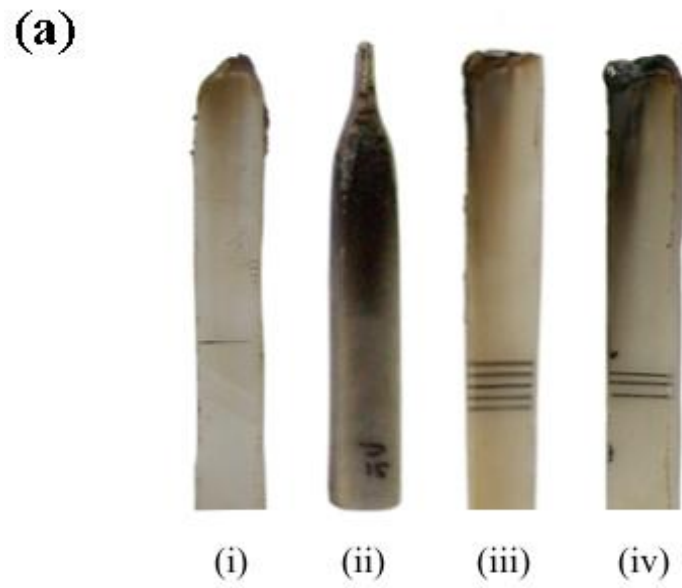
Contrarily, when 20 wt% ADP was incorporated alone, there were significant improvements, e.g. both specimens (PA-ADP 20 and PA/GF-ADP 20) obtained V-0, the best rating of UL-94, and increased LOI values of 32.7 and 30.7 O<sub>2</sub>%, respectively. These improvements were especially due to the very effective “flame inhibition” action of ADP, and also its “charring” action as shown in Figure 3.2(a)(iii) and (b)(iii).

Table 3.1 indicates that when the amount of ADP was replaced with 1, 3, 5, 7 wt% ZB, then all specimens keep not only V-0 rating of UL-94, but also some of them could have higher LOI values. For example, for each group, replacement of amount of ADP with 3 wt% ZB leads to highest LOI value (i.e. more than 33 O<sub>2</sub>%). This enhancement is basically due to the additional contribution of “gas and condensed phase barrier” actions of ZB.

**Table 3.1** Results of UL-94 and LOI Flammability Tests

<b>Specimens</b>	<b>UL-94 Rating<sup>a</sup></b>	<b>LOI<sup>b</sup> (%O<sub>2</sub>)</b>
PA	V-2	26.1
PA-ZB 20	V-2	24.3
PA-ADP 20	V-0	32.7
PA-ADP 19-ZB 1	V-0	32.3
PA-ADP 17-ZB 3	V-0	33.5
PA-ADP 15-ZB 5	V-0	30.7
PA-ADP 13-ZB 7	V-0	29.1
PA/GF	V-2	23.3
PA/GF-ZB 20	V-2	25.1
PA/GF-ADP 20	V-0	30.7
PA/GF-ADP 19-ZB 1	V-0	33.1
PA/GF-ADP 17-ZB 3	V-0	32.1
PA/GF-ADP 15-ZB 5	V-0	31.3
PA/GF-ADP 13-ZB 7	V-0	28.3

<sup>a</sup>Rating of UL-94 standard, <sup>b</sup> Limiting oxygen index



**Figure 3.1** Photographs of the Representative Specimens after UL-94 Test:  
(a) PA Based Materials; (i) PA, (ii) PA-ZB 20, (iii) PA-ADP 20,  
(iv) PA-ADP 17-ZB 3  
(b) PA/GF Based Materials; (i) PA/GF, (ii) PA/GF-ZB 20, (iii) PA/GF-ADP 20,  
(iv) PA/GF-ADP 17-ZB 3

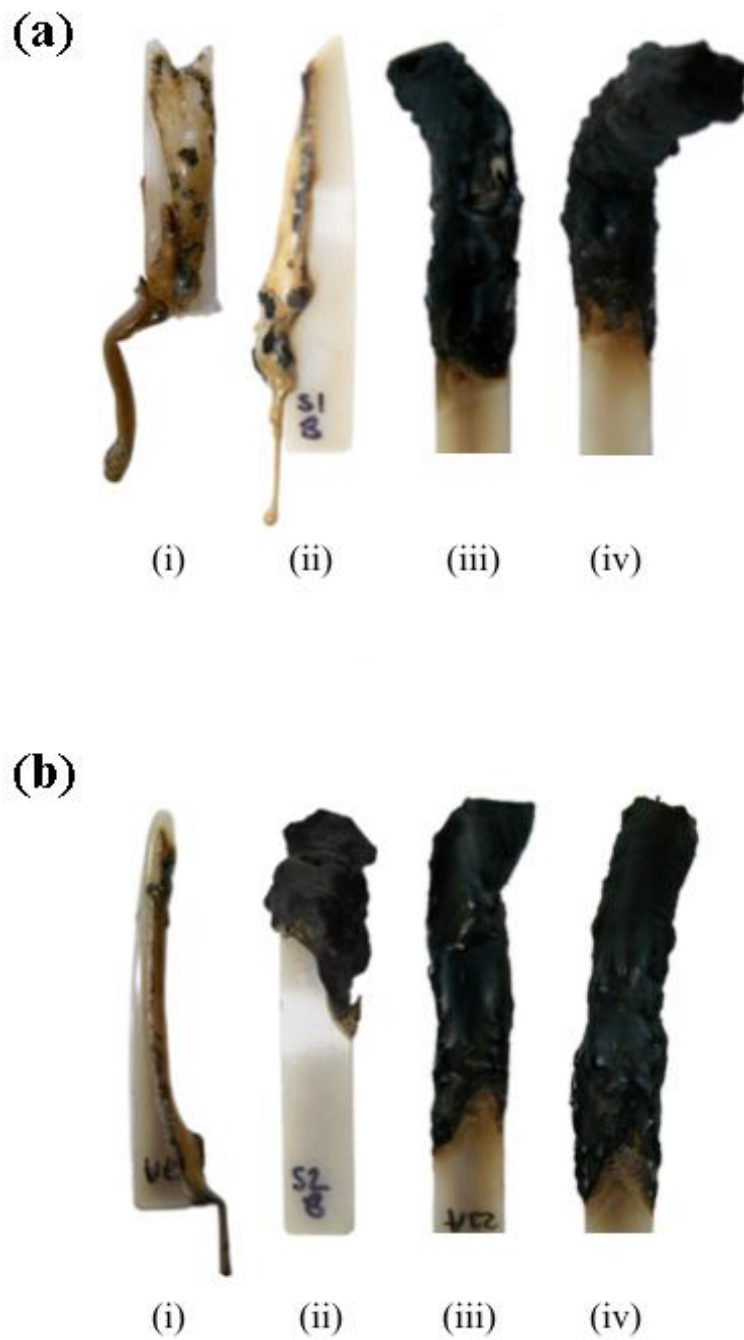


**Figure 3.2** Photographs of the Representative Specimens after LOI Test:  
**(a)** PA Based Materials; **(i)** PA, **(ii)** PA-ZB 20, **(iii)** PA-ADP 20,  
**(iv)** PA-ADP 17-ZB 3  
**(b)** PA/GF Based Materials; **(i)** PA/GF, **(ii)** PA/GF-ZB 20, **(iii)** PA/GF-ADP 20,  
**(iv)** PA/GF-ADP 17-ZB 3

### 3.1.2 SEM Analysis of LOI Chars

Burned tips of the representative LOI specimens were examined under SEM in order to compare their O<sub>2</sub>% values. Figure 3.3(i) and 3.4(i) show that specimens without flame retardants have very smooth surfaces with no charring. When 20 wt% ZB was added to the specimens, there was no charring, either (Figure 3.3(ii) and 3.4(ii)). Because, addition of ZB increases melt flow index of the specimen leading to dripping during burning.

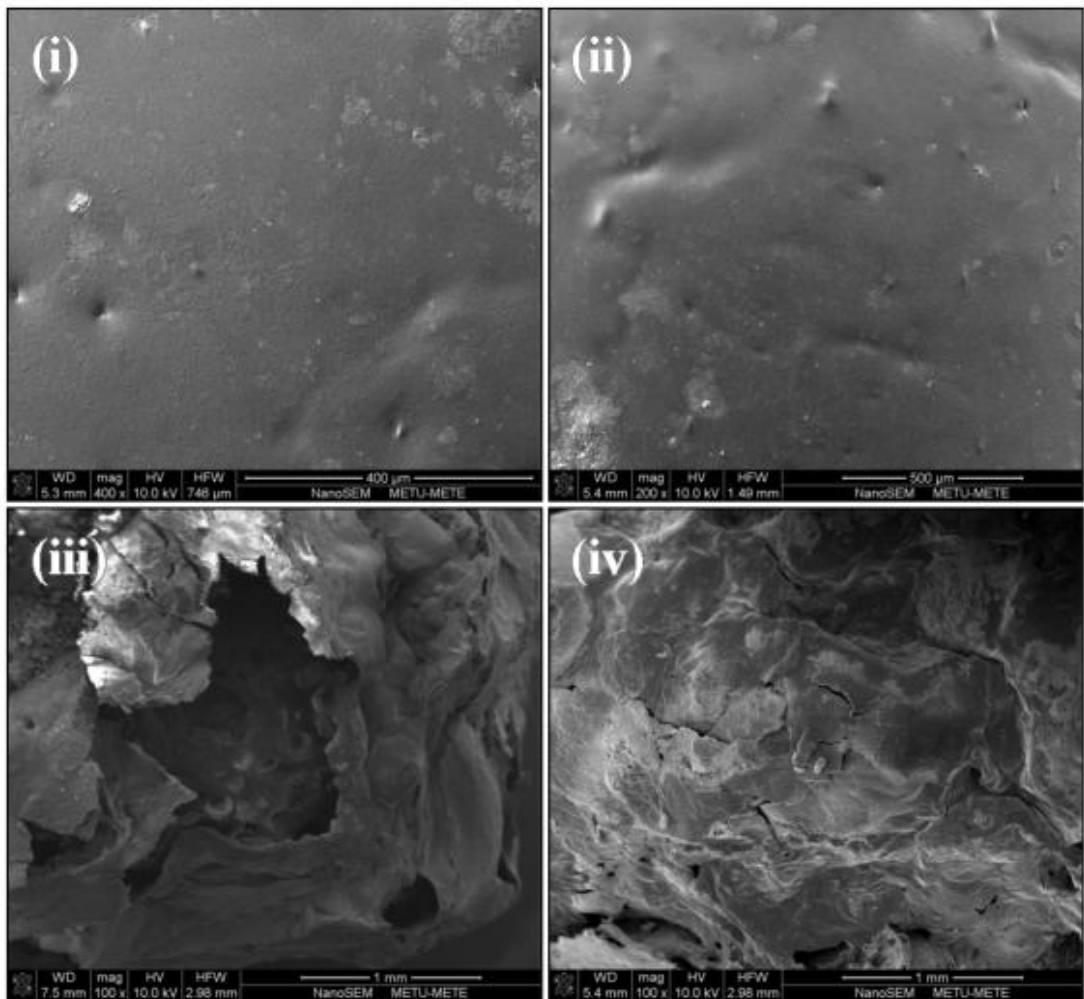


**Figure 3.3** SEM Images Showing Surface Char Barriers of the Representative PA Based Materials:

(i) PA, (ii) PA-ZB 20, (iii) PA-ADP 20, (iv) PA-ADP 13-ZB 7

Figure 3.3(iii) and 3.4(iii) show that the use of 20 wt% ADP leads to formation of certain level of rather continuous and strong char layers on the surface of the specimens increasing their LOI values significantly. When certain amount of ADP was replaced with ZB (Figure 3.3(iv) and 3.4(iv)), barrier action of charred layers could be more effective.

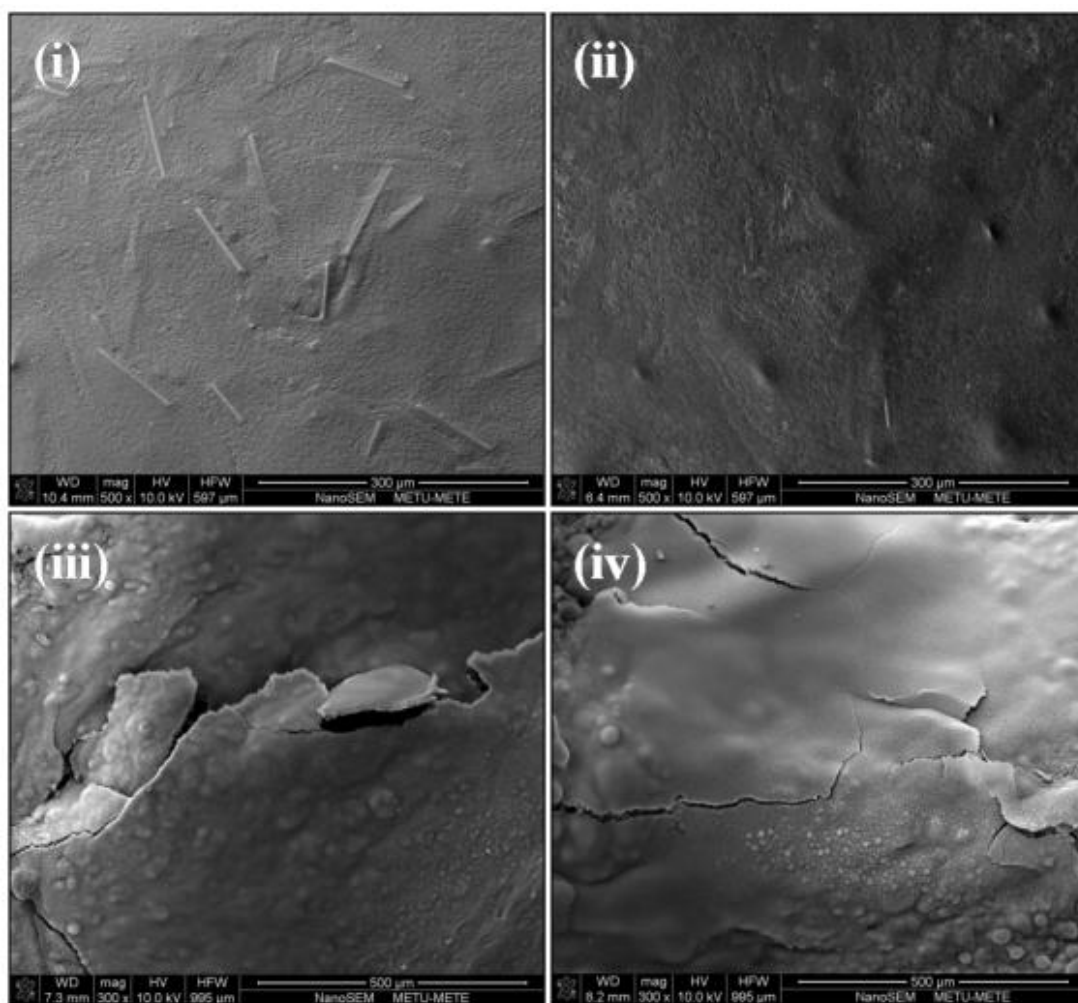


**Figure 3.4** SEM Images Showing Surface Char Barriers of the Representative PA/GF Based Materials:

(i) PA/GF, (ii) PA/GF-ZB 20, (iii) PA/GF-ADP 20, (iv) PA/GF-ADP 15-ZB 5

### 3.1.3 Mass Loss Cone Calorimetry Analysis

Mass loss cone calorimetry (MLC) was conducted to measure fire performances of all specimens. After the test, first, visual examination of the remaining char structures were done as given in Figures 3.5 and 3.6. These figures simply show that the char yield increases after incorporation of ADP and ZB. Then, the most significant plots, i.e. “heat release rate” (HRR) and “mass loss rate” (MLR) curves were plotted (Figures 3.7 and 3.8). Finally, all important fire performance parameters were determined and tabulated in Table 3.2.

Figures 3.7 and 3.8 indicate that HRR and MLR curves of both PA and PA/GF were suppressed after adding 20 wt% ZB alone or 20 wt% ADP alone. Moreover, these figures show that when certain amount of ADP was replaced with ZB, i.e. when ADP and ZB were used together, the suppressions were much more significant.

For instance, Table 3.2 shows that, when 20 wt% ZB alone was added, the suppression in the “peak heat release rate” (PHRR) values of PA and PA/GF were 48% and 50%, respectively. These suppressions were 32% and 75% when 20 wt% ADP alone was added. On the other hand, when certain amount of ADP was replaced with ZB, there were more significant suppressions, e.g. when 15 wt% ADP and 5 wt% ZB were used together, the suppression in PHRR values could be as much as 82%. Note that, the trend in the suppression of the “total heat evolved” (THE) values is almost the same.

In terms of time related MLC parameters, Table 3.2 indicates that use of both ZB and ADP alone or together delayed the periods of “time to ignition” (TTI) values a little bit further, while the delays in the values of “time to peak heat release rate” (TPHRR) were much longer. Nevertheless, the most significant time extensions were observed in the values of “total burning time” (TBT). Table 3.2 shows that, when ZB and ADP were used together, TBT periods of PA and PA/GF could be extended more than three times.

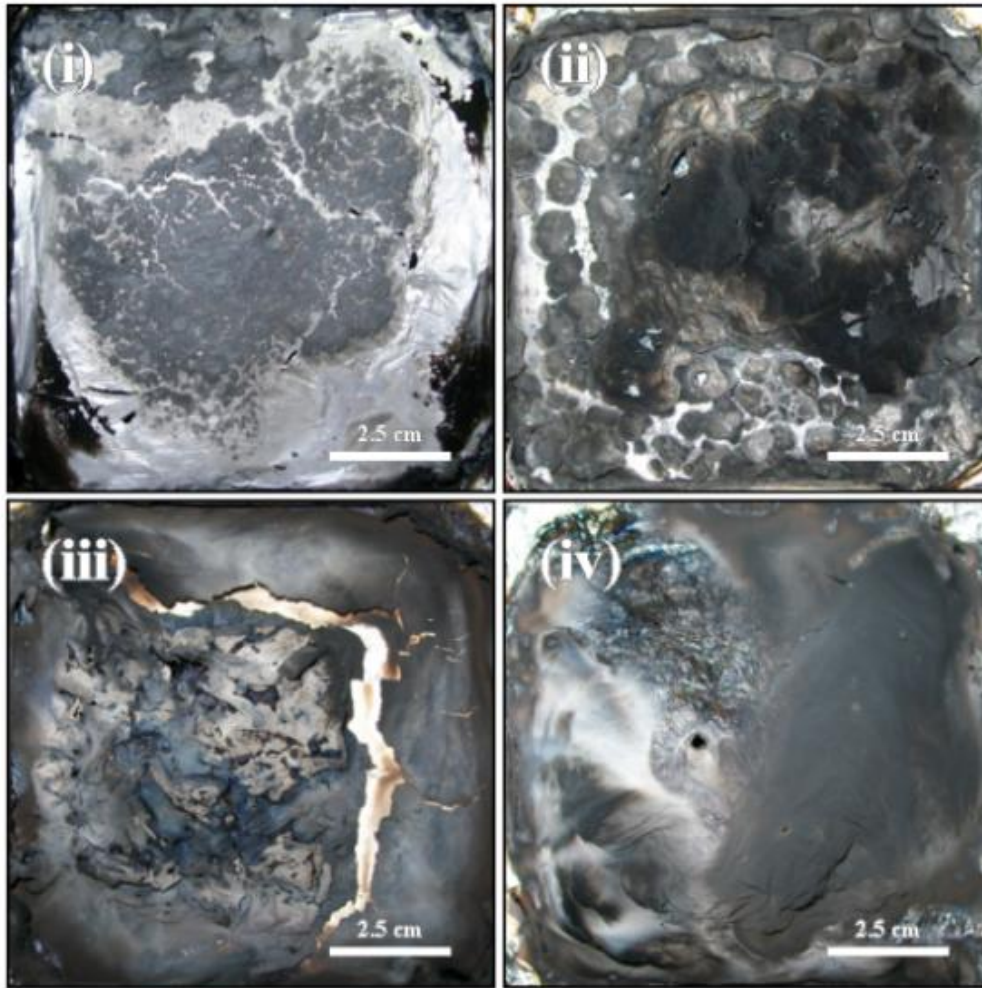


**Figure 3.5** Photographs of the Remaining Char Structure of MLC Specimens of the Representative PA Based Materials: (i) PA, (ii) PA-ZB 20, (iii) PA-ADP 20, (iv) PA-ADP 15-ZB 5

In order to have additional data about the contribution of a material to the fire propagation rate, two different indices can be calculated from the MLC parameters. The first index is called “fire growth index” (FGI) which is the ratio of PHRR/TTI, the second one is named as “fire growth rate index” (FIGRA) which is the ratio of PHRR/TPHRR. Use of any flame retardant decreases these indices, i.e. decreases fire propagation rate. Table 3.2 again shows that use of ZB and ADP together decreased values of these two indices considerably.

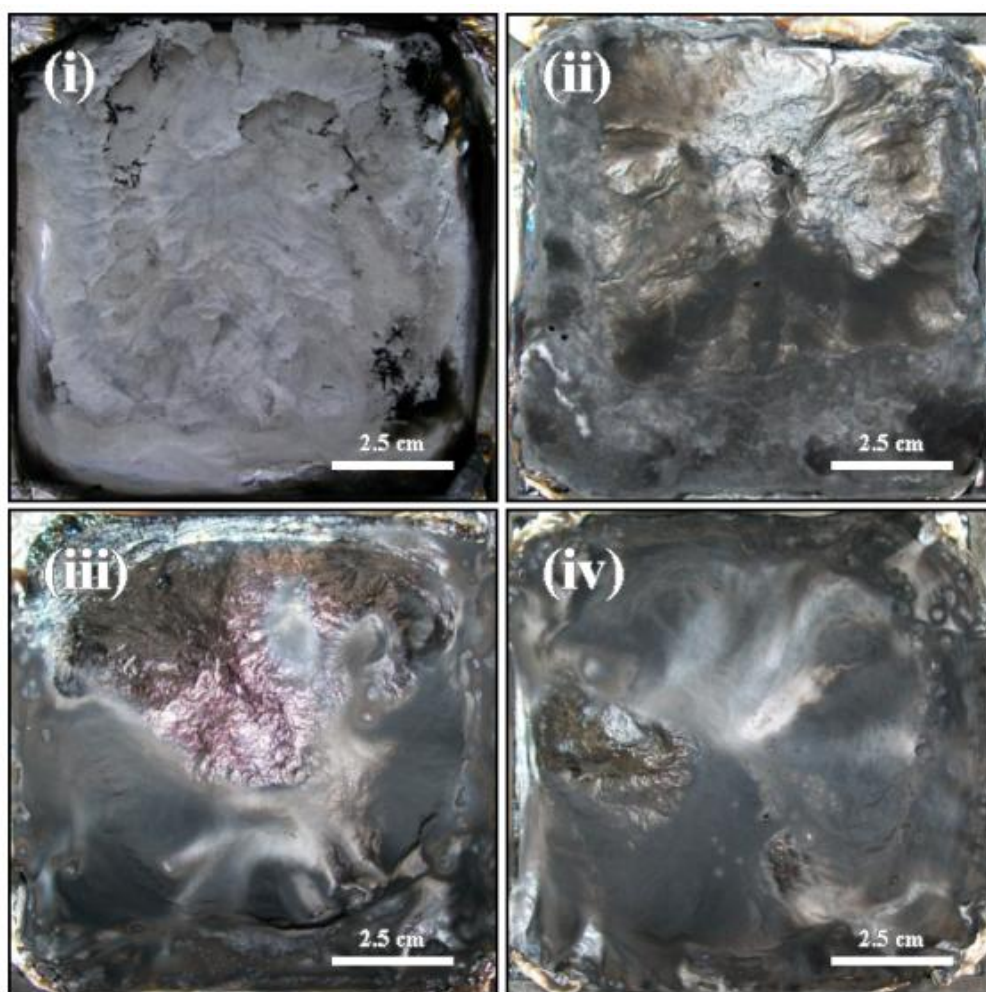


**Figure 3.6** Photographs of the Remaining Char Structure of MLC Specimens of the Representative PA/GF Based Materials: (i) PA/GF, (ii) PA/GF-ZB 20, (iii) PA/GF-ADP 20, (iv) PA/GF-ADP 15-ZB 5

The ratio of THE/TML (total heat evolved/total mass loss) and % char yield data might give information about the flame retardancy mechanisms of the specimens. Table 3.2 reveals that the values of THE/TML ratio decreased when ADP was incorporated. This means, ADP might basically act in the gaseous phase mechanisms. On the other hand, Table 3.2 shows that use of ZB increases % char residue considerably, indicating the effectiveness of condensed phase physical char formation.

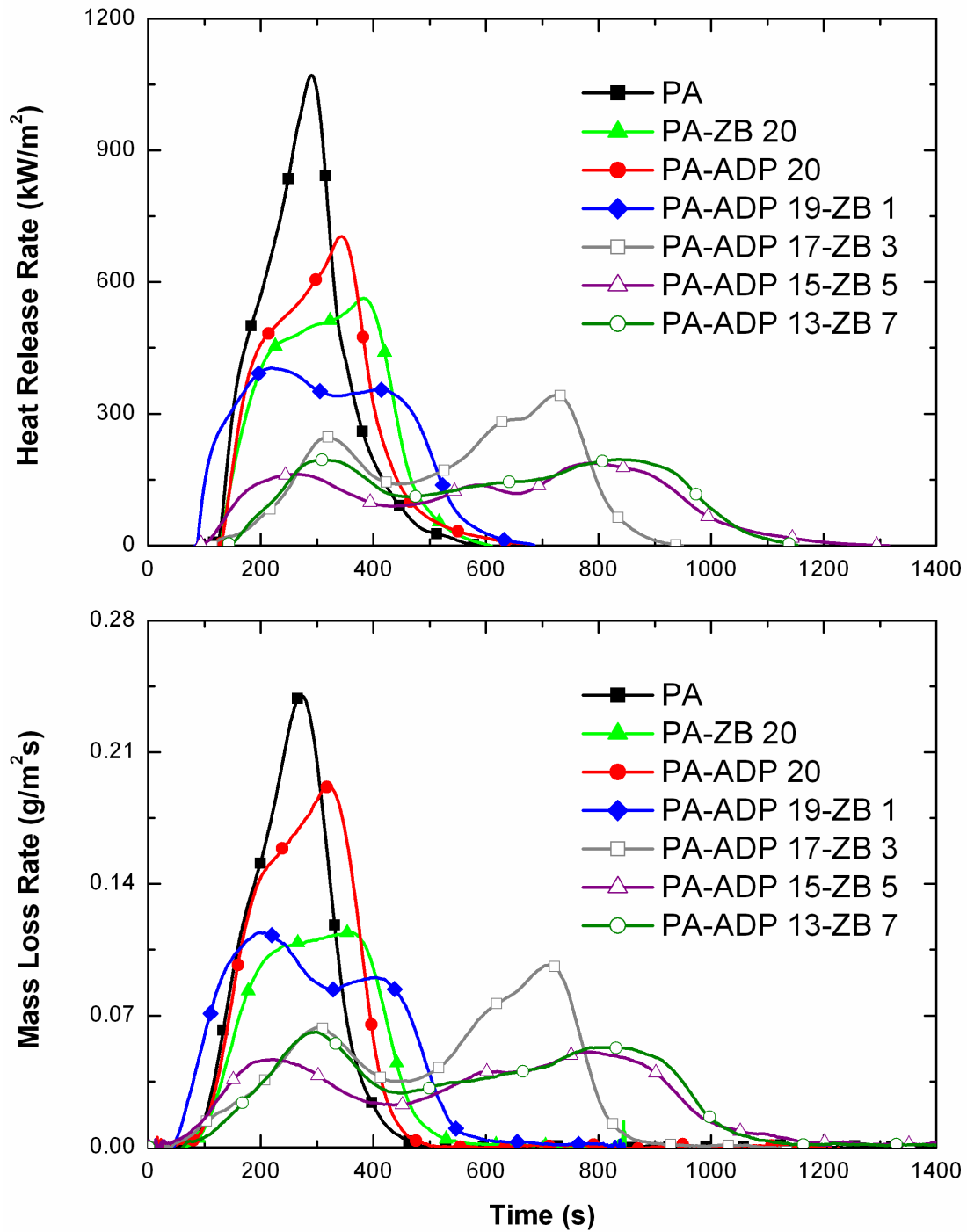


**Figure 3.7** Heat Release Rate and Mass Loss Rate Curves for the PA Based Materials

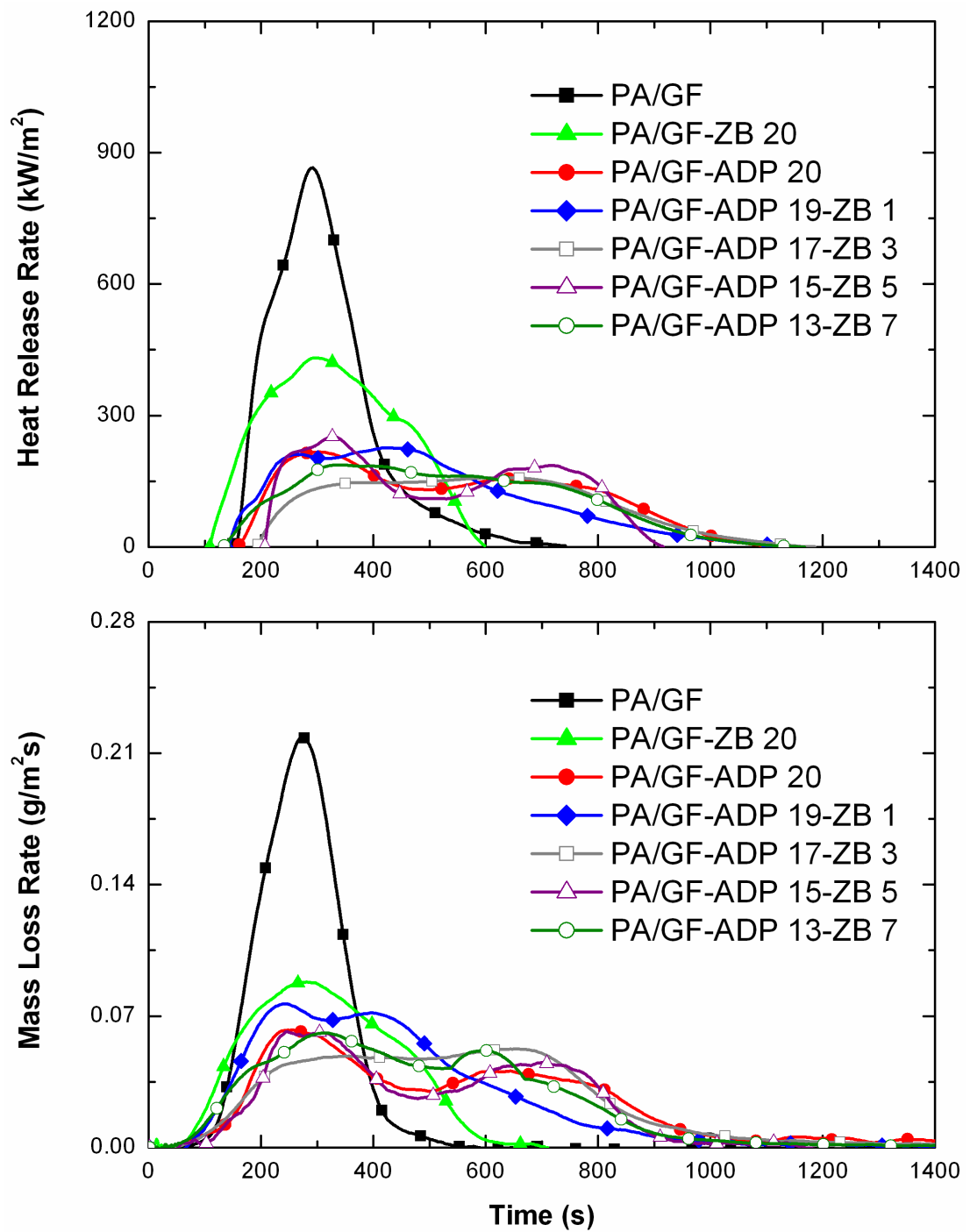


**Figure 3.8** Heat Release Rate and Mass Loss Rate Curves for the PA/GF Based Materials

**Table 3.2** Mass Loss Cone Calorimeter Parameters of the Specimens

Specimens	PHRR <sup>a</sup> (kW/m <sup>2</sup> )	THE <sup>b</sup> (MJ/m <sup>2</sup> )	TTI <sup>c</sup> (s)	TPHRR <sup>d</sup> (s)	TBT <sup>e</sup> (s)	FGI <sup>f</sup> (kW/m <sup>2</sup> .s)	FIGRA <sup>g</sup> (kW/m <sup>2</sup> .s)	THE/TML <sup>h</sup> (MJ/m <sup>2</sup> .g)	Char Yield (%)
PA	1055	171	96	302	437	11.0	3.5	4.2	0.2
PA-ZB 20	554	146	103	368	587	5.4	1.5	4.5	20.1
PA-ADP 20	716	151	108	350	477	6.6	2.0	3.5	2.3
PA-ADP 19-ZB 1	407	146	65	241	644	6.3	1.7	3.6	8.8
PA-ADP 17-ZB 3	346	135	84	720	953	4.1	0.5	3.4	10.9
PA-ADP 15-ZB 5	193	122	61	792	688	3.2	0.2	3.4	18.6
PA-ADP 13-ZB 7	198	128	111	821	1602	1.8	0.2	3.3	16.1
PA/GF	868	159	108	291	563	8.0	3.0	4.1	15.0
PA/GF-ZB 20	434	133	69	294	596	6.3	1.5	4.5	34.7
PA/GF-ADP 20	219	114	112	326	1354	2.0	0.7	3.4	31.3
PA/GF-ADP 19-ZB 1	227	113	116	422	1541	2.0	0.5	3.1	24.4
PA/GF-ADP 17-ZB 3	161	98	108	594	1579	1.5	0.3	2.7	25.5
PA/GF-ADP 15-ZB 5	256	107	137	330	1192	1.9	0.8	3.6	31.1
PA/GF-ADP 13-ZB 7	191	109	102	321	1385	1.9	0.6	3.1	30.3

<sup>a</sup> PHRR: peak heat release rate

<sup>b</sup> THE: total heat evolved

<sup>c</sup> TTI: time to ignition

<sup>d</sup> TPHRR: time to peak heat release rate

<sup>e</sup> TBT: total burning time

<sup>f</sup> FGI: fire growth index, where FGI=PHRR/TTI

<sup>g</sup> FIGRA: fire growth index rate, where FIGRA=PHRR/TPHRR

<sup>h</sup> THE/TML: ratio of total heat evolved/total mass loss

### 3.1.4 Flame Retardancy Mechanisms

It is known that phosphorus based flame retardants can function effectively when incorporated into polymers containing oxygen in pendant groups or in the backbone. It is also generally accepted that phosphorus compounds either react with the polymer during decomposition, or get oxidized to phosphoric acid to promote charring in the condensed phase. Phosphorus compounds can also volatilize into gas phase and get oxidized to  $\text{HPO}_2\bullet$ ,  $\text{PO}\bullet$ ,  $\text{PO}_2\bullet$ , and  $\text{HPO}\bullet$  radicals acting as  $\text{H}\bullet$  and  $\text{OH}\bullet$  scavengers to suppress combustion chain reaction.

Therefore, since polyamide-6 is an oxygen containing polymer, ADP may act both in the “condensed” phase and the “gaseous” phase [29,30,34]. When ADP was vaporized during fire, it might get oxidized to radicals mentioned above which would scavenge very harmful  $\text{H}\bullet$  and  $\text{OH}\bullet$  hot radicals. This gaseous phase action, which is called “flame inhibition”, is considered to be the dominant mechanism of ADP suppressing the combustion reactions effectively.

When ADP was oxidized to phosphoric acid during fire, it might lead to formation of char layers which would insulate the material from fire and oxygen. ADP could form two-layer protective barrier; a carbon based char and an inorganic residue layer such as aluminum phosphate. This condensed phase action, which is called “barrier effect”, can be considered as a secondary mechanism enhancing the flame retardancy.

It should be noted that ADP vaporization would be improved when lower external heat fluxes were applied, e.g. during LOI tests. Then, “gas phase action” of ADP would be dominant. On the other hand, when higher external heat fluxes were applied, e.g. during MLC tests, decomposition of ADP would be improved. Then, decomposed phosphinate ions would induce formation of carbon char layers and aluminum phosphate residue, i.e. “condensed phase action” of ADP would be also operative.

The main mechanism of ZB is also barrier formation which could take place both in the condensed phase and the gas phase. ZB dehydrates endothermically which absorb the heat of combustion, and the released water vapor dilutes oxygen and gaseous flammable components. This mechanism is considered as the gas phase barrier action. During fire, ZB also produces a glassy layer over the polymer surface, which is considered as the condensed phase barrier action.

When ZB and ADP were used together, those mechanisms mentioned above would be also operative. The main contribution of ZB to ADP would be again in the formation of barrier layers. It is believed that, when they are used together, an additional inorganic barrier, i.e. boron phosphate /aluminum phosphate layers would form, as also discussed by Braun et.al. [29]. Another advantage of ZB would be its well-known ability of smoke and afterglow suppression.

Of course, another contribution to the condensed phase barrier mechanism would take place by the short glass fibers used in the PA/GF based specimens which would increase the effectiveness of char barriers via reinforcing or stabilizing their structure.

In order to clarify these flame retardancy mechanisms further, three additional analyses (thermogravimetric analysis, X-ray diffraction and evolved gas analysis) were conducted and discussed in the following sections.

### **3.1.5 Thermogravimetric Analysis**

Since results of each group were very similar, thermogravimetric (TG) and differential thermogravimetric (DTG) curves are given in Figure 3.9 only for the representative compositions of the PA based materials, while the thermal degradation parameters derived from these curves are tabulated in Table 3.3 for neat ZB, ADP and the representative compositions of the both PA and PA/GF based materials.

These curves showed that neat PA decomposes in one step with maximum mass loss rate at around 460°C leaving very little residue. On the contrary, due to the 15 wt% glass fiber reinforcements, PA/GF specimen formed considerable amount of residue. It is known that during decomposition, polyamide-6 releases water, ammonia, carbon monoxide, carbon dioxide, and certain hydrocarbon fragments.

Figure 3.9 shows that when ZB and ADP were added, TG and DTG curves shift slightly to lower temperatures. Therefore, Table 3.3 reveals that, not only maximum mass loss rate temperatures ( $T_{DTG\text{-peak}}$ ), but also 10 wt% and 50 wt% degradation temperatures ( $T_{10\text{ wt\%}}$  and  $T_{50\text{ wt\%}}$ ) of the PA and PA/GF specimens were lowered.

On the other hand, Table 3.3 also indicates that addition of ZB increases amount of residue significantly, for instance, use of 20 wt% ZB lead to more than 15 wt% residue. It is seen than use of ADP also resulted in residue formation considerably. Thus, TG analysis supported the physical barrier formation mechanisms of ZB and ADP discussed in the previous section.

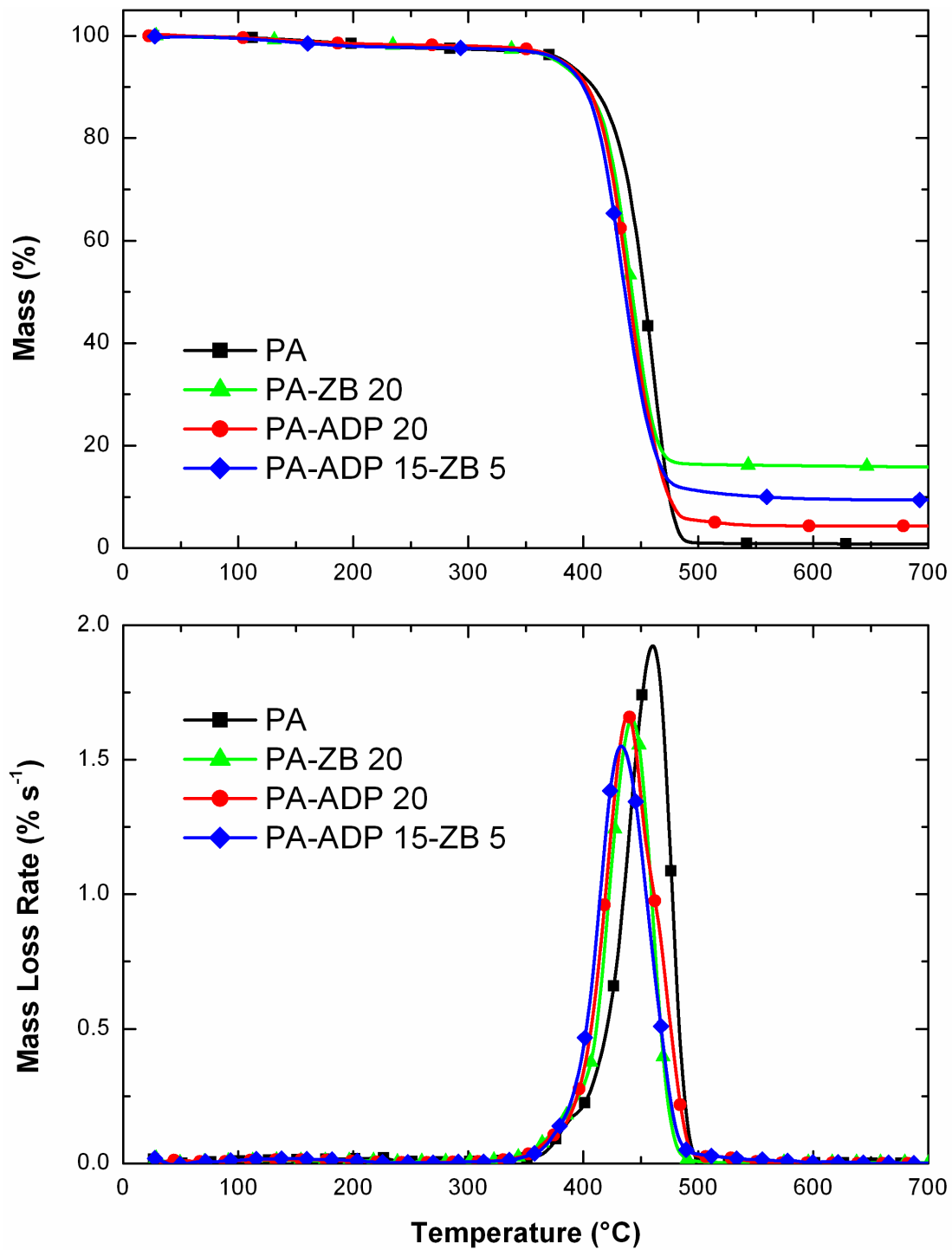


**Figure 3.9** Thermogravimetric (TG) and Differential Thermogravimetric (DTG) Curves for the Representative PA Based Materials

**Table 3.3** Thermal Degradation Parameters of the Representative Specimens Determined from TG and DTG Curves

Specimens	T <sub>DTG-Peak 1</sub> <sup>a</sup> (°C)	T <sub>DTG-Peak 2</sub> <sup>b</sup> (°C)	T <sub>10 wt%</sub> <sup>c</sup> (°C)	T <sub>50 wt%</sub> <sup>d</sup> (°C)	% Residue at 600 °C
ZB	242	415	428	-	85.8
ADP		496	459	494	15.8
PA	-	460	408	452	0.9
PA-ZB 20	-	442	403	443	16.1
PA-ADP 20	-	436	404	439	4.4
PA-ADP 15-ZB 5	-	426	401	437	9.6
PA/GF		465	416	455	14.8
PA/GF-ZB 20	-	435	409	443	31.5
PA/GF-ADP 20		430	395	436	18.2
PA/GF-ADP 15-ZB 5	-	438	408	443	21.6

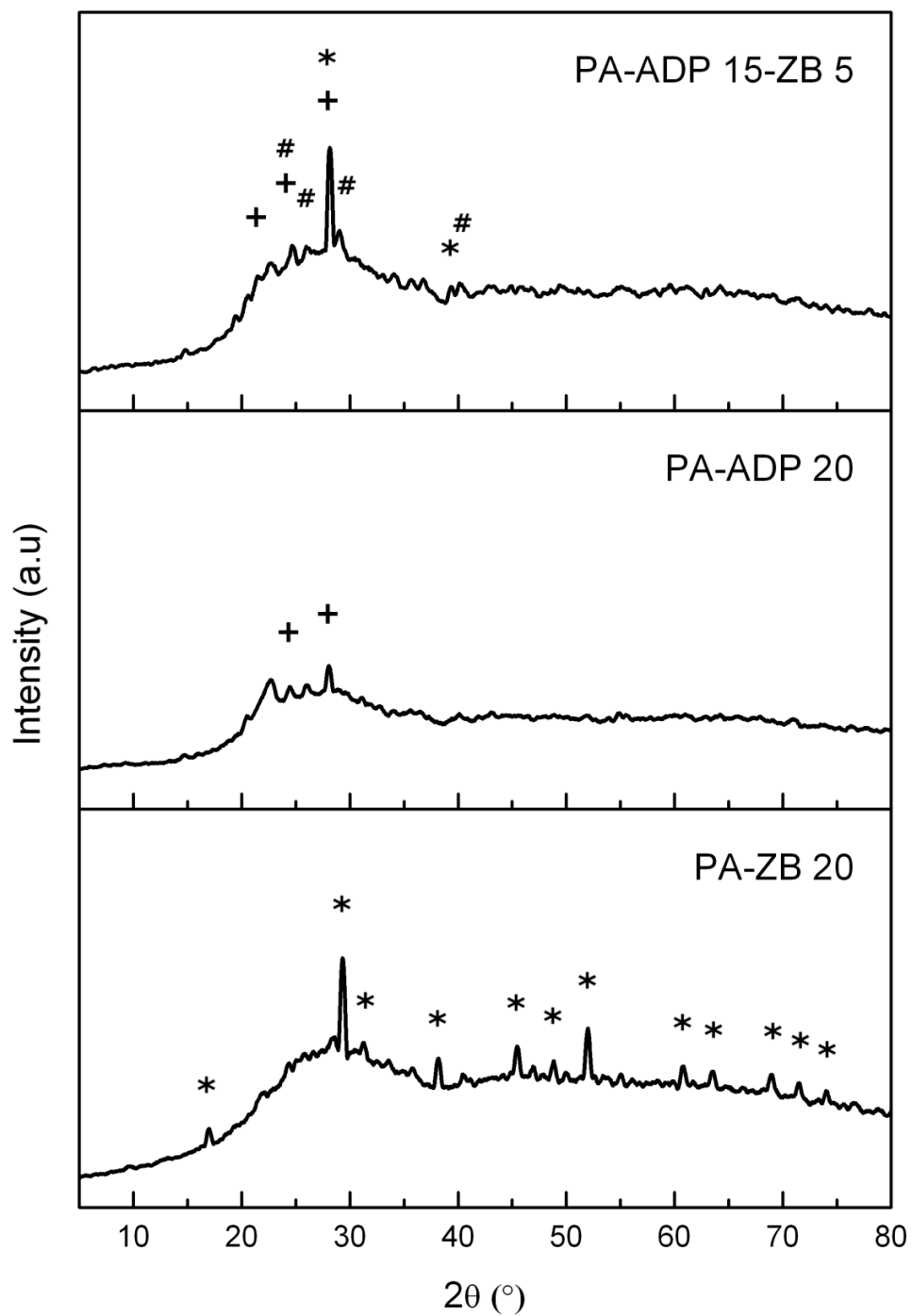
<sup>a</sup> T<sub>DTG-Peak 1</sub>: first peak temperature in DTG curve<sup>b</sup> T<sub>DTG-Peak 2</sub>: second peak temperature in DTG curve<sup>c</sup> T<sub>10 wt%</sub>: thermal degradation temperature for 10% mass loss<sup>d</sup> T<sub>50 wt%</sub>: thermal degradation temperature for 50% mass loss

### 3.1.6 XRD Analysis of MLC Residues

In order to reveal crystal structure of the phases in the char layers, XRD analyses were conducted on the MLC chars of the representative specimens of each group. Since results of each group were very similar, XRD diffractograms are provided in Figure 3.10 only for the PA based materials.

Figure 3.10 shows that when ZB was added alone, three forms of dehydrated zinc borate ( $\text{Zn}(\text{BO}_2)_2$ ,  $\text{ZnB}_4\text{O}_7$  and  $\text{Zn}_4\text{B}_6\text{O}_{13}$ ) peaks were seen. When ADP was used alone, peaks of its main decomposition phase, i.e. peaks of aluminum phosphate ( $\text{AlPO}_4$ ) were seen. When ZB and ADP were added together, apart from their decomposition phases of dehydrated zinc borate and aluminum phosphate, additional peaks for boron phosphate ( $\text{BPO}_4$ ) could be observed.

Thus, it can be stated that, apart from the expected decomposition byproducts, no other phases were formed in the chars of the MLC specimens. This could be interpreted as another confirmation of the physical barrier mechanism of especially ZB, and also partly for ADP.



\* : Dehydrated zinc borate  $ZnB_4O_7$ , Card no: 24-1438, or  $Zn_4B_6O_{13}$ , Card no: 27-1487, or  $Zn(BO_2)_2$ , Card no: 39-1126

+ : Aluminum phosphate  $AlPO_4$ , Card no: 46-0695

# : Boron phosphate  $BPO_4$ , Card no: 11-0237, 12-0380, 34-0132

**Figure 3.10** XRD Patterns of the MLC Residues of the Representative PA Based Materials

### 3.1.7 Evolved Gas Analysis

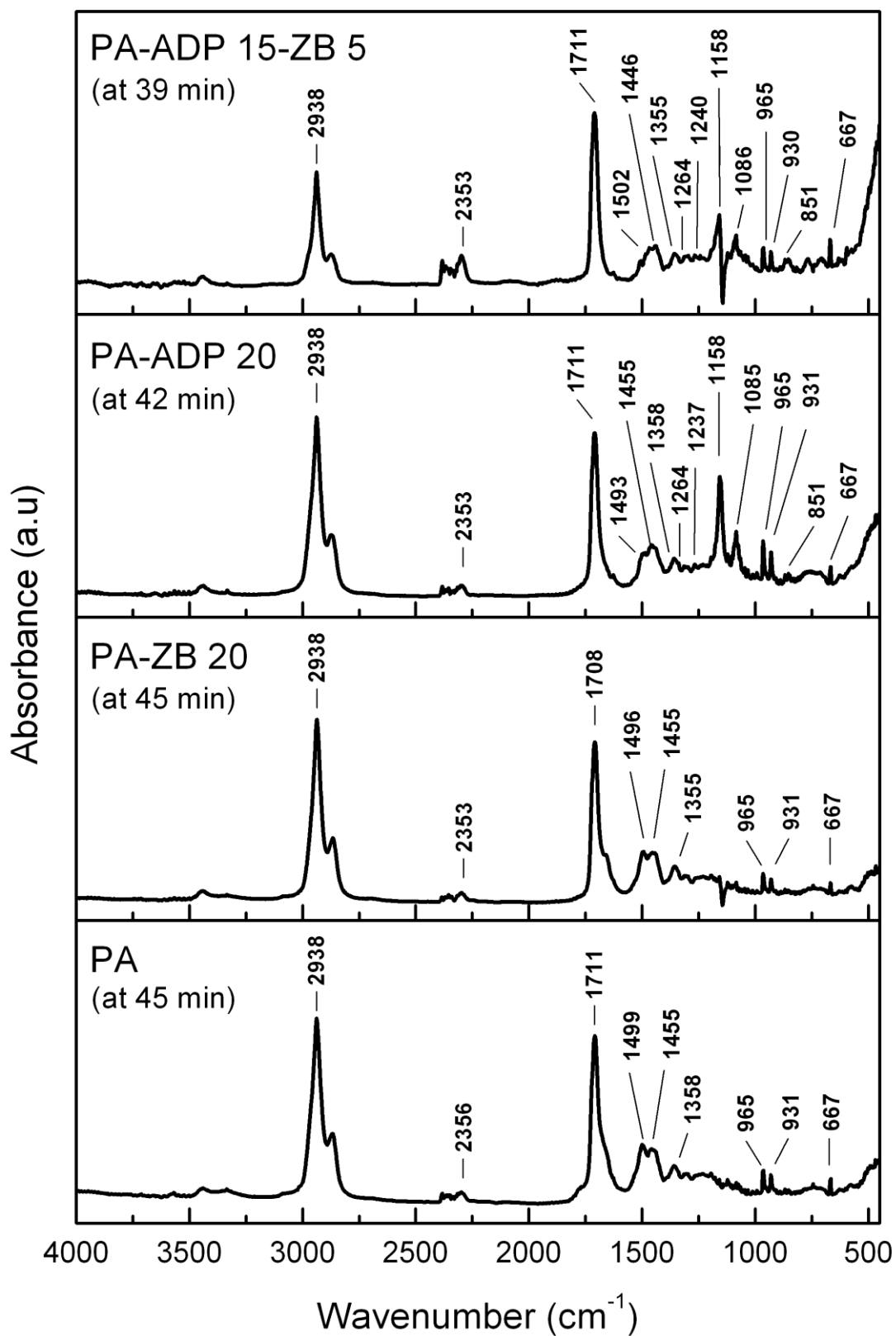
In order to support gas phase action of the flame retardants, volatile decomposition products of the representative specimens of each group were examined using a TGA-FTIR coupled system. Since results of each group were very similar, evolved gas analysis spectra are given in Figure 3.11 only for the PA based materials.

Figure 3.11 shows that spectrum of neat PA specimen at 45 min exhibited characteristic bands of ammonia (N-H bending at 965 and 931  $\text{cm}^{-1}$ ), carbon dioxide (C=O stretching at 2356  $\text{cm}^{-1}$  and C=O bending at 667  $\text{cm}^{-1}$ ),  $\epsilon$ -caprolactam (C=O stretching at 1711  $\text{cm}^{-1}$  and C-N stretching at 1358  $\text{cm}^{-1}$ ), hydrocarbons (C-H stretching at 2938  $\text{cm}^{-1}$  and C-H bending at 1455  $\text{cm}^{-1}$ ), water (H-O-H bending at 1499  $\text{cm}^{-1}$ ). These decomposition products are in accordance with the literature [29,30,66].

When ZB alone was added, it was seen in the spectrum of PA-ZB 20 at 45 min that there is no contribution of ZB decomposition.

On the other hand, PA-ADP 20 spectrum at 42 min exhibited additional characteristic bands of  $\text{PO}_2^-$  anion (1158 and 1085  $\text{cm}^{-1}$ ), P-O-P stretching (851  $\text{cm}^{-1}$ ) and P=O stretching (1264 and 1237  $\text{cm}^{-1}$ ). These volatile products could be interpreted as the confirmation of gas phase flame inhibition mechanism of ADP [29,30,66].

Since the use of ZB and ADP together leads to no additional gas phase mechanism, spectrum of PA-ADP 15-ZB 5 specimen exhibited no additional band.



**Figure 3.11** Evolved Gas Analysis Spectra of the Representative PA Based Materials

### 3.1.8 Tensile Testing for Mechanical Properties

In order to observe influences of ZB and ADP on the mechanical performance of all the specimens studied, a minimum of five samples for each formulation were subjected to tension tests. Figure 3.12 shows tensile stress-strain behavior of the specimens, while Table 3.4 gives determined mechanical properties.

Figure 3.12 and Table 3.4 shows that when 20 wt% ZB alone was added to neat PA, its modulus and strength values increased. The increase in Young's modulus is 53%, in yield strength 31%, and in tensile strength 15%. These increases should be due to the decreased chain mobility of the PA matrix by the fine sized (12.3  $\mu\text{m}$ ) rigid and strong inorganic ZB particles. Thus, its ductility (i.e. % elongation at break) decreased considerably.

However, when 20 wt% ADP was incorporated into neat PA, except modulus its other mechanical properties decreased. These decreases were 17% in yield strength, 14% in tensile strength, and 91% in elongation at break. These decreases could be basically due to the very coarse size (42.3  $\mu\text{m}$ ) and rather weak organic structure of ADP particles.

Therefore, Table 3.4 indicates that, when ZB and ADP were used together in PA, their mechanical properties are lower compared to the values of ZB alone, but higher compared to the values of ADP alone.

As expected, when 15 wt% short glass fiber reinforcements were filled, modulus and strength values increased significantly. Compared to PA, these increases in the specimen of PA/GF are 64% for Young's modulus, 36% for yield strength, and 34% for tensile strength. Of course, the reason for these improvements is the well known composite strengthening mechanism, i.e. very effective load transfer from the matrix to the fiber reinforcements.

In this PA/GF based group, Table 3.4 shows that, use of ZB and ADP, alone or together, lead to no decrease in Young's modulus values; but there are substantial decreases in the strength and ductility values. These decreases should be due to the lowered efficiency of load transfer mechanism.

Fracture surfaces of the tensile test specimens were also examined via SEM in order to reveal morphology of the fracture surfaces and distribution of the flame retardants. Figures 3.13 and 3.14 show that very smooth fracture surfaces of PA and PA/GF specimens transformed into very rough morphology when ZB and ADP were incorporated. It is also seen that flame retardants ZB and ADP, and the fiber reinforcement GF were all distributed rather uniformly having certain level of interfacial bonding with the PA matrix.

**Table 3.4** Tensile Mechanical Properties of the Specimens

<b>Specimens</b>	<b>Young's Modulus (GPa)</b>	<b>Yield Strength (MPa)</b>	<b>Tensile Strength (MPa)</b>	<b>Elongation at break (%)</b>
PA	1.96 ± 0.08	40.3 ± 3.4	54.2 ± 0.7	58.3 ± 3.5
PA-ZB 20	2.99 ± 0.06	52.9 ± 0.4	62.1 ± 1.6	18.0 ± 1.3
PA-ADP 20	2.43 ± 0.17	33.3 ± 3.9	46.6 ± 0.3	9.0 ± 0.4
PA-ADP 19-ZB 1	2.62 ± 0.06	39.6 ± 1.2	45.3 ± 0.4	12.8 ± 1.1
PA-ADP 17-ZB 3	2.49 ± 0.12	36.5 ± 3.5	44.3 ± 1.6	8.8 ± 0.6
PA-ADP 15-ZB 5	2.34 ± 0.18	30.3 ± 3.8	46.3 ± 1.2	6.6 ± 0.7
PA-ADP 13-ZB 7	2.52 ± 0.06	38.1 ± 1.2	46.6 ± 0.4	6.2 ± 1.1
PA/GF	3.22 ± 0.04	54.8 ± 2.9	72.5 ± 0.6	8.8 ± 0.4
PA/GF-ZB 20	3.89 ± 0.03	54.6 ± 1.8	61.3 ± 0.7	4.6 ± 0.4
PA/GF-ADP 20	3.46 ± 0.08	42.8 ± 3.4	57.7 ± 0.3	5.1 ± 0.1
PA/GF-ADP 19-ZB 1	3.89 ± 0.04	51.5 ± 0.2	56.0 ± 0.2	4.1 ± 0.2
PA/GF-ADP 17-ZB 3	3.93 ± 0.03	53.0 ± 1.3	59.0 ± 0.3	4.0 ± 0.2
PA/GF-ADP 15-ZB 5	3.89 ± 0.04	50.7 ± 0.5	55.0 ± 0.2	3.8 ± 0.1
PA/GF-ADP 13-ZB 7	3.63 ± 0.06	47.4 ± 0.8	50.1 ± 0.7	4.0 ± 0.2

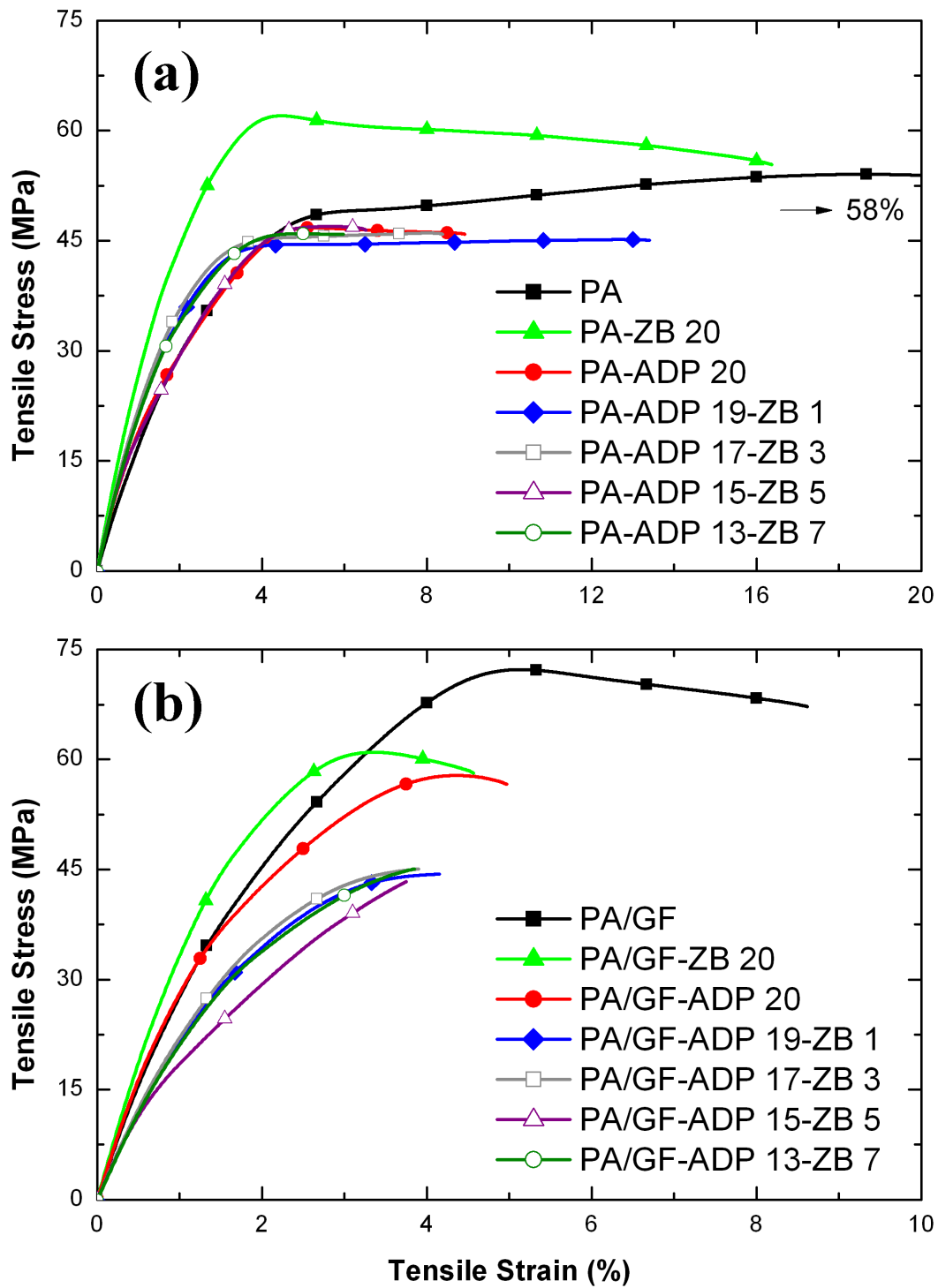


**Figure 3.12** Tensile Stress-Strain Curves of the (a) PA and (b) PA/GF Based Materials

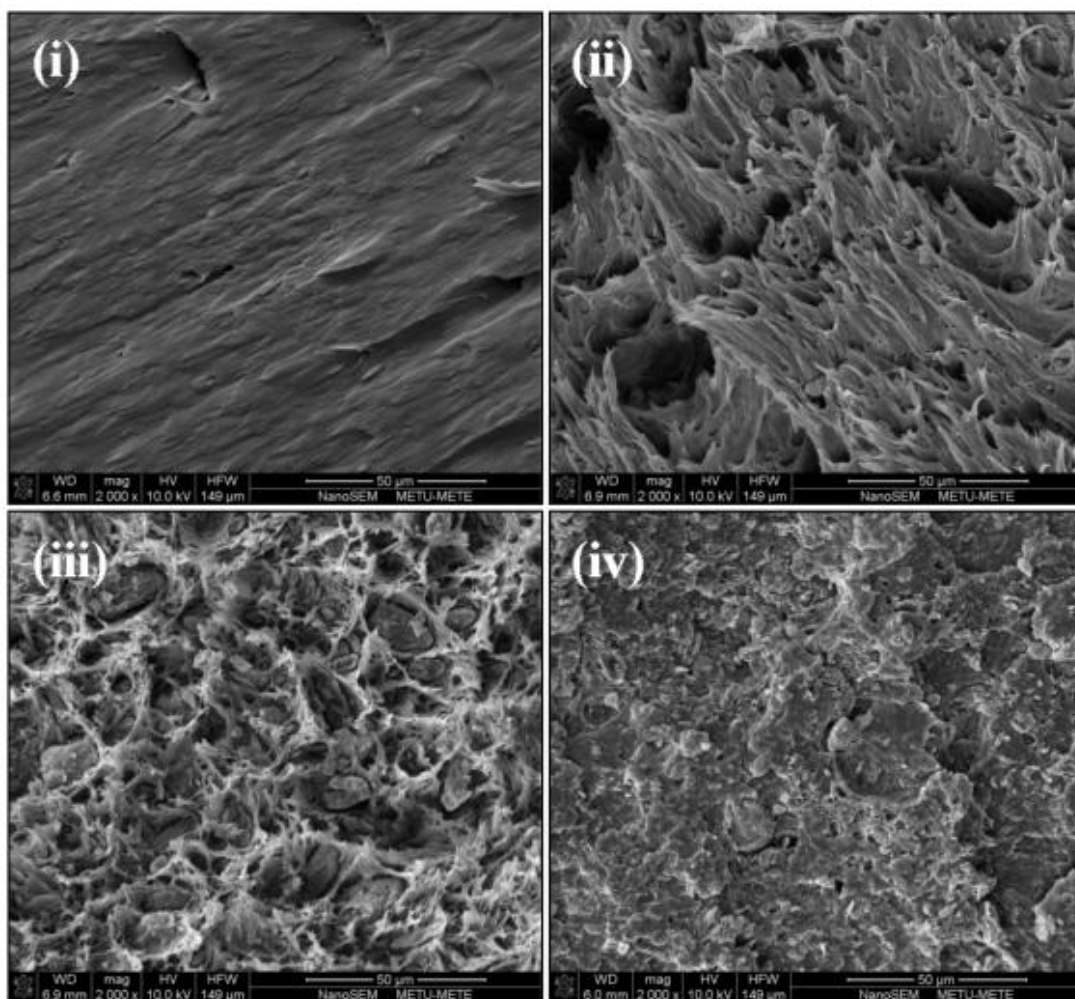


**Figure 3.13** SEM Fractographs of the Representative PA Based Materials:

(i) PA, (ii) PA-ZB 20, (iii) PA-ADP 20, (iv) PA-ADP 15-ZB 5

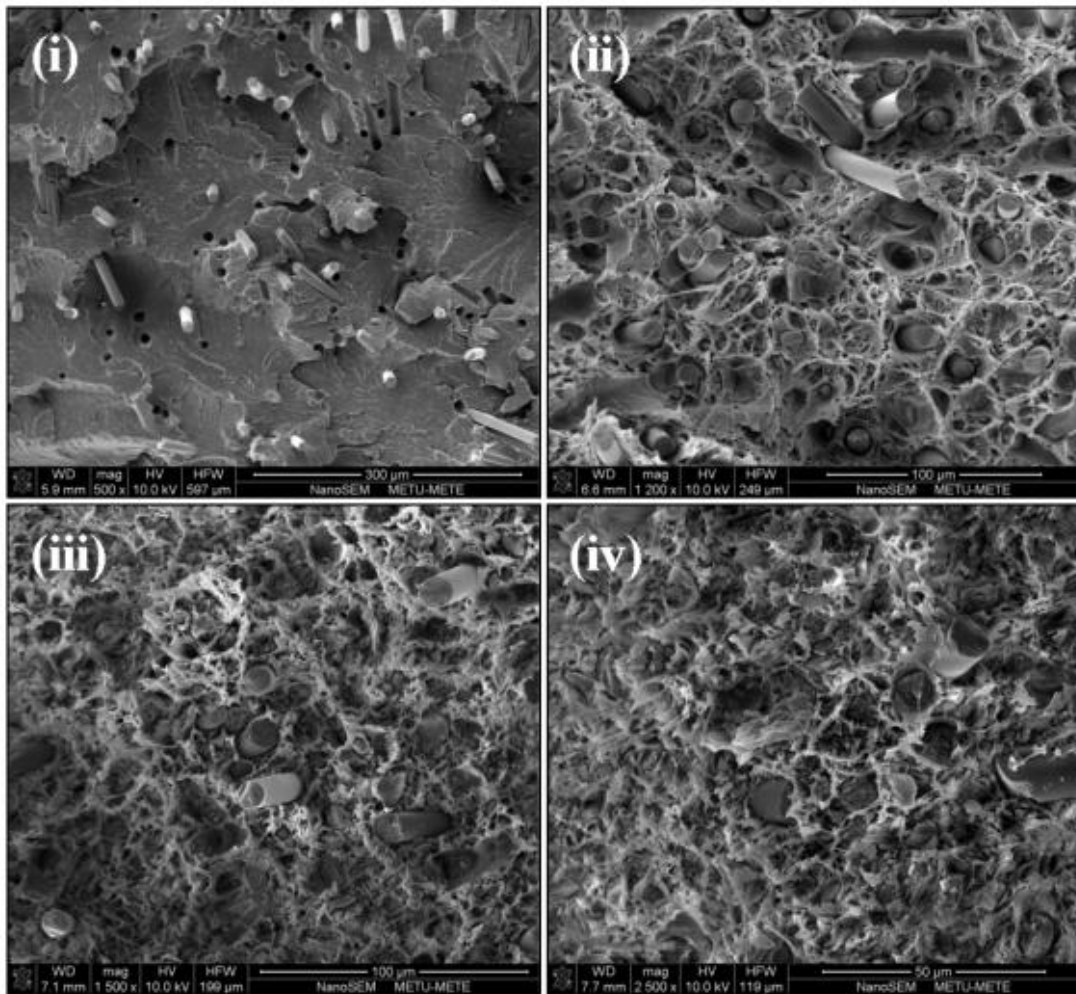


**Figure 3.14** SEM Fractographs of the Representative PA/GF Based Materials:  
(i) PA/GF, (ii) PA/GF-ZB 20, (iii) PA/GF-ADP20, (iv) PA/GF-ADP 15-ZB 5

## **3.2 EFFECTS OF BORON OXIDE AND BORIC ACID**

To evaluate flame retardancy enhancement of BO and BA, the control sample material was chosen as PA or PA/GF with 20 wt% ADP type organophosphorus compound. Then, amount of ADP was replaced with certain amounts of BO or BA. These replacements were 1, 3 and 5 wt% for the PA based group, while only 3 and 5 wt% for the PA/GF based group. In order to observe effects of BO or BA alone, specimens having only 10 wt% BO or BA were also produced. Unfortunately, due to the compounding problems in the laboratory size twin-screw extruder, production of specimens with 20 wt% BO or BA were not possible. Designations and compositions of the specimens produced for this second part of the thesis are given in Table 2.3 and the results are discussed below.

### **3.2.1 UL-94 and LOI Flammability Tests**

Results of UL-94 and LOI flammability tests are tabulated in Table 3.5, while appearances of the representative specimens after these two tests are given in Figure 3.15 and 3.16, respectively. It is seen that both PA and PA/GF specimens have V-2 rating from UL-94 tests, and LOI values of 26.1 and 23.3 O<sub>2</sub>%, respectively.

Due to its very high efficiency, when 20 wt% ADP was incorporated alone, there were significant improvements, e.g. both specimens (PA-ADP 20 and PA/GF-ADP 20) obtained V-0, the best rating of UL-94, and increased LOI values of 32.7 and 30.7 O<sub>2</sub>%, respectively. These improvements were especially due to the very effective “flame inhibition” action of ADP, and also its “charring” action as shown in Figure 3.16(a)(iv) and (b)(iv).

When BO or BA was used alone or when certain amount of ADP was replaced with BO or BA, Table 3.5 indicates that UL-94 ratings were kept, but there were no further improvements in the LOI values.

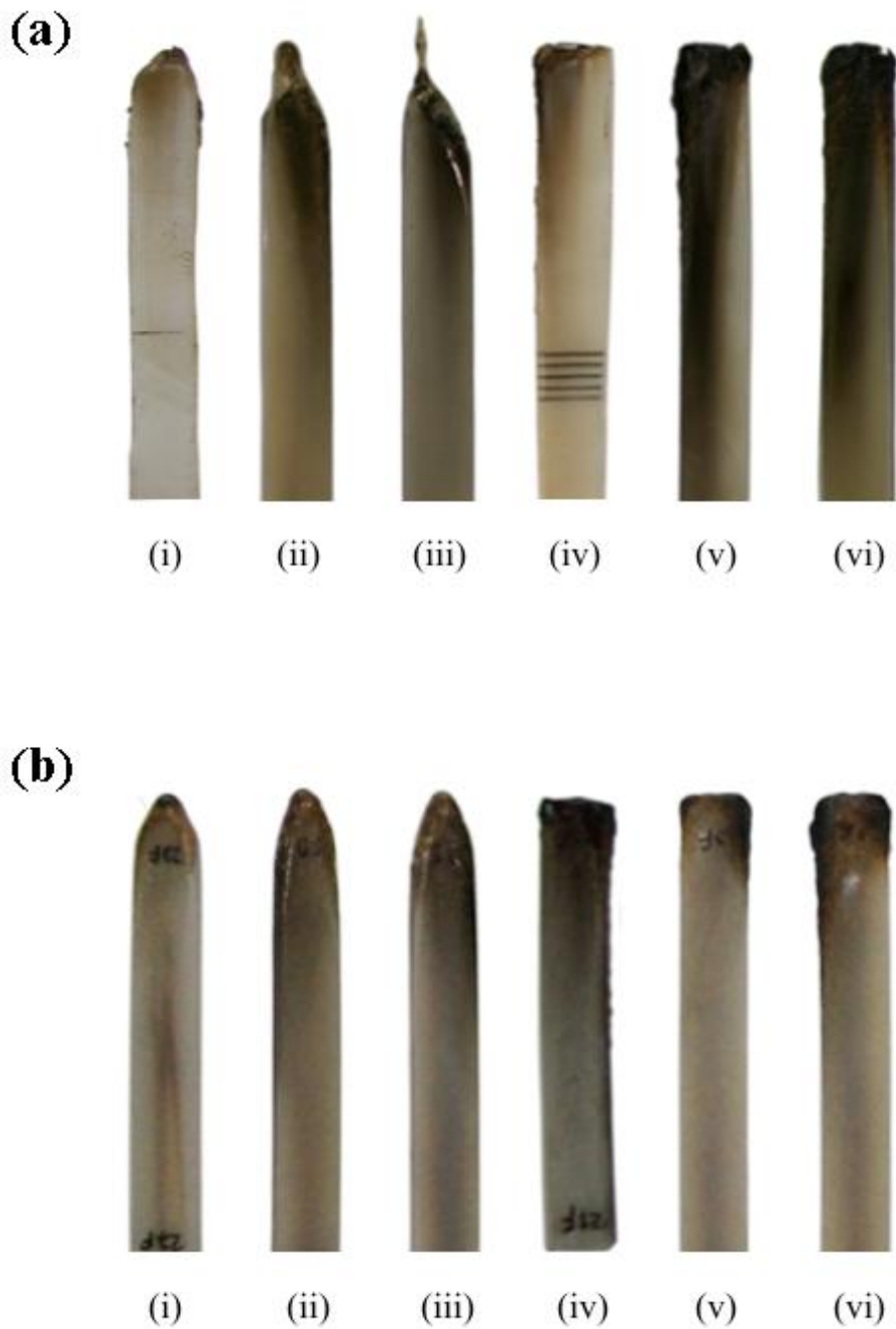


**Figure 3.15** Photographs of the Representative Specimens after UL-94 Test:  
**(a)** PA Based Materials: **(i)** PA, **(ii)** PA-BO 10, **(iii)** PA-BA 10, **(iv)** PA-ADP 20,  
**(v)** PA-ADP 15-BO 5, **(vi)** PA-ADP 15-BA 5  
**(b)** PA/GF Based Materials; **(i)** PA/GF, **(ii)** PA/GF-BO 10, **(iii)** PA/GF-BA 10,  
**(iv)** PA/GF-ADP 20, **(v)** PA/GF-ADP 15-BO 5, **(vi)** PA/GF-ADP 15-BA 5

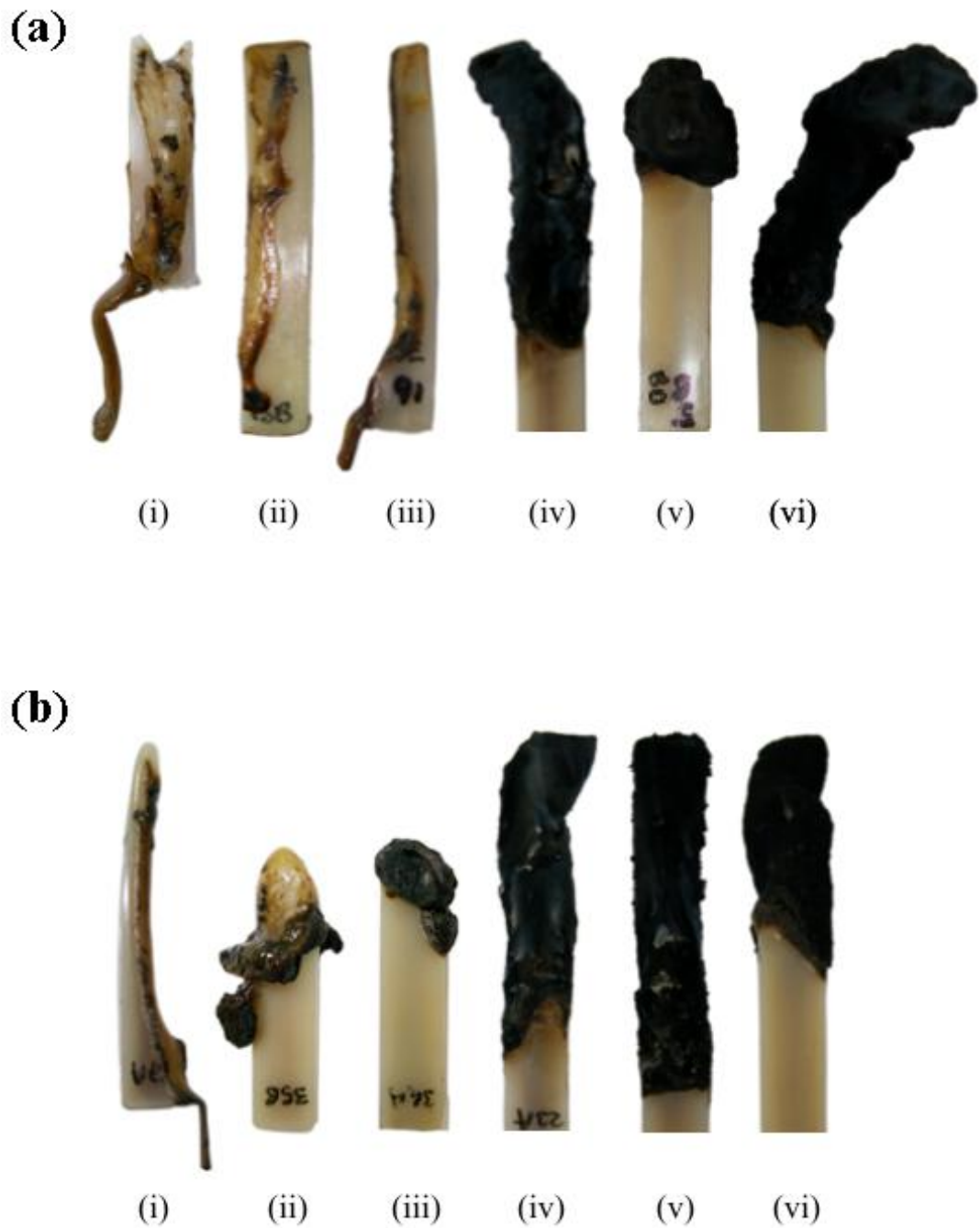


**Figure 3.16** Photographs of the Representative Specimens after LOI Test:  
**(a)** PA Based Materials: **(i)** PA, **(ii)** PA-BO 10, **(iii)** PA-BA 10, **(iv)** PA-ADP 20,  
**(v)** PA-ADP 15-BO 5, **(vi)** PA-ADP 15-BA 5  
**(b)** PA/GF Based Materials; **(i)** PA/GF, **(ii)** PA/GF-BO 10, **(iii)** PA/GF-BA 10,  
**(iv)** PA/GF-ADP 20, **(v)** PA/GF-ADP 15-BO 5, **(vi)** PA/GF-ADP 15-BA 5

**Table 3.5** Results of UL-94 and LOI Flammability Tests

<b>Specimens</b>	<b>UL-94 Rating<sup>a</sup></b>	<b>LOI<sup>b</sup> (%O<sub>2</sub>)</b>
PA	V-2	26.1
PA-BO 10	V-2	25.2
PA-BA 10	V-2	25.8
PA-ADP 20	V-0	32.7
PA-ADP 19-BO 1	V-0	32.1
PA-ADP 17-BO 3	V-0	29.3
PA-ADP 15-BO 5	V-0	28.6
PA-ADP 19-BA 1	V-0	31.5
PA-ADP 17-BA 3	V-0	32.1
PA-ADP 15-BA 5	V-0	30.1
PA/GF	V-2	23.3
PA/GF-BO 10	V-2	22.9
PA/GF-BA 10	V-2	23.1
PA/GF-ADP 20	V-0	30.7
PA/GF-ADP 17-BO 3	V-0	29.9
PA/GF-ADP 15-BO 5	V-0	28.4
PA/GF-ADP 17-BA 3	V-0	29.3
PA/GF-ADP 15-BA 5	V-0	28.1

<sup>a</sup>Rating of UL-94 standard, <sup>b</sup> Limiting oxygen index

### 3.2.2 SEM Analysis of LOI Chars

Burned tips of the representative LOI specimens were examined via SEM in order to compare their O<sub>2</sub>% values. Figures 3.17(i) and 3.18(i) show that specimens without flame retardants have very smooth surfaces with no charring. When 10 wt% BO or BA were added to the specimens, there were no charring, either (Figures 3.17(ii), (iii) and 3.18(ii), (iii)). Because, addition of BO or BA increase melt flow index of the specimen leading to dripping during burning.

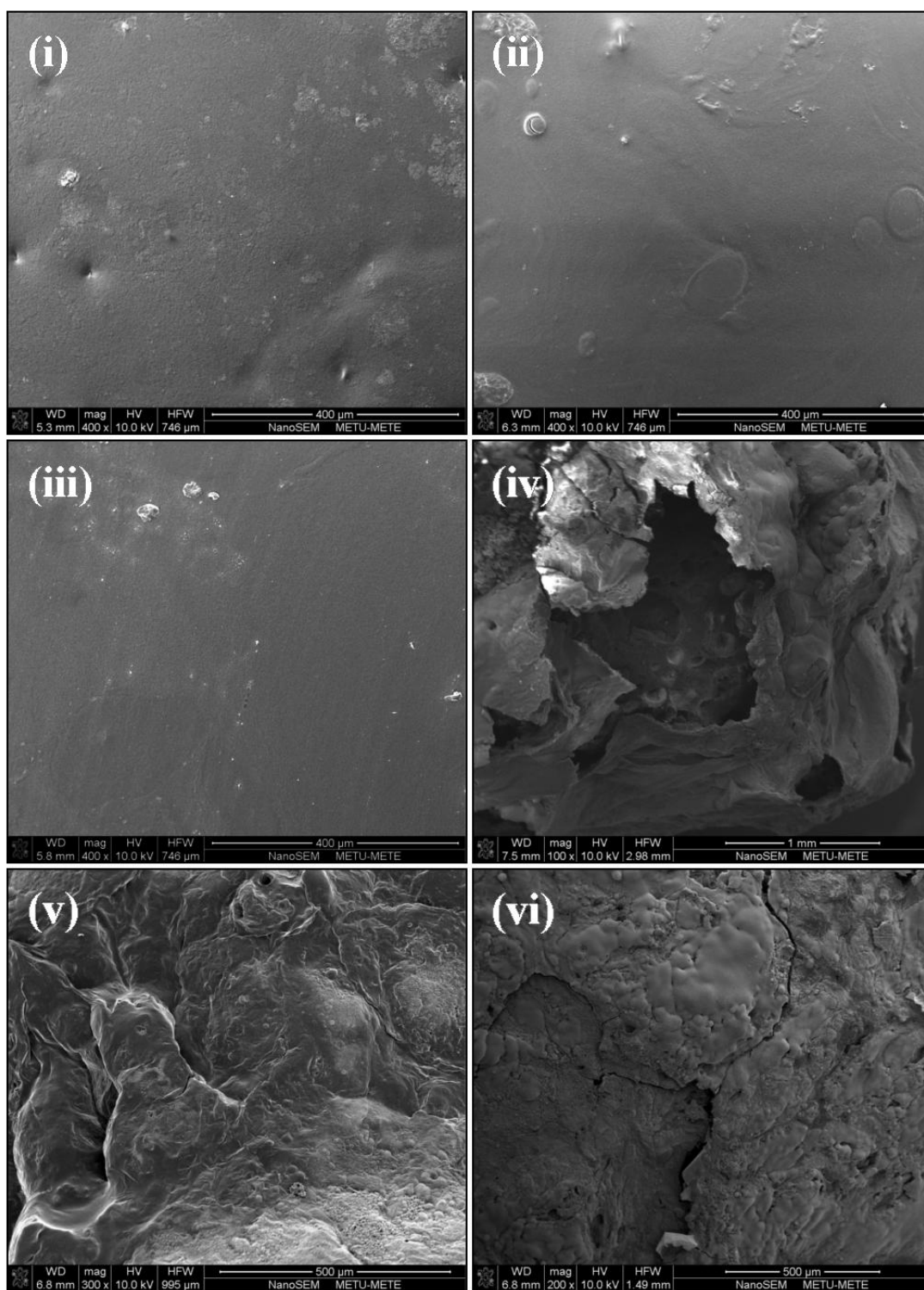


**Figure 3.17** SEM Images Showing Surface Char Barriers of the Representative PA Based Materials: **(i)** PA, **(ii)** PA-BO 10, **(iii)** PA-BA 10, **(iv)** PA-ADP 20, **(v)** PA-ADP 15-BO 5, **(vi)** PA-ADP 15-BA 5

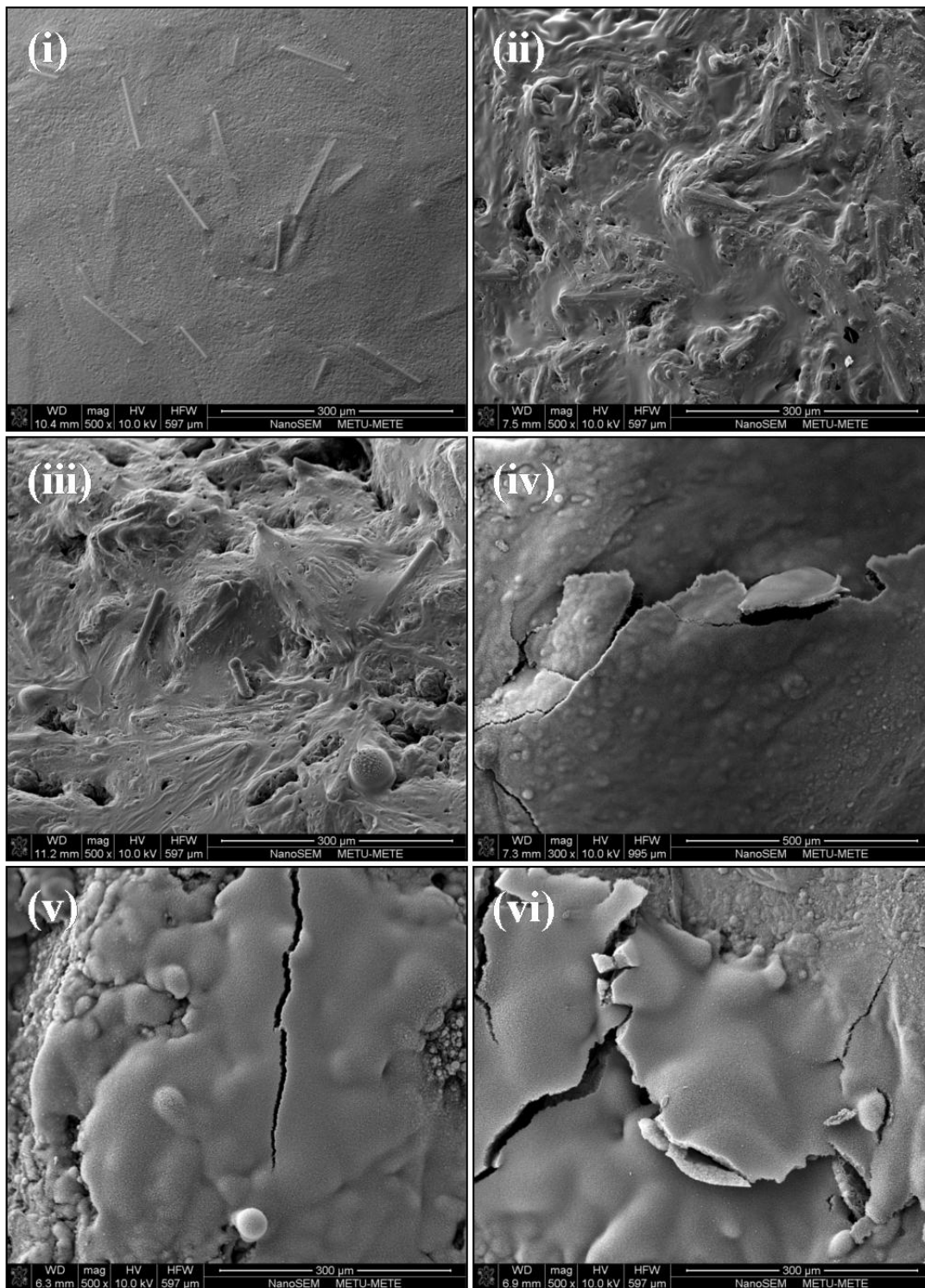


**Figure 3.18** SEM Images Showing Surface Char Barriers of the Representative PA/GF Based Materials: **(i)** PA/GF, **(ii)** PA/GF-BO 10, **(iii)** PA/GF-BA 10, **(iv)** PA/GF-ADP 20, **(v)** PA/GF-ADP 15-BO 5, **(vi)** PA/GF-ADP 15-BA 5

Figures 3.17(iv) and 3.18(iv) show that the use of 20 wt% ADP leads to formation of certain level of char layers on the surface of the specimens increasing their LOI values significantly. When certain amount of ADP was replaced with BO or BA (Figures 3.17(v), (vi) and 3.18(v), (vi)), there were slight contributions to the char formation; however, this was not sufficient to further increase LOI values.

### 3.2.3 Mass Loss Cone Calorimetry Analysis

Mass loss cone calorimetry (MLC) was conducted to measure fire performances of all specimens. After the test, first, visual examination of the remaining char structures were done as given in Figures 3.19 and 3.20. These figures simply show that the char yield increases after incorporation of ADP, BO and BA. Then, the most significant plots, i.e. heat release rate (HRR) and mass loss rate (MLR) curves were plotted (Figures 3.21 and 3.22). Finally, all the important fire performance parameters were determined and tabulated in Table 3.6.

Figures 3.21 and 3.22 indicated that HRR and MLR curves of both PA and PA/GF were suppressed after adding 10 wt% BO or BA alone, or 20 wt% ADP alone. Figure 3.21 also shows that when certain amount of ADP was replaced by BO or BA, i.e. when ADP and BO or BA were used together, the suppressions were much more significant in the PA based materials; but, as shown in Figure 3.22, this was not the case for the PA/GF based materials.

For instance, Table 3.6 shows that, when 10 wt% BO alone were added, the suppression in the “peak heat release rate” (PHRR) values of PA and PA/GF were 30% and 42%, respectively, when 10 wt% BA alone were added suppressions were 22% and 50%, respectively. PHRR suppressions in each group were 32% and 75%, respectively, when 20 wt% ADP alone was added. On the other hand, when certain amount of ADP was replaced with BO or BA in the PA based materials, there were more significant suppressions, e.g. when 17 wt% ADP and 3 wt% BO were used

together, the suppression in PHRR values could be as much as 84%, while this suppression was as much as 86% when 17 wt% ADP and 3 wt% BA were used together. Note that, the trend in the suppression of the total heat evolved (THE) values were almost the same, for the PA based materials. Unfortunately, for the PA/GF based materials, due to the high efficiency of glass fibers, replacement of ADP with BO or BA resulted in no further suppressions in PHRR and THE values.

In terms of time related MLC parameters, Table 3.6 indicates that in each group use of BO, BA or ADP alone or together resulted in no significant delays in “time to ignition” (TTI) periods, or “time to peak heat release rate” (TPHRR) periods. However, there were significant time extensions in the values of “total burning time” (TBT). Table 3.6 shows that, when BO and ADP or BA and ADP were used together, TBT periods of PA and PA/GF could be extended more than two times.

In order to have additional data about the contribution of material to the fire propagation rate, two different indices can be calculated from the MLC parameters. The first index is called “fire growth index” (FGI) which is the ratio of PHRR/TTI, the second one is named as “fire growth rate index” (FIGRA) which is the ratio of PHRR/TPHRR. Use of any flame retardant decreases these indices, i.e. decreases fire propagation rate. Table 3.6 shows that use of BO and ADP or BA and ADP together decreased values of these two indices considerably especially for the PA based materials.

The ratio of THE/TML (total heat evolved/total mass loss) and % char yield data might give information about the flame retardancy mechanism of the specimens. Table 3.6 reveals that the value of THE/TML ratio decreased when ADP was incorporated. This means, ADP might basically act in the gaseous phase mechanisms. On the other hand, Table 3.6 shows that again especially in the PA based materials, use of BO or BA increases % char residue considerably, indicating the effectiveness of condensed phase physical char formation.

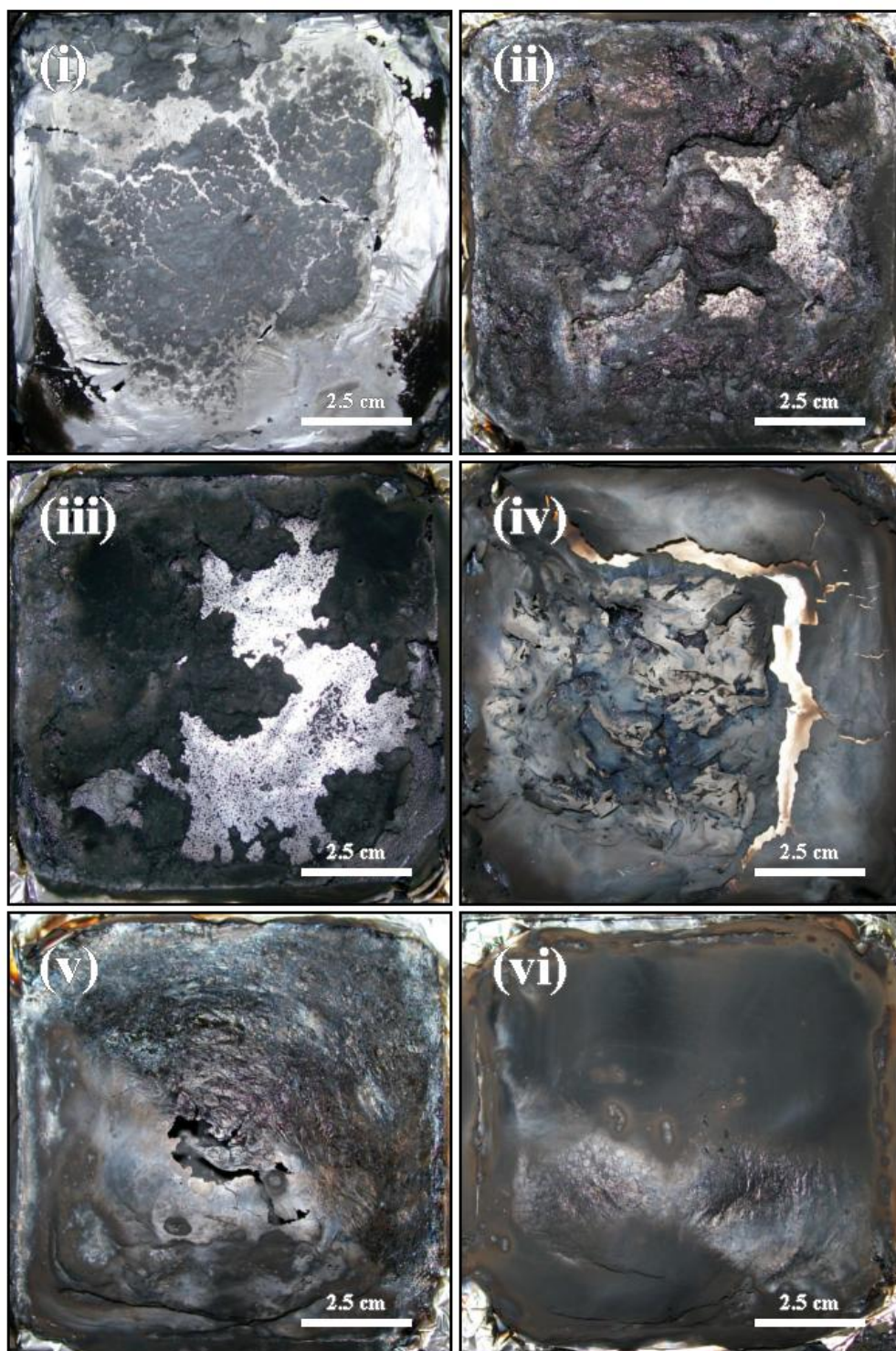


**Figure 3.19** Photographs of the Remaining Char Structure of MLC Specimens of the Representative PA Based Materials: (i) PA, (ii) PA-BO 10, (iii) PA-BA 10, (iv) PA-ADP 20, (v) PA-ADP 15-BO 5, (vi) PA-ADP 15-BA 5

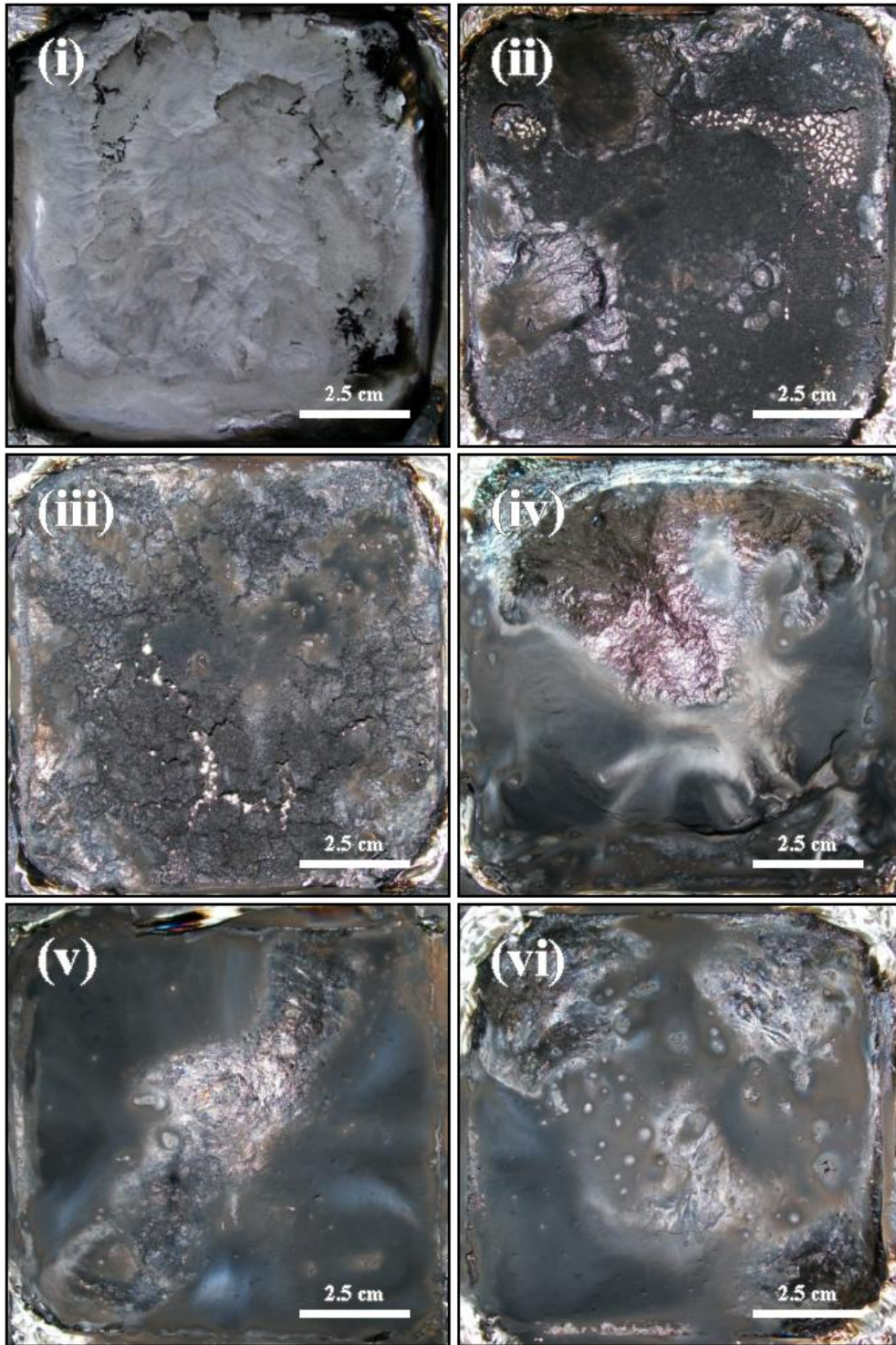


**Figure 3.20** Photographs of the Remaining Char Structure of MLC Specimens of the Representative PA/GF Based Materials: (i) PA/GF, (ii) PA/GF-BO 10, (iii) PA/GF-BA 10, (iv) PA/GF-ADP 20, (v) PA/GF-ADP 15-BO 5, (vi) PA/GF-ADP 15-BA 5

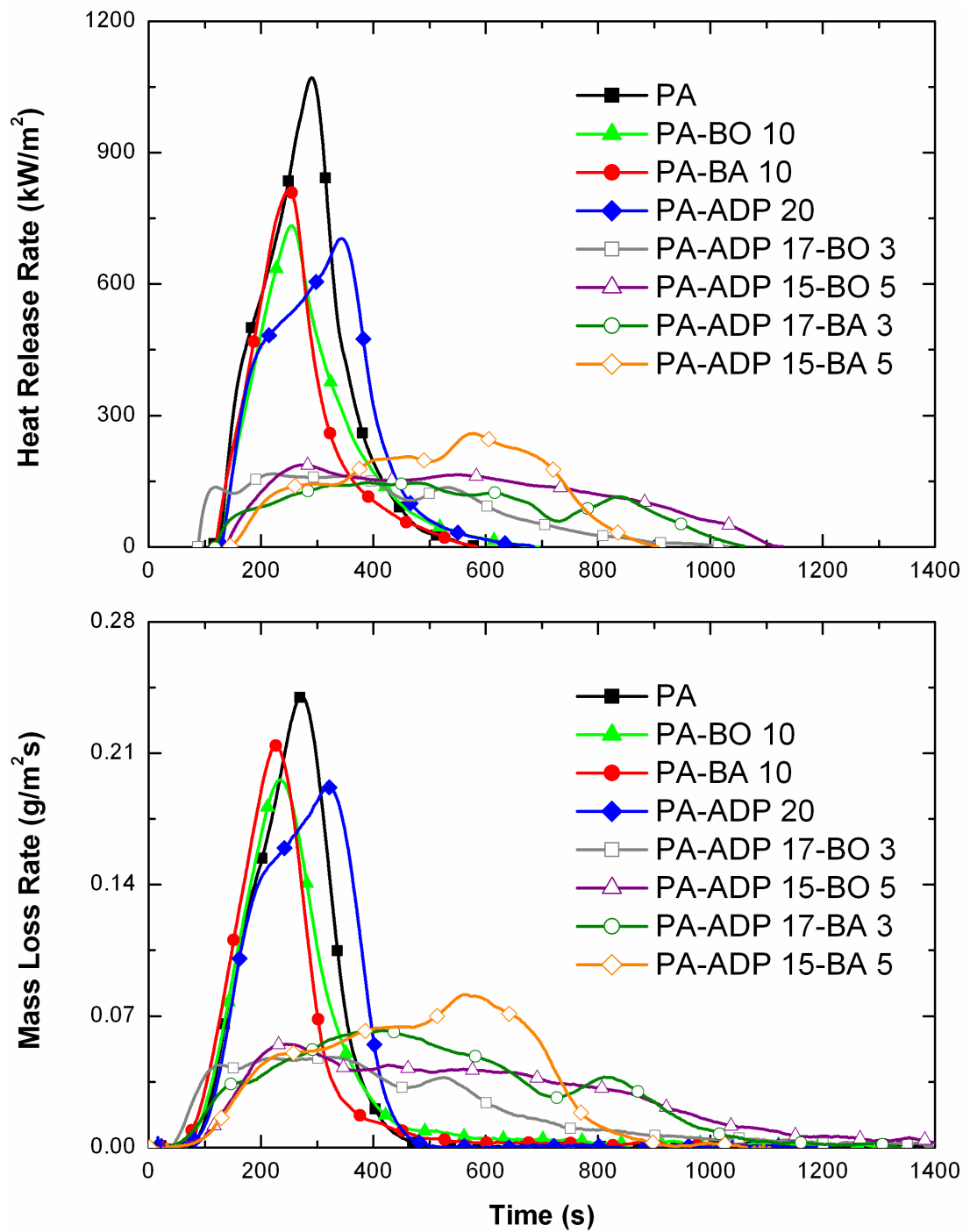


**Figure 3.21** Heat Release Rate and Mass Loss Rate Curves for the PA Based Materials

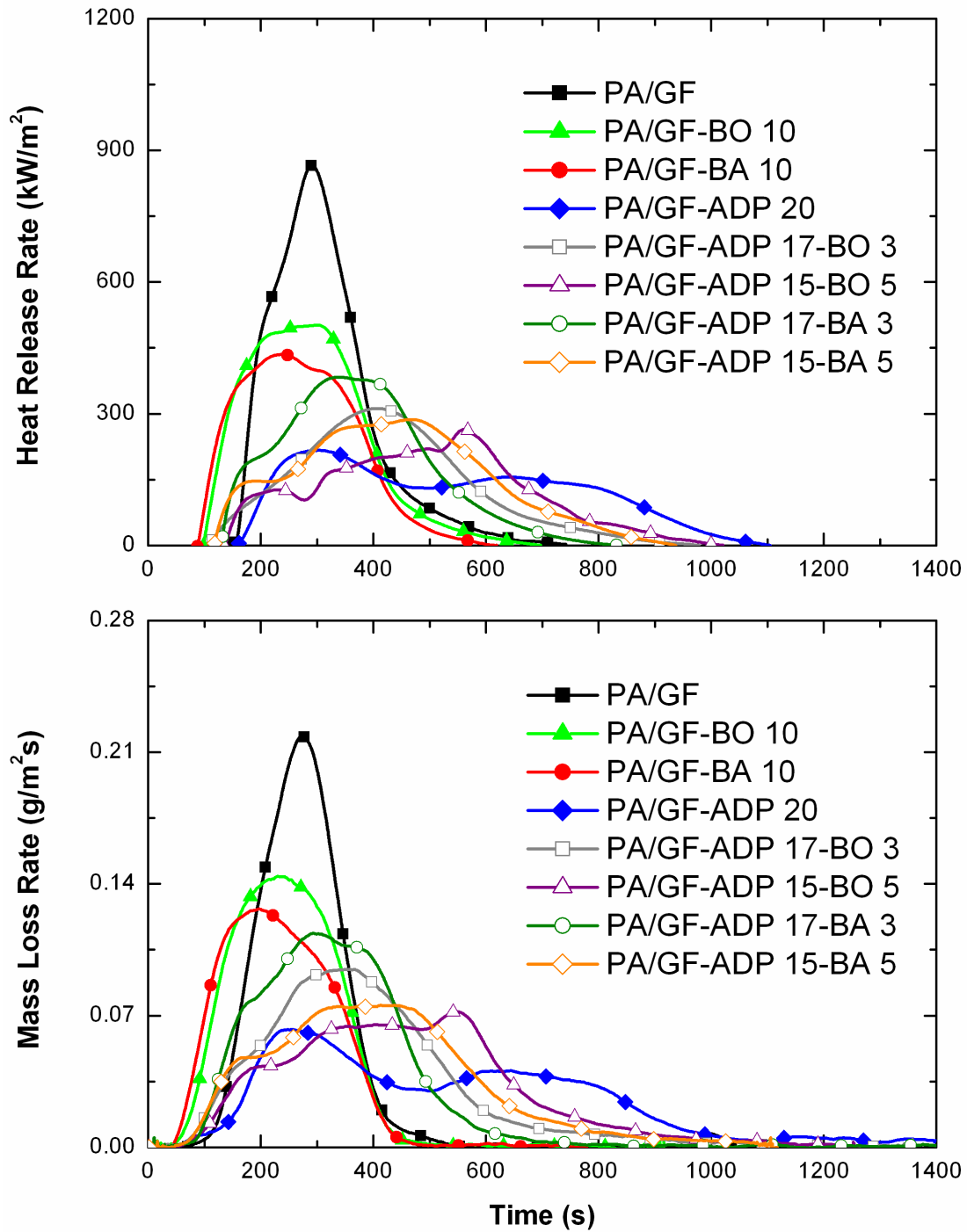


**Figure 3.22** Heat Release Rate and Mass Loss Rate Curves for the PA/GF Based Materials

**Table 3.6** Mass Loss Cone Calorimeter Parameters of the Specimens

Specimens	PHRR <sup>a</sup> (kW/m <sup>2</sup> )	THE <sup>b</sup> (MJ/m <sup>2</sup> )	TTI <sup>c</sup> (s)	TPHRR <sup>d</sup> (s)	TBT <sup>e</sup> (s)	FGI <sup>f</sup> (kW/m <sup>2</sup> .s)	FIGRA <sup>g</sup> (kW/m <sup>2</sup> .s)	THE/TML <sup>h</sup> (MJ/m <sup>2</sup> .g)	Char Yield (%)
PA	1055	171	96	302	437	11.0	3.5	4.2	0.2
PA-BO 10	738	125	105	254	1272	7.0	2.9	3.4	10.8
PA-BA 10	819	118	92	256	1009	8.9	3.2	3.4	7.3
PA-ADP 20	716	151	108	350	477	6.6	2.0	3.5	2.3
PA-ADP 19-BO 1	413	143	92	458	1044	4.5	0.9	3.5	7.4
PA-ADP 17-BO 3	168	84	67	200	1372	2.5	0.8	3.0	14.2
PA-ADP 15-BO 5	193	120	95	277	1085	2.0	0.7	3.2	14.6
PA-ADP 19-BA 1	446	124	106	359	805	4.2	1.2	3.0	6.1
PA-ADP 17-BA 3	148	92	88	383	1338	1.7	0.4	2.3	11.0
PA-ADP 15-BA 5	263	113	96	578	914	2.7	0.5	2.9	9.9

<sup>a</sup> PHRR: peak heat release rate

<sup>b</sup> THE: total heat evolved

<sup>c</sup> TTI: time to ignition

<sup>d</sup> TPHRR: time to peak heat release rate

<sup>e</sup> TBT: total burning time

<sup>f</sup> FGI: fire growth index, where FGI=PHRR/TTI

<sup>g</sup> FIGRA: fire growth index rate, where FIGRA=PHRR/TPHRR

<sup>h</sup> THE/TML: ratio of total heat evolved/total mass loss

**Table 3.6** Mass Loss Cone Calorimeter Parameters of the Specimens Continued

Specimens	PHRR <sup>a</sup> (kW/m <sup>2</sup> )	THE <sup>b</sup> (MJ/m <sup>2</sup> )	TTI <sup>c</sup> (s)	TPHRR <sup>d</sup> (s)	TBT <sup>e</sup> (s)	FGI <sup>f</sup> (kW/m <sup>2</sup> .s)	FIGRA <sup>g</sup> (kW/m <sup>2</sup> .s)	THE/TML <sup>h</sup> (MJ/m <sup>2</sup> .g)	Char Yield (%)
PA/GF	868	159	108	291	563	8.0	3.0	4.1	15.0
PA/GF-BO 10	507	135	70	299	568	7.2	1.7	3.8	19.3
PA/GF-BA 10	437	117	56	241	455	7.8	1.8	3.5	18.9
PA/GF-ADP 20	219	114	112	326	1354	2.0	0.7	3.4	31.3
PA/GF-ADP 17-BO 3	312	111	91	396	1102	3.4	0.8	3.1	24.6
PA/GF-ADP 15-BO 5	264	108	108	552	1089	2.4	0.5	3.0	25.6
PA/GF-ADP 17-BA 3	384	124	102	321	794	3.8	1.2	3.3	22.1
PA/GF-ADP 15-BA 5	292	123	95	475	992	3.1	0.6	3.5	26.3

<sup>a</sup> PHRR: peak heat release rate

<sup>b</sup> THE: total heat evolved

<sup>c</sup> TTI: time to ignition

<sup>d</sup> TPHRR: time to peak heat release rate

<sup>e</sup> TBT: total burning time

<sup>f</sup> FGI: fire growth index, where FGI=PHRR/TTI

<sup>g</sup> FIGRA: fire growth index rate, where FIGRA=PHRR/TPHRR

<sup>h</sup> THE/TML: ratio of total heat evolved/total mass loss

### 3.2.4 Flame Retardancy Mechanisms

As discussed in Section 3.1.4 before, flame retardancy mechanism of ADP may be in the “condensed” and “gaseous” phase. When ADP was vaporized during fire, it might get oxidized to  $\text{HPO}_2\bullet$ ,  $\text{PO}\bullet$ ,  $\text{PO}_2\bullet$ , and  $\text{HPO}\bullet$  radicals which would scavenge very harmful  $\text{H}\bullet$  and  $\text{OH}\bullet$  hot radicals. This gaseous phase action is called “flame inhibition”. When ADP was oxidized to phosphoric acid during fire, it might lead to formation of two-layer protective barrier; a carbon based char and an inorganic residue layer of aluminum phosphate. This condensed phase action is called as the “barrier effect”.

Due to the extremely limited number of literature in any polymeric matrix material, flame retardancy mechanism of BO and BA are not well-established. As discussed by Ibibikcan and Kaynak [40], the main mechanism of BO is “condensed” phase barrier formation, while for BA, barrier mechanism could be both in the “condensed” and “gaseous” phase.

During fire, BO softens around  $350^\circ\text{C}$  and flows above  $450^\circ\text{C}$  forming a protective vitreous glassy layer thereby insulating the underlying material from heat and oxygen.

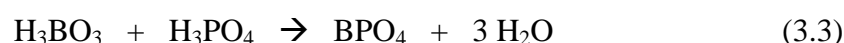
On the other hand, BA releases water at around  $150^\circ\text{C}$  and produces metaboric acid according to the Reaction 3.1, and then another water release takes place at around  $265^\circ\text{C}$ , this time with the formation of BO (Reaction 3.2);



Thus, these two-steps endothermic dehydration reactions of BA will absorb the heat of combustion, and the released water vapor will dilute the oxygen and the gaseous flammable compounds during fire. This mechanism could be considered as the

“gas phase barrier” action. Of course, BO formed after Reaction 3.2 would contribute as the “condensed phase barrier” action.

When ADP was used together with BO and BA, all these mechanisms discussed above would cooperate. Moreover, there could be an additional physical char layer contribution when BA and ADP were used together. Because, according to the Reaction 3.3;



BA could react with phosphoric acid (a combustion byproduct of ADP) to form boron phosphate, i.e. an additional inorganic barrier layer.

Of course, another contribution to the condensed phase barrier mechanism would take place by the short glass fibers used in the PA/GF based specimens which would increase the effectiveness of char barriers via reinforcing or stabilizing their structure. In this PA/GF group, since effectiveness of fiber reinforcement were very high, additional contribution of BO and BA were not observed.

In order to clarify these flame retardancy mechanisms further, three additional analyses (thermogravimetric analysis, X-ray diffraction and evolved gas analysis) were conducted and discussed in the following sections.

### **3.2.5 Thermogravimetric Analysis**

Since results of each group were very similar, thermogravimetric (TG) and differential thermogravimetric (DTG) curves are given in Figure 3.23 only for the representative PA based materials, while the thermal degradation parameters derived from these curves are tabulated in Table 3.7 for neat BO, BA, ADP and the representative specimens of both PA and PA/GF based materials.

These curves showed that neat PA decomposes in one step with maximum mass loss rate at around 460°C leaving very little residue. On the contrary, due to the 15 wt% glass fiber reinforcements, PA/GF specimen formed considerable amount of residue. It is known that during decomposition, polyamide-6 releases water, ammonia, carbon monoxide, carbon dioxide, and certain hydrocarbon fragments.

Figure 3.23 shows that when BO, BA and ADP were added, TG and DTG curves shift slightly to lower temperatures. Therefore, Table 3.7 reveals that, not only maximum mass loss rate temperatures ( $T_{DTG\text{-peak}}$ ), but also 10 wt% and 50 wt% degradation temperatures ( $T_{10\text{ wt\%}}$  and  $T_{50\text{ wt\%}}$ ) of the PA and PA/GF specimens were lowered.

On the other hand, Table 3.7 also indicates that addition of BO or BA increases amount of residue significantly, for instance, use of 10 wt% BO leads to more than 12 wt% residue, while use of 10 wt% BA lead to more than 8 wt% residue. It is seen than use of ADP also resulted in residue formation considerably. Thus, TG analysis supported the physical barrier formation mechanisms of BO, BA and ADP discussed in the previous section.

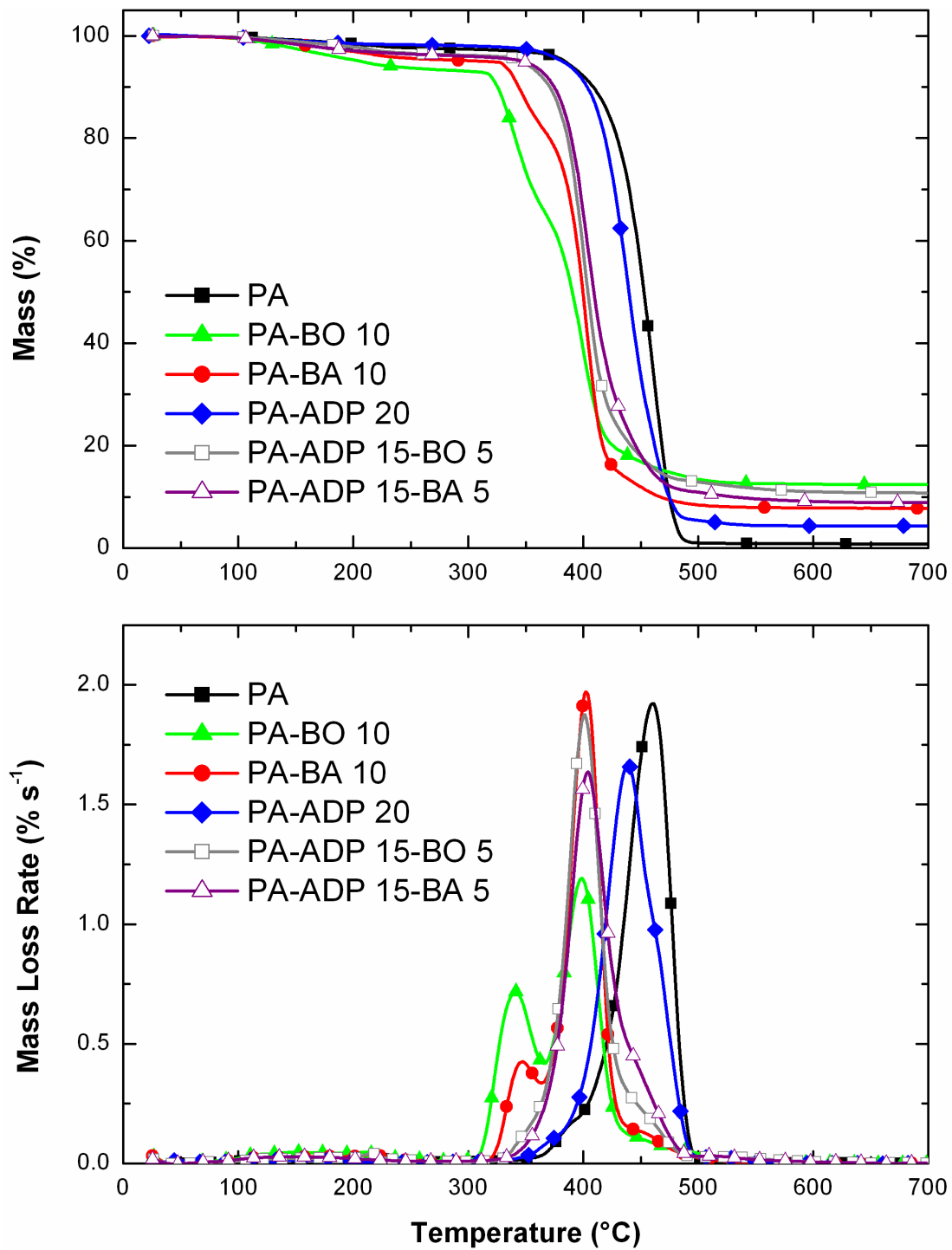


**Figure 3.23** Thermogravimetric (TG) and Differential Thermogravimetric (DTG) Curves for the Representative PA Based Materials

**Table 3.7** Thermal Degradation Parameters of the Representative Specimens Determined from TG and DTG Curves

Specimens	T <sub>DTG-Peak 1</sub> <sup>a</sup> (°C)	T <sub>DTG-Peak 2</sub> <sup>b</sup> (°C)	T <sub>10 wt%</sub> <sup>c</sup> (°C)	T <sub>50 wt%</sub> <sup>d</sup> (°C)	% Residue at 600 °C
BO	106	161	182	-	81.1
BA	153	213	137	-	55.9
ADP	-	496	459	494	15.8
PA	-	460	408	452	0.9
PA-BO 10	334	392	326	391	12.5
PA-BA 10	341	397	346	400	7.9
PA-ADP 20	-	436	404	439	4.4
PA-ADP 15-BO 5	210	395	370	404	11.0
PA-ADP 15-BA 5	-	399	374	409	9.1
PA/GF	-	465	416	455	14.8
PA/GF-BO 10	349	402	372	407	22.3
PA/GF-BA 10	338	402	349	405	19.7
PA/GF-ADP 20	-	430	395	436	18.2
PA/GF-ADP 15-BO 5	-	396	376	410	25.5
PA/GF-ADP 15-BA 5	101	397	368	409	23.9

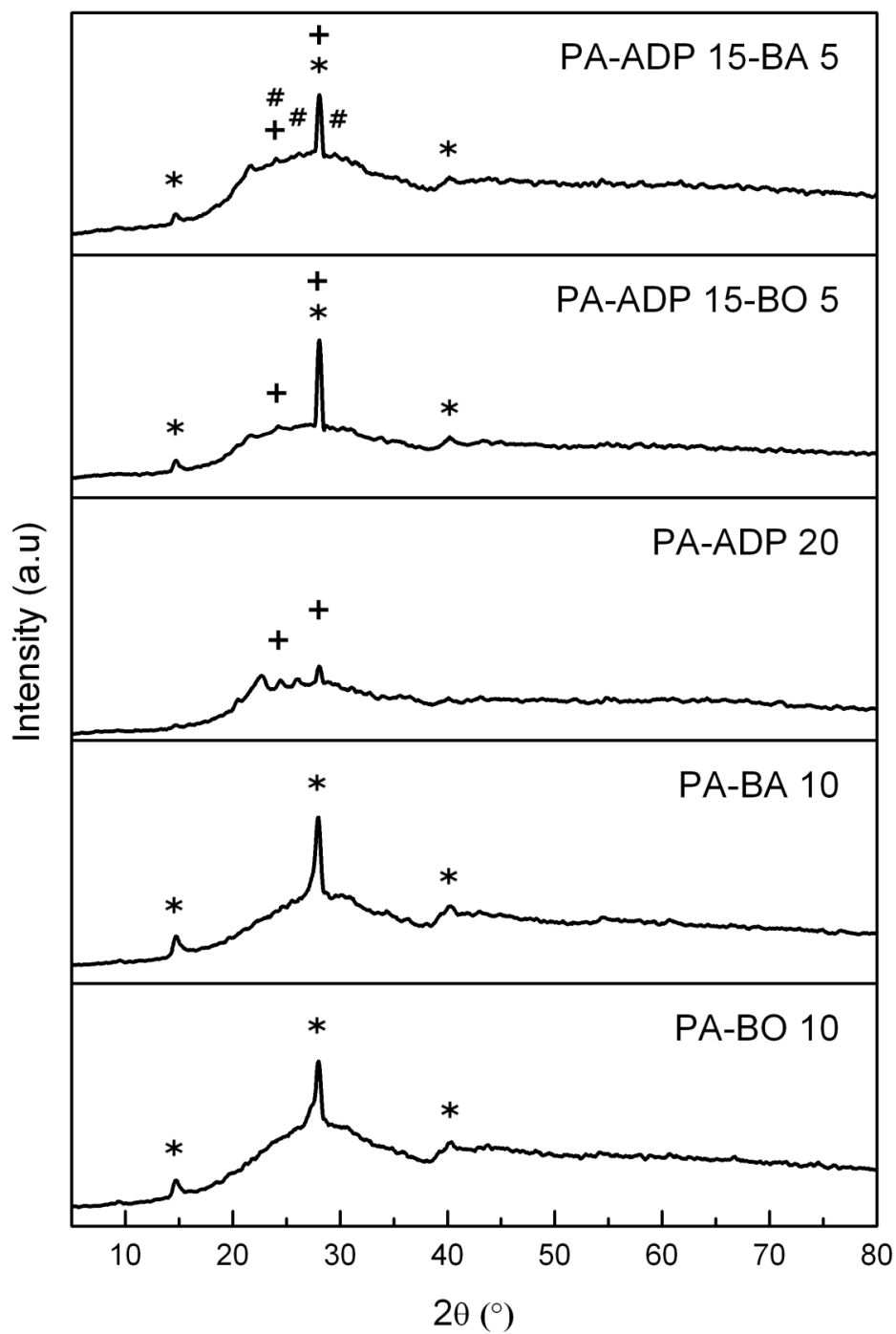
<sup>a</sup> T<sub>DTG-Peak 1</sub>: first peak temperature in DTG curve<sup>b</sup> T<sub>DTG-Peak 2</sub>: second peak temperature in DTG curve<sup>c</sup> T<sub>10 wt%</sub>: thermal degradation temperature for 10% mass loss<sup>d</sup> T<sub>50 wt%</sub>: thermal degradation temperature for 50% mass loss

### 3.2.6 XRD Analysis of MLC Residues

In order to reveal crystal structure of the phases in the char layers, XRD analyses were conducted on the MLC chars of representative specimens of each group. Since results of each group were very similar, XRD diffractograms are provided in Figure 3.24 only for the PA based materials.

Figure 3.24 shows that when BO or BA was added alone, their only decomposition product boron oxide ( $B_2O_3$ ) peaks were seen. When ADP was used alone, peaks of its main decomposition phase, i.e. peaks of aluminum phosphate ( $AlPO_4$ ) were seen. When BO and ADP were added together, no additional peaks were observed. But, when BA and ADP were used together, apart from their decomposition phases, additional peaks for boron phosphate ( $BPO_4$ ) could be observed.

Thus, it can be stated that, apart from the expected decomposition byproducts, no other phases were formed in the chars of the MLC specimens. This could be interpreted as another confirmation of the physical barrier mechanism of especially BO and BA, and also partly for ADP.



\* : Boron oxide  $B_2O_3$ , Card no: 6-0297  
 + : Aluminum phosphate  $AlPO_4$ , Card no: 46-0695  
 # : Boron phosphate  $BPO_4$ , Card no: 11-0237, 12-0380, 34-0132

**Figure 3.24** XRD Patterns of the MLC Residues of the Representative PA Based Materials

### 3.2.7 Evolved Gas Analysis

In order to support gas phase action of the flame retardants, volatile decomposition products of the representative specimens of each group were examined using a TGA-FTIR coupled system. Since results of each group were very similar, evolved gas analysis spectra are given in Figure 3.25 only for the PA based materials.

As discussed in Section 3.1.7 before, Figure 3.25 shows that spectrum of neat PA specimen at 45 min exhibited characteristic bands of ammonia (N-H bending at 965 and 931  $\text{cm}^{-1}$ ), carbon dioxide (C=O stretching at 2356  $\text{cm}^{-1}$  and C=O bending at 667  $\text{cm}^{-1}$ ),  $\epsilon$ -caprolactam (C=O stretching at 1711  $\text{cm}^{-1}$  and C-N stretching at 1358  $\text{cm}^{-1}$ ), hydrocarbons (C-H stretching at 2938  $\text{cm}^{-1}$  and C-H bending at 1455  $\text{cm}^{-1}$ ), water (H-O-H bending at 1499  $\text{cm}^{-1}$ ).

When BO or BA was used alone, it was seen in the spectrum of PA-BO 10 at 38 min and PA-BA 10 at 37 min that these were no additional contribution of BO or BA decomposition.

On the other hand, as also stated in Section 3.1.7, PA-ADP 20 spectrum at 42 min exhibited additional characteristic bands of  $\text{PO}_2^-$  anion (1158 and 1085  $\text{cm}^{-1}$ ), P-O-P stretching (851  $\text{cm}^{-1}$ ) and P=O stretching (1264 and 1237  $\text{cm}^{-1}$ ). These volatile products could be interpreted as the confirmation of gas phase flame inhibition mechanism of ADP.

Since the use of BO and ADP or BA and ADP together result in no additional gas phase mechanism, spectrum of PA-ADP 15-BO 5 or PA-ADP 15-BA 5 specimens exhibited no additional bands.

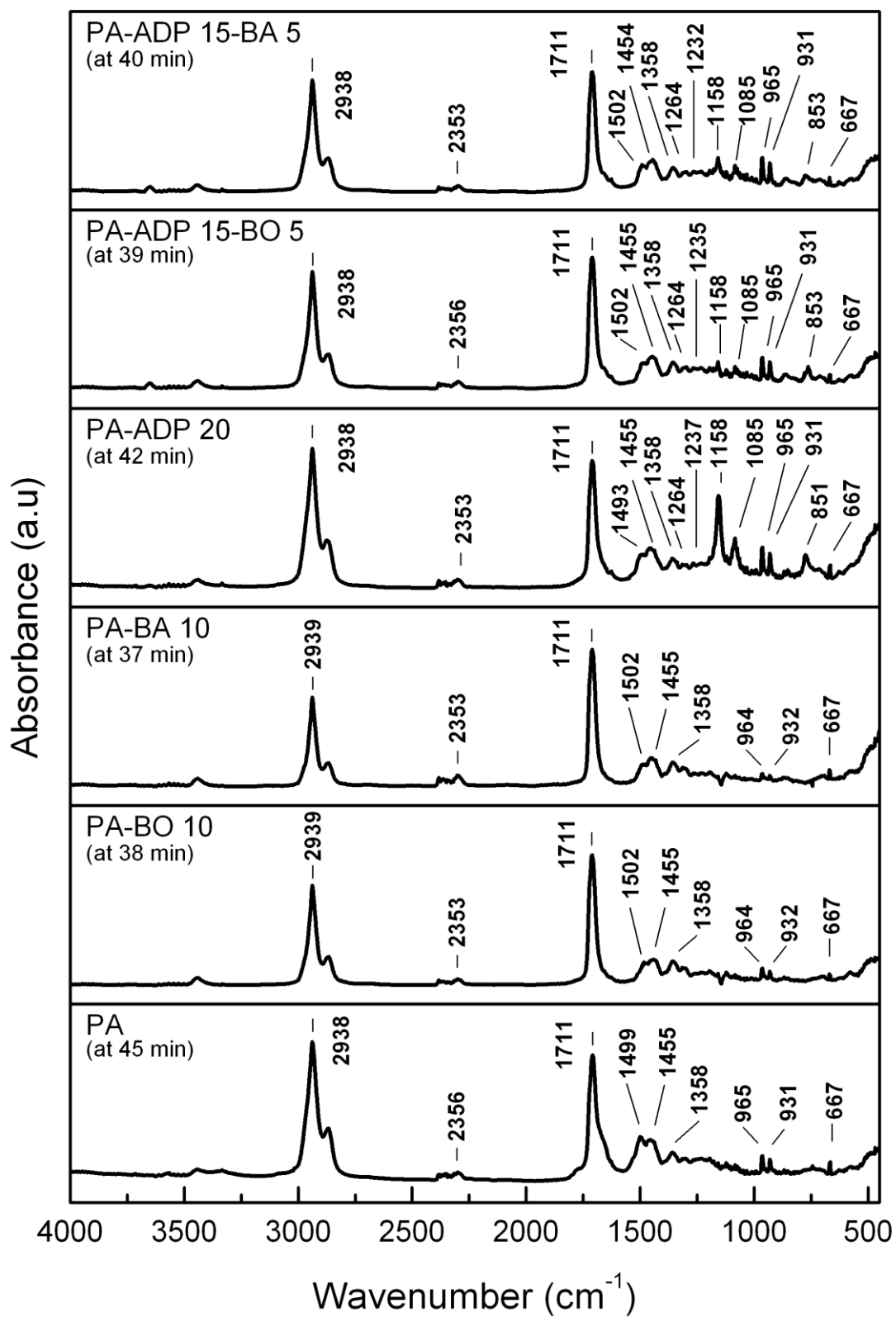


**Figure 3.25** Evolved Gas Analysis Spectra of the Representative PA Based Materials

### 3.2.8 Tensile Testing for Mechanical Properties

In order to observe influences of BO, BA and ADP on the mechanical performance of all the studied specimens, a minimum of five samples for each formulation were subjected to tension tests. Figure 3.26 shows tensile stress-strain behavior of the specimens, while Table 3.8 gives determined mechanical properties.

Figure 3.26 and Table 3.8 shows that use of each of BO, BA, and ADP alone, or in combinations of ADP-BO or ADP-BA, all increases elastic modulus of both base materials PA and PA/GF significantly. For example use of 10 wt% BO increases modulus of PA by 57%; use of 15 wt% ADP with 5 wt% BA increases modulus of PA/GF by 37%. These increases should be due to the decreased chain mobility of the PA matrix by rigid inorganic structures of BO and BA and organometallic structure of ADP particles. Consequently, decreased chain mobility also resulted in significant reduction in the ductility levels, i.e. % elongation at break values of the matrix.

As discussed in Section 3.1.8 before, when 15 wt% short glass fiber reinforcements were filled, not only elastic modulus but also strength values increased significantly. Compared to PA, these increases in the specimen of PA/GF were 64% for Young's modulus and 34% for tensile strength. Of course, the reason for these improvements is the well known composite strengthening mechanism, i.e. very effective load transfer from the matrix to the silane sized fiber reinforcements.

Table 3.8 shows that, use of BO, BA and ADP, alone or together, all resulted in substantial decreases in the tensile strength values. These decreases should be especially due to the lowered efficiency of load transfer mechanism from the matrix to non-surface treated particles of BO, BA, or ADP, having very low aspect ratio either.

Fracture surfaces of the tensile test specimens were also examined via SEM in order to reveal morphology of the fracture surfaces and distribution of the flame retardants.

Figures 3.27 and 3.28 show that very smooth fracture surfaces of PA and PA/GF specimens transformed into rather rough morphology when ADP was incorporated leading to lower reductions in the strength and ductility values compared to the higher reductions of BO or BA. These figures also indicate that all flame retardants (i.e. BO, BA and ADP) were distributed rather uniformly; but, their interfacial interactions with the PA matrix were very limited basically due to their untreated surface.

**Table 3.8** Tensile Mechanical Properties of the Specimens

<b>Specimens</b>	<b>Young's Modulus (GPa)</b>	<b>Tensile Strength (MPa)</b>	<b>Elongation at break (%)</b>
PA	1.96 ± 0.08	54.2 ± 0.7	58.3 ± 3.5
PA-BO 10	3.08 ± 0.05	28.0 ± 2.7	1.2 ± 0.1
PA-BA 10	2.75 ± 0.09	36.7 ± 3.2	2.2 ± 0.3
PA-ADP 20	2.43 ± 0.17	46.6 ± 0.3	9.0 ± 0.4
PA-ADP 19-BO 1	2.61 ± 0.04	44.8 ± 0.5	4.7 ± 0.1
PA-ADP 17-BO 3	2.90 ± 0.07	43.8 ± 2.6	2.6 ± 0.1
PA-ADP 15-BO 5	2.88 ± 0.04	23.9 ± 2.0	1.4 ± 0.1
PA-ADP 19-BA 1	2.55 ± 0.05	44.9 ± 0.5	7.7 ± 1.6
PA-ADP 17-BA 3	2.80 ± 0.04	46.8 ± 2.7	3.1 ± 0.4
PA-ADP 15-BA 5	2.69 ± 0.14	44.2 ± 5.0	2.9 ± 0.4
PA/GF	3.22 ± 0.04	72.5 ± 0.6	8.8 ± 0.4
PA/GF-BO 10	3.89 ± 0.10	44.3 ± 2.2	1.6 ± 0.2
PA/GF-BA 10	4.20 ± 0.02	34.6 ± 1.9	1.1 ± 0.1
PA/GF-ADP 20	3.46 ± 0.08	57.7 ± 0.3	5.1 ± 0.1
PA/GF-ADP 17-BO 3	4.39 ± 0.08	54.6 ± 2.6	1.9 ± 0.2
PA/GF-ADP 15-BO 5	4.47 ± 0.10	43.0 ± 3.2	1.3 ± 0.1
PA/GF-ADP 17-BA 3	4.29 ± 0.06	62.2 ± 1.8	2.8 ± 0.3
PA/GF-ADP 15-BA 5	4.40 ± 0.05	55.1 ± 1.0	2.0 ± 0.1

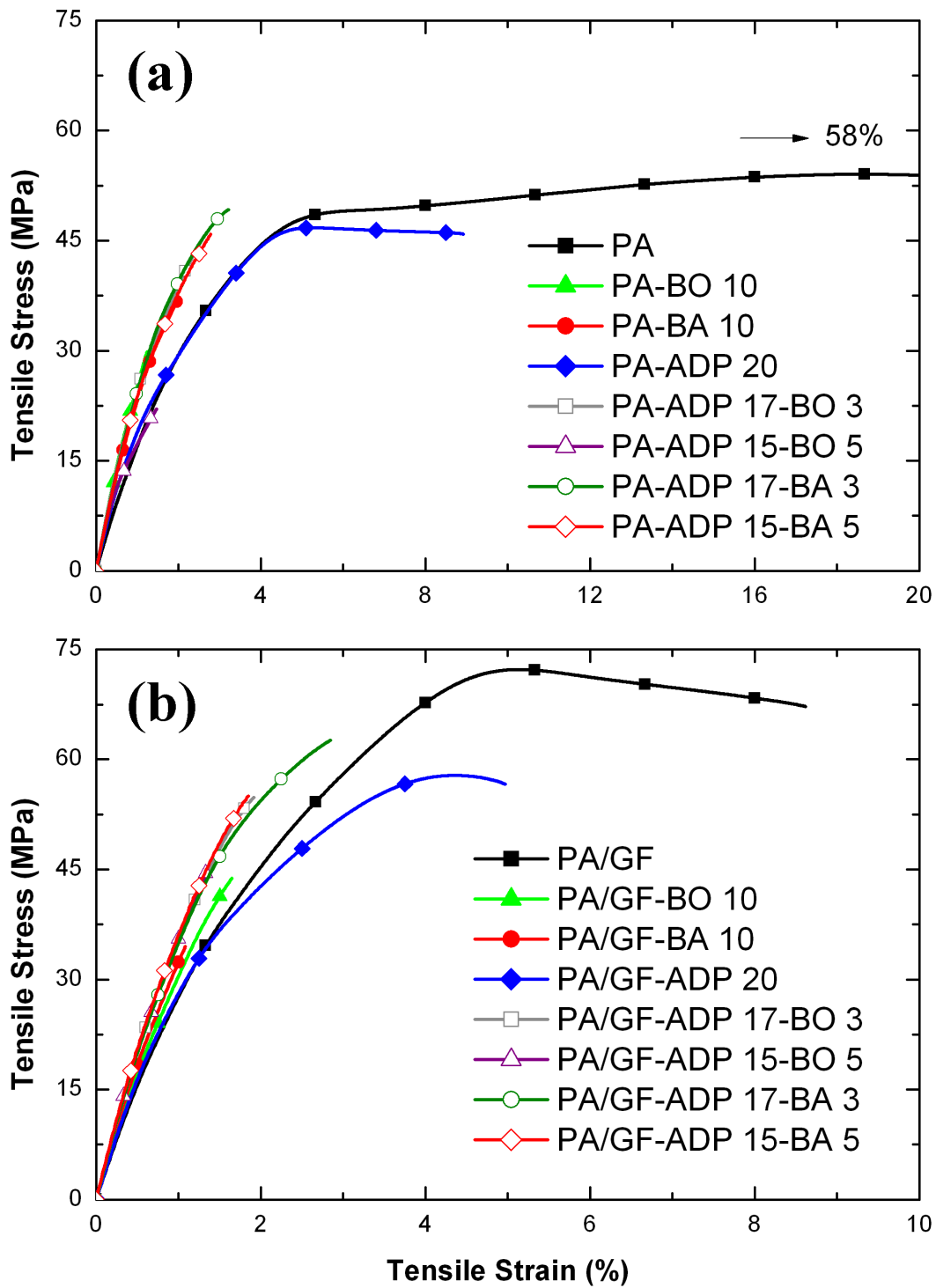


**Figure 3.26** Tensile Stress-Strain Curves of the (a) PA and (b) PA/GF Based Materials

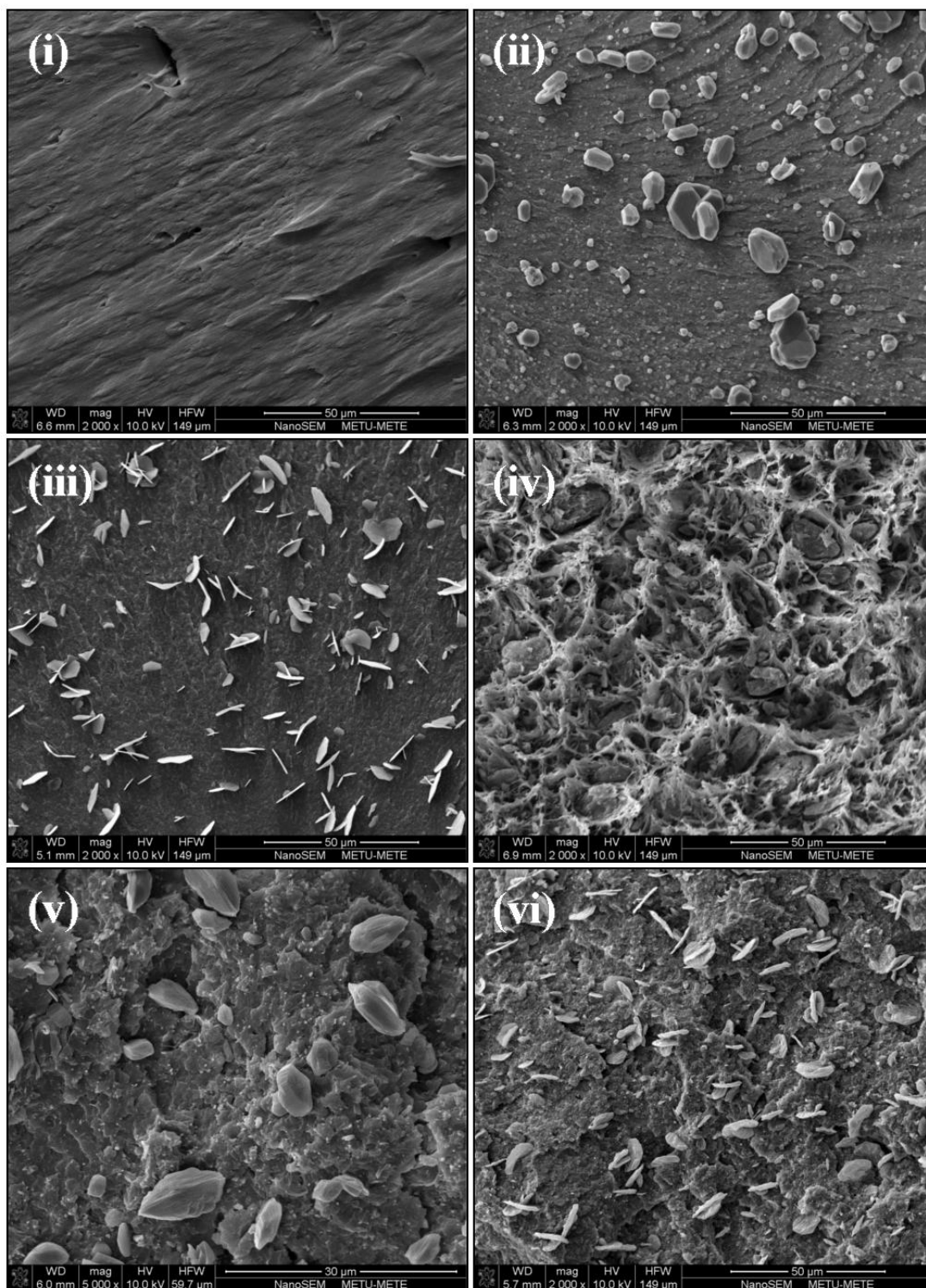


**Figure 3.27** SEM Fractographs of the Representative PA Based Materials:

(i) PA, (ii) PA-BO 10, (iii) PA-BA 10, (iv) PA-ADP 20,

(v) PA-ADP 15-BO 5, (vi) PA-ADP 15-BA 5

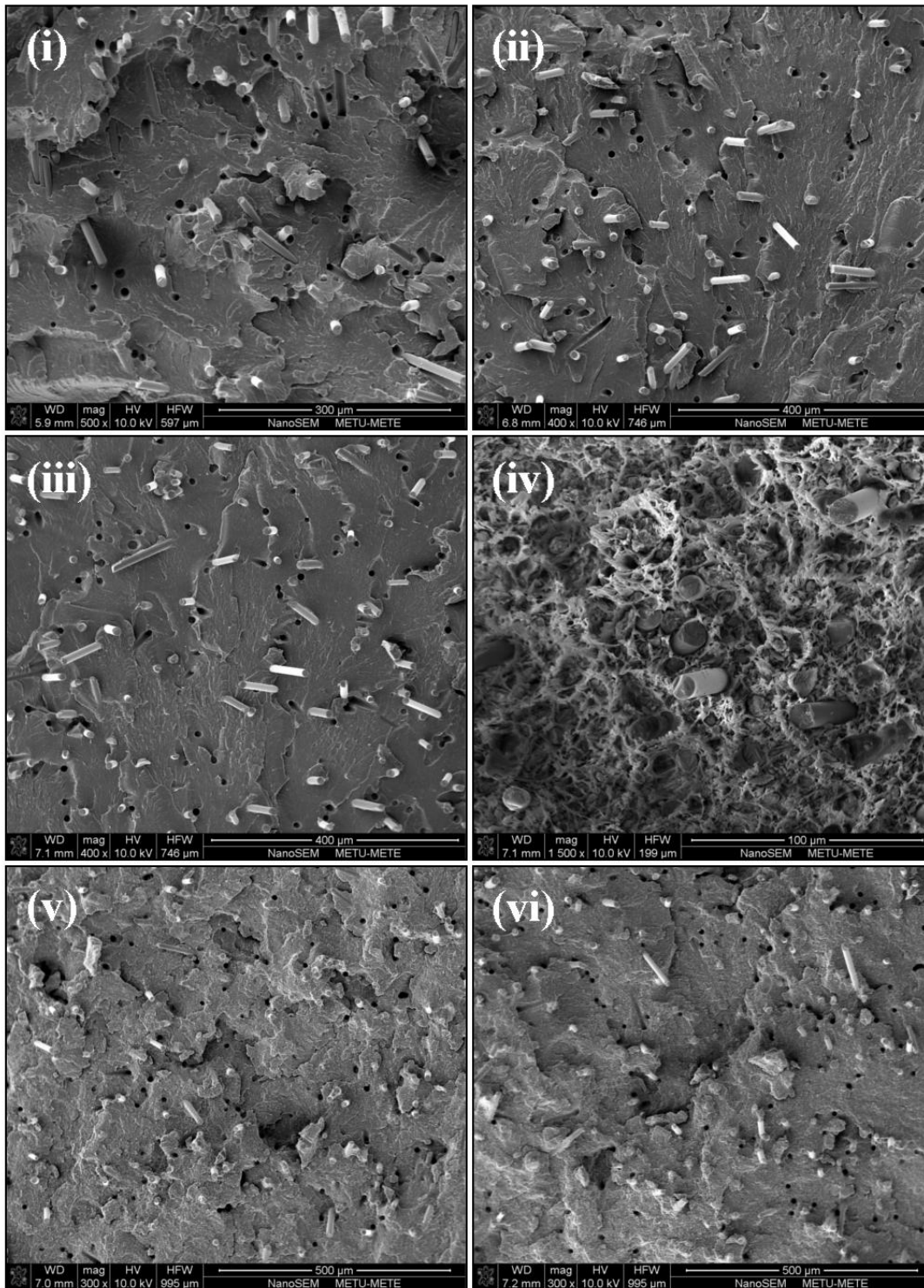


**Figure 3.28** SEM Fractographs of the Representative PA/GF Based Materials:  
 (i) PA/GF, (ii) PA/GF-BO 10, (iii) PA/GF-BA 10,  
 (iv) PA/GF-ADP 20, (v) PA/GF-ADP 15-BO 5, (vi) PA/GF-ADP 15-BA 5

### 3.3 EFFECTS OF NANOCCLAYS

In order to evaluate flame retardancy contribution of NC, the control sample material was chosen as PA or PA/GF with 20 wt% ADP type organophosphorus compound. In order to observe the effects of NC alone, first of all, specimens having only 5 wt% NC were produced for each group. Then, in order to reveal effects of using NC together with ADP, the amount of ADP was replaced with 5 wt% NC. Synergistic contribution of NC was also studied when used together with ZB (zinc borate). For this purpose, replacement of ADP was with 5 wt% NC plus 5 wt% ZB for each group. Designations and compositions of the specimens produced for this third part of the thesis are given in Table 2.4 and the results are discussed below.

#### 3.3.1 Nanocomposite Structure

Prior to investigation of flame retardancy behavior, it was important to reveal whether nanocomposite structure was obtained or not. For this purpose, first XRD and TEM analyses were performed to evaluate dispersibility and intercalation/exfoliation level of NC silicate layers in PA and PA/GF matrices.

Nanoclay used in this study (Cloisite 30B) impart a sharp XRD peak at  $2\theta = 4.90^\circ$  corresponding to an interlayer spacing (calculated from Bragg's law) of 1.8 nm. XRD patterns of all nanocomposite specimens in Figure 3.29 show that NC peak shifts to around  $1.84^\circ$  corresponding to the interlayer spacing of around 4.8 nm. Therefore, increase of gallery distance from 1.8 to 4.8 nm indicates that silicate layers are very well "intercalated" by the PA molecular chains.

Figure 3.29 also shows that XRD peaks of nanocomposite specimens have rather lower and broad intensity compared to NC structure. These broad and low intensity peaks could be interpreted as "partial exfoliation", but not as complete exfoliation of the silicate layers. Because, decrease in the sharpness and intensity of these peaks

could also be due to the attenuation and absorption of the reflections by the presence of other elements in the structure (such as aluminum in ADP and GF, and zinc and boron in ZB) having high levels of attenuation coefficients.

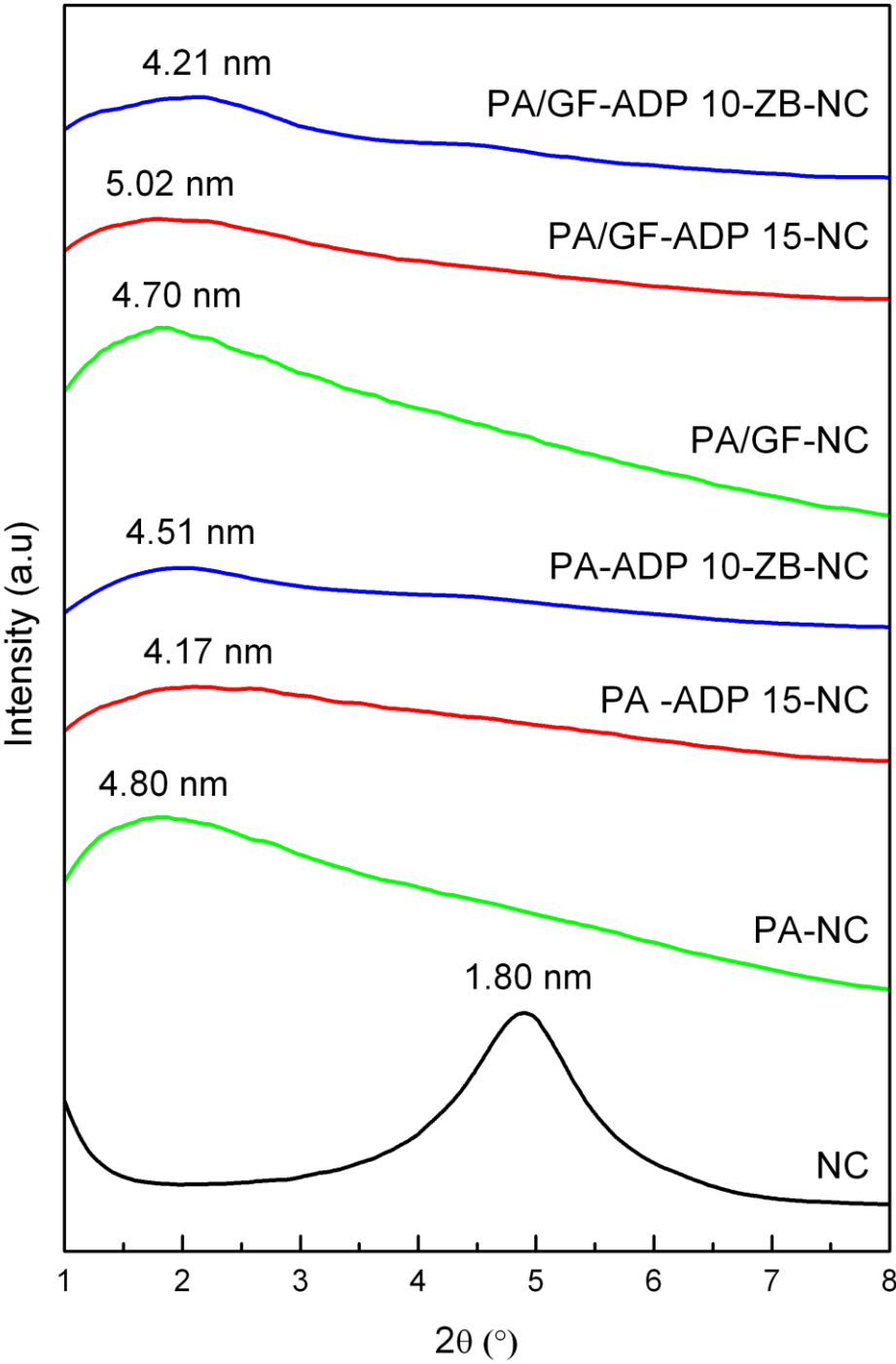


**Figure 3.29** XRD Patterns of the Nanoclay and Nanocomposite Specimens

To evaluate dispersion of NC and to support intercalation/exfoliation findings of XRD, nanocomposite specimens were also investigated by TEM analysis. Lower magnification images (Figures 3.30(i) and (ii)) show that NCs were homogeneously distributed in PA matrix. Medium and higher magnification images (Figures 3.30(iii) and (iv)) revealed that NC silicate layers were very well intercalated with certain level of exfoliation.

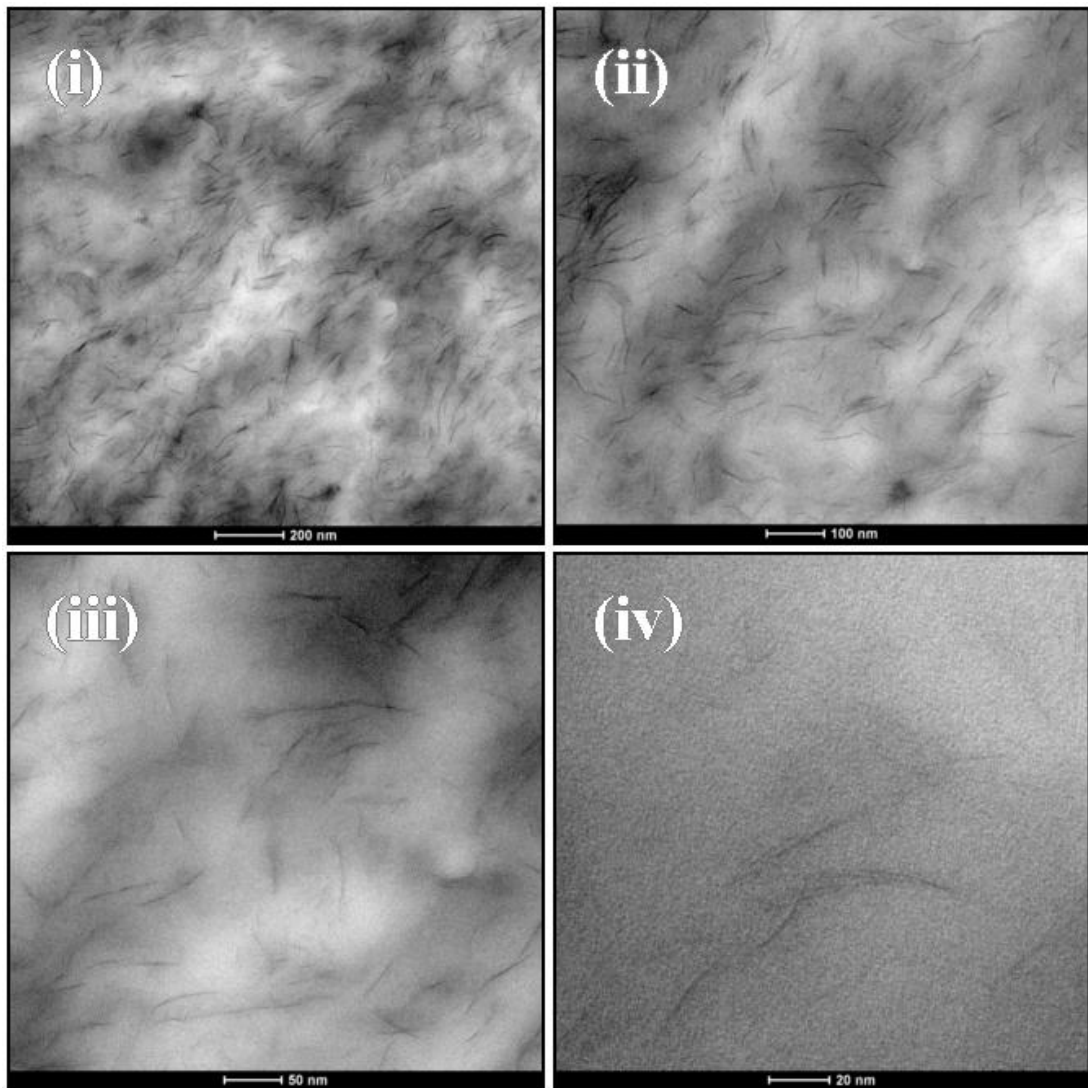


**Figure 3.30** TEM Images Showing (i) and (ii) Uniform Distribution, (iii) and (iv) Intercalated and Partly Exfoliated Structure of NC Silicate Layers in PA Matrix

### 3.3.2 UL-94 and LOI Flammability Tests

Results of UL-94 and LOI flammability tests are tabulated in Table 3.9, while photographs of the specimens after these two tests are given in Figures 3.31 and 3.32, respectively. It is seen that both PA and PA/GF specimens have V-2 rating from UL-94 tests, and LOI values of 26.1 and 23.3 O<sub>2</sub>%, respectively. It is seen in Table 3.9 that addition of 5 wt% NC alone into PA and PA/GF matrices lead to no improvements in UL-94 rating and LOI values.

As expected, when PA and PA/GF were loaded with novel flame retardant ADP as 20 wt%, there were significant improvements, e.g. both specimens (PA-ADP 20 and PA/GF-ADP 20) obtained V-0, the best rating of UL-94, and increased LOI values of 32.7 and 30.7 O<sub>2</sub>%, respectively. These improvements were especially due to the very effective “flame inhibition” action of ADP, and also its “charring” action as shown in Figure 3.32(a)(iii) and (b)(iii).

Table 3.9 indicates that when 5 wt% of ADP was replaced with NC, then each specimen (i.e. PA-ADP 15-NC and PA/GF-ADP 15-NC) not only keep the best UL-94 rating of V-0, but they also increase LOI values further to 34.9 and 35.1 %O<sub>2</sub>, respectively. This further contribution of NC was especially due to the further physical barrier mechanism of intercalated silica layers. On the other hand, when 10 wt% of ADP was replaced with 5 wt% ZB plus 5 wt% NC together, although V-0 ratings were kept, there were no further improvements in the LOI values.

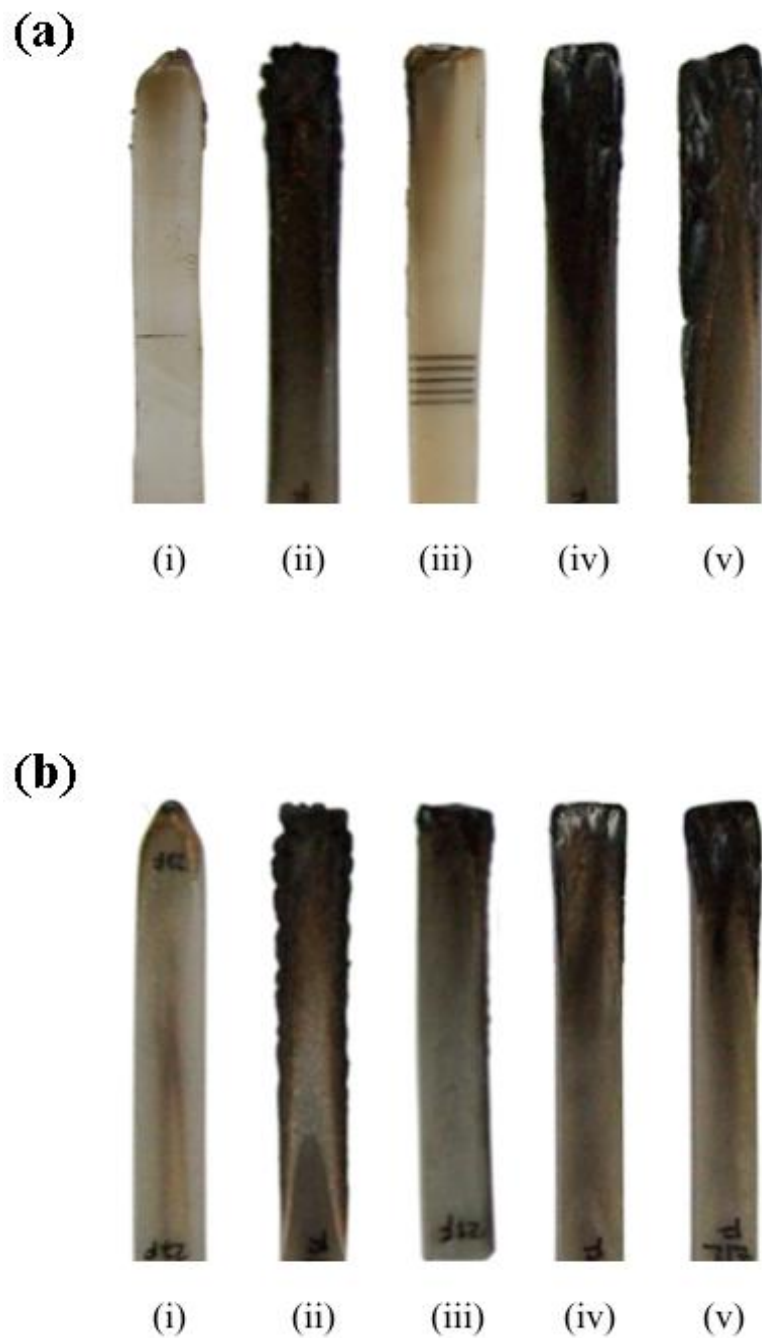


**Figure 3.31** Photographs of the Specimens after UL-94 Test:

**(a)** PA Based Materials; **(i)** PA, **(ii)** PA-NC, **(iii)** PA-ADP 20, **(iv)** PA-ADP 15-NC, **(v)** PA-ADP 10-ZB-NC

**(b)** PA/GF Based Materials; **(i)** PA/GF, **(ii)** PA/GF-NC, **(iii)** PA/GF-ADP 20, **(iv)** PA/GF-ADP 15-NC, **(v)** PA/GF-ADP 10-ZB-NC

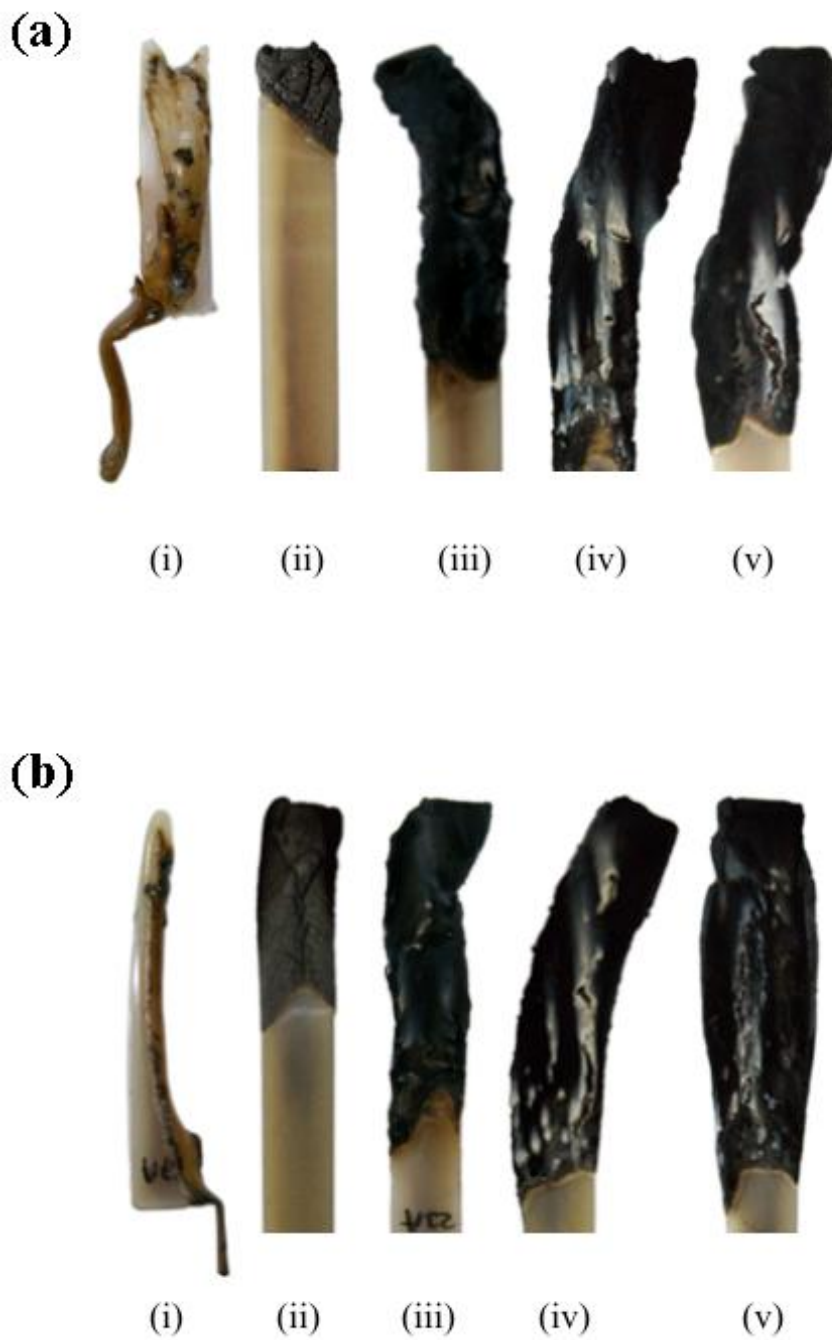


**Figure 3.32** Photographs of the Specimens after LOI Test:

**(a)** PA Based Materials; **(i)** PA, **(ii)** PA-NC, **(iii)** PA-ADP 20, **(iv)** PA-ADP 15-NC, **(v)** PA-ADP 10-ZB-NC

**(b)** PA/GF Based Materials; **(i)** PA/GF, **(ii)** PA/GF-NC, **(iii)** PA/GF-ADP 20, **(iv)** PA/GF-ADP 15-NC, **(v)** PA/GF-ADP 10-ZB-NC

**Table 3.9** Results of UL-94 and LOI Flammability Tests

Specimens	UL-94 Rating <sup>a</sup>	LOI <sup>b</sup> (%O <sub>2</sub> )
PA	V-2	26.1
PA-NC	Fail	24.5
PA-ADP 20	V-0	32.7
PA-ADP 15-NC	V-0	34.9
PA-ADP 10-ZB-NC	V-0	31.3
PA/GF	V-2	23.3
PA/GF-NC	Fail	23.1
PA/GF-ADP 20	V-0	30.7
PA/GF-ADP 15-NC	V-0	35.1
PA/GF-ADP 10-ZB-NC	V-0	30.9

<sup>a</sup>Rating of UL-94 standard, <sup>b</sup> Limiting oxygen index

### 3.3.3 SEM Analysis of LOI Chars

Burned tips of the LOI specimens were examined under SEM in order to evaluate their O<sub>2</sub>% values. Figures 3.33(i) and 3.34(i) show that specimens without flame retardants have very smooth surfaces with no charring. When 5 wt% NC were added to these specimens, Figure 3.33(ii) and 3.34(ii) show that there were certain level of rather porous char layer formation. However, as Table 3.9 indicates, this level of char barrier was not sufficient for any improvement in LOI values.

Figure 3.33 (iii) and 3.34(iii) show that the use of 20 wt% ADP leads to formation of certain level of rather continuous and strong char layers on the surface of the specimens increasing their LOI values significantly. When 5 wt% of ADP was replaced with NC (Figures 3.33(iv) and 3.34(iv)), it is seen that char barrier structure becomes more continuous and stronger, leading to further improvements in LOI values.

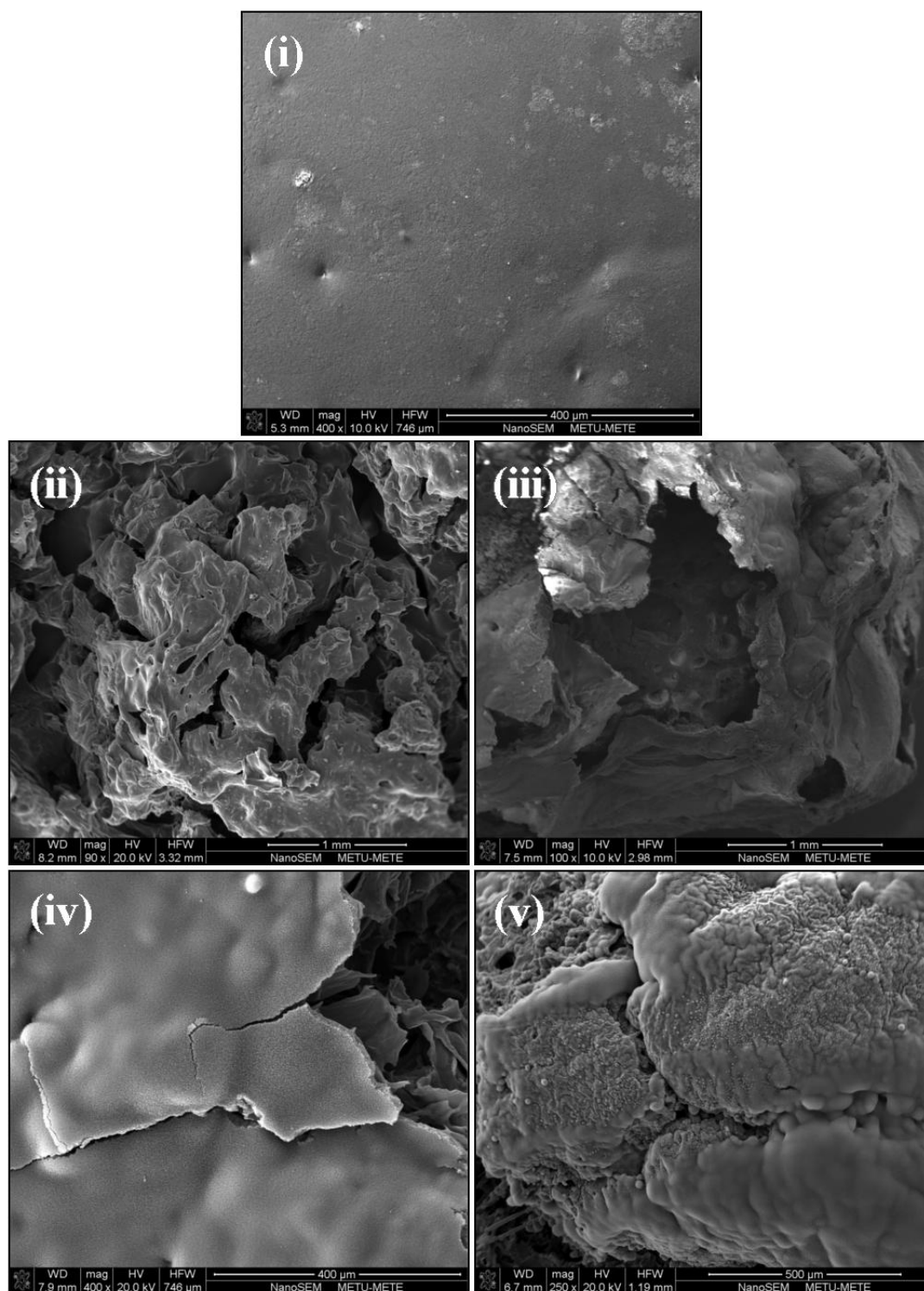


**Figure 3.33** SEM Images Showing Surface Char Barriers of the PA Based Materials:  
 (i) PA, (ii) PA-NC, (iii) PA-ADP 20, (iv) PA-ADP 15-NC,  
 (v) PA-ADP 10-ZB-NC

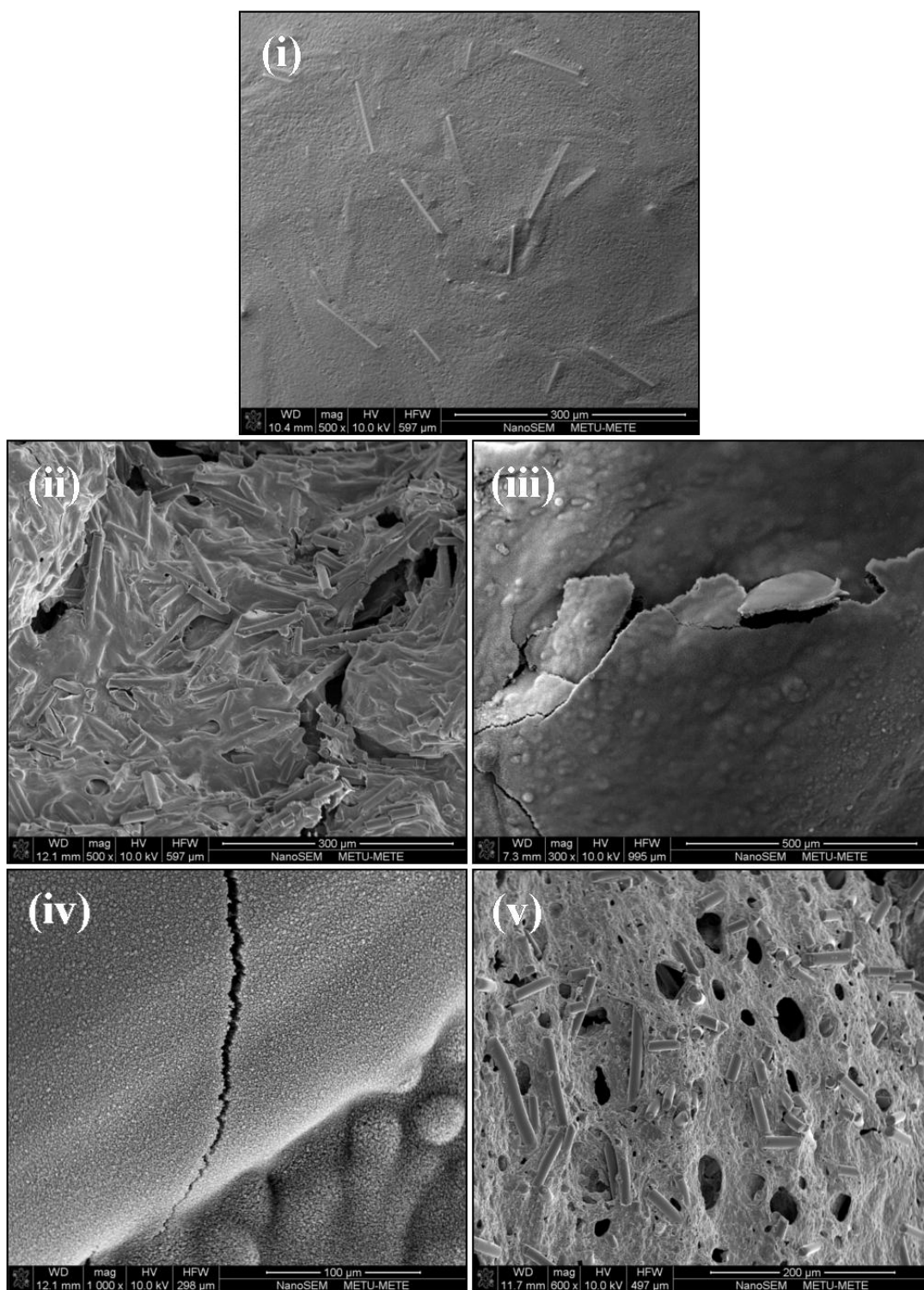


**Figure 3.34** SEM Images Showing Surface Char Barriers of the PA/GF Based Materials: (i) PA/GF, (ii) PA/GF-NC, (iii) PA/GF-ADP 20, (iv) PA/GF-ADP 15-NC, (v) PA/GF-ADP 10-ZB-NC

Replacement of ADP with ZB plus NC together (Figures 3.33(v) and 3.34 (v)) make the char structure more porous again, consequently no further improvement in LOI values.

### 3.3.4 Mass Loss Cone Calorimetry Analysis

Mass loss cone calorimetry (MLC) was conducted to measure fire performances of all specimens. After the test, first, visual examination of the remaining char structures were done as given in Figures 3.35 and 3.36. These figures simply show that char formation increases after incorporation of not only ADP and ZB but also with NC. Then, two important curves, i.e. “heat release rate” (HRR) and “mass loss rate” (MLR) curves were drawn (Figures 3.37 and 3.38). Consequently, all the important fire performance parameters were determined and tabulated in Table 3.10.

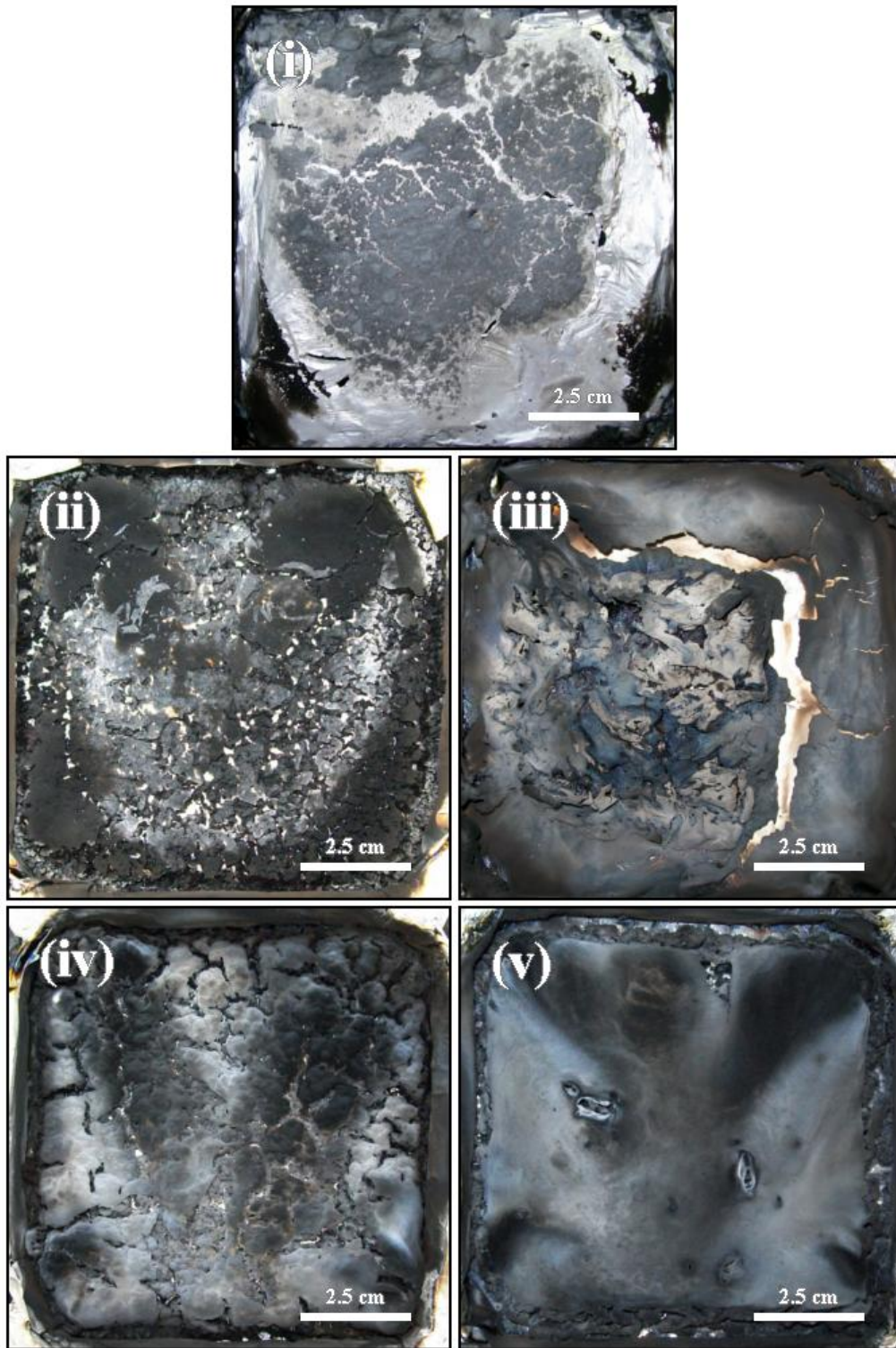
Figures 3.37 and 3.38 show that HRR and MLR curves of PA and PA/GF based materials were suppressed after adding 5 wt% NC alone or 20 wt% ADP alone. Moreover, these figures also show that when 5 wt% of ADP was replaced by NC, i.e. when ADP and NC were used together, there were more significant suppressions. Similarly, when 10 wt% of ADP was replaced with ZB plus NC together, further suppressions were obtained.

Table 3.10 for instance shows that, when 5 wt% NC alone were used, the suppression in the “peak heat release rate” (PHRR) values of PA and PA/GF were 55% and 61%, respectively. These suppressions were 32% and 75% when 20 wt% ADP alone was used. On the other hand, when 5 wt% of ADP was replaced with NC, suppressions were much more significant, i.e. as much as 65% in PA, and 76% in PA/GF based materials. When 10 wt% of ADP was replaced with ZB plus NC together, PHRR suppressions reached 72% and 80%, respectively. It can be also noted that, the trend in the suppressions of the “total heat evolved” (THE) values were similar.

Time related MLC parameters in Table 3.10 indicate that use of both NC and ADP alone or together resulted in no significant changes in the periods of “time to ignition” (TTI) values and “time to peak heat release rate” (TPHRR) values. However, there were very significant time extensions in the values of “total burning time” (TBT). Table 3.10 shows that, use of NC alone or together with ADP delay the TBT periods as much as two times for PA and three times for PA/GF based materials.

Contribution of additives to the fire propagation rate of materials can be evaluated by two indices determined from the MLC parameters. The first index is called “fire growth index” (FGI) which is the ratio of PHRR/TTI, the second one is named as “fire growth rate index” (FIGRA) which is the ratio of PHRR/TPHRR. It is expected that use of any flame retardant should decrease these indices, i.e. decrease the fire propagation rate. Table 3.10 shows that use of NC and ADP alone or together decreased the values of these two indices considerably in the PA and PA/GF materials.

The ratio of THE/TML (total heat evolved/total mass loss) and % char yield data can be used to evaluate main flame retardancy mechanisms of the specimens. Table 3.10 reveals that the values of THE/TML ratio decreased especially when ADP was used alone. This could be interpreted as that, ADP basically acts in the “gaseous phase” mechanism. On the other hand, Table 3.10 shows that addition of NC in all combinations increases % char residue considerably, which could be interpreted as its “condensed phase” mechanism as discussed below.



**Figure 3.35** Photographs of the Remaining Char Structure of MLC Specimens of the PA Based Materials: (i) PA, (ii) PA-NC, (iii) PA-ADP 20, (iv) PA-ADP 15-NC, (v) PA-ADP 10-ZB-NC

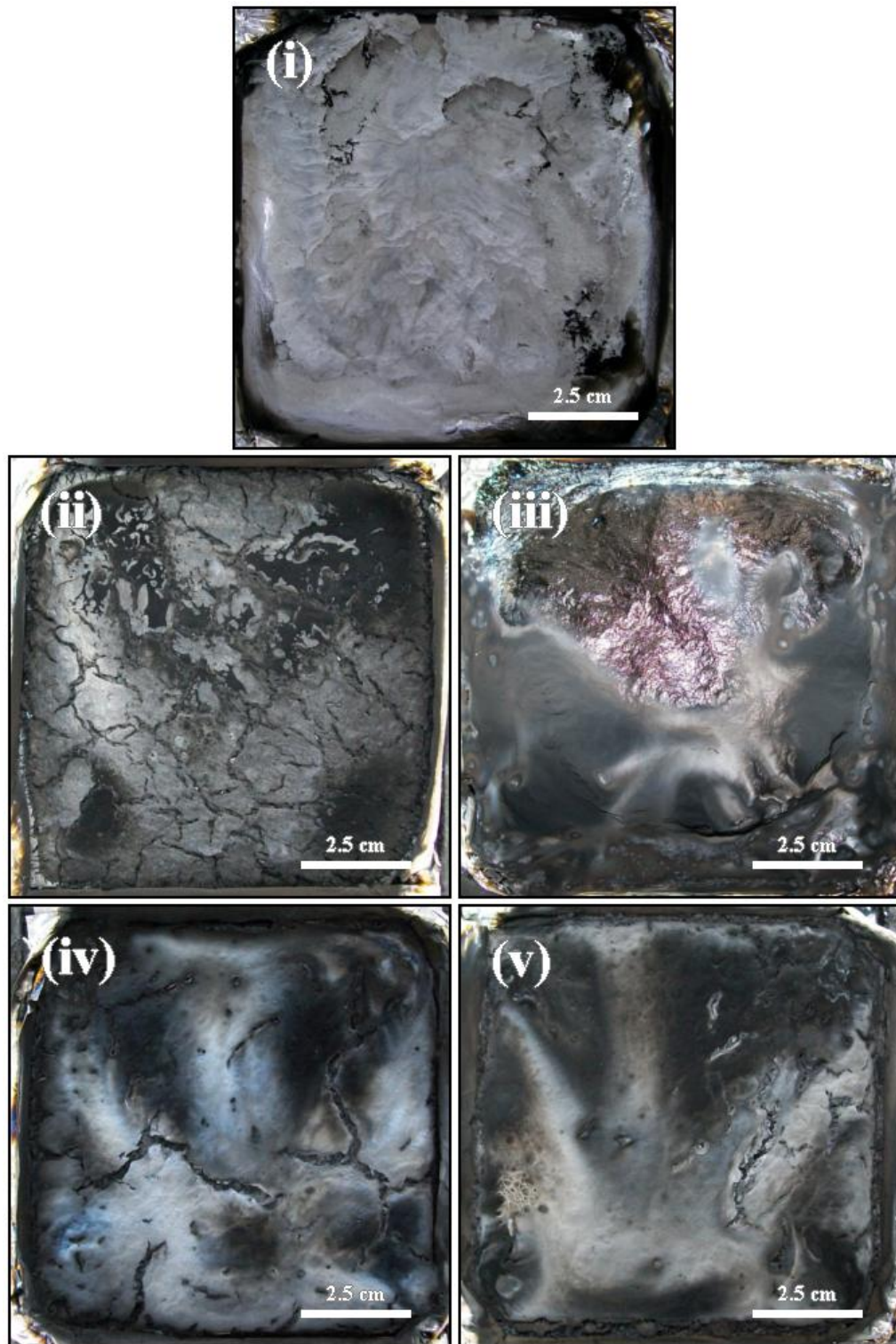


**Figure 3.36** Photographs of the Remaining Char Structure of MLC Specimens of the PA/GF Based Materials: (i) PA/GF, (ii) PA/GF-NC, (iii) PA/GF-ADP 20, (iv) PA/GF-ADP 15-NC, (v) PA/GF-ADP 10-ZB-NC

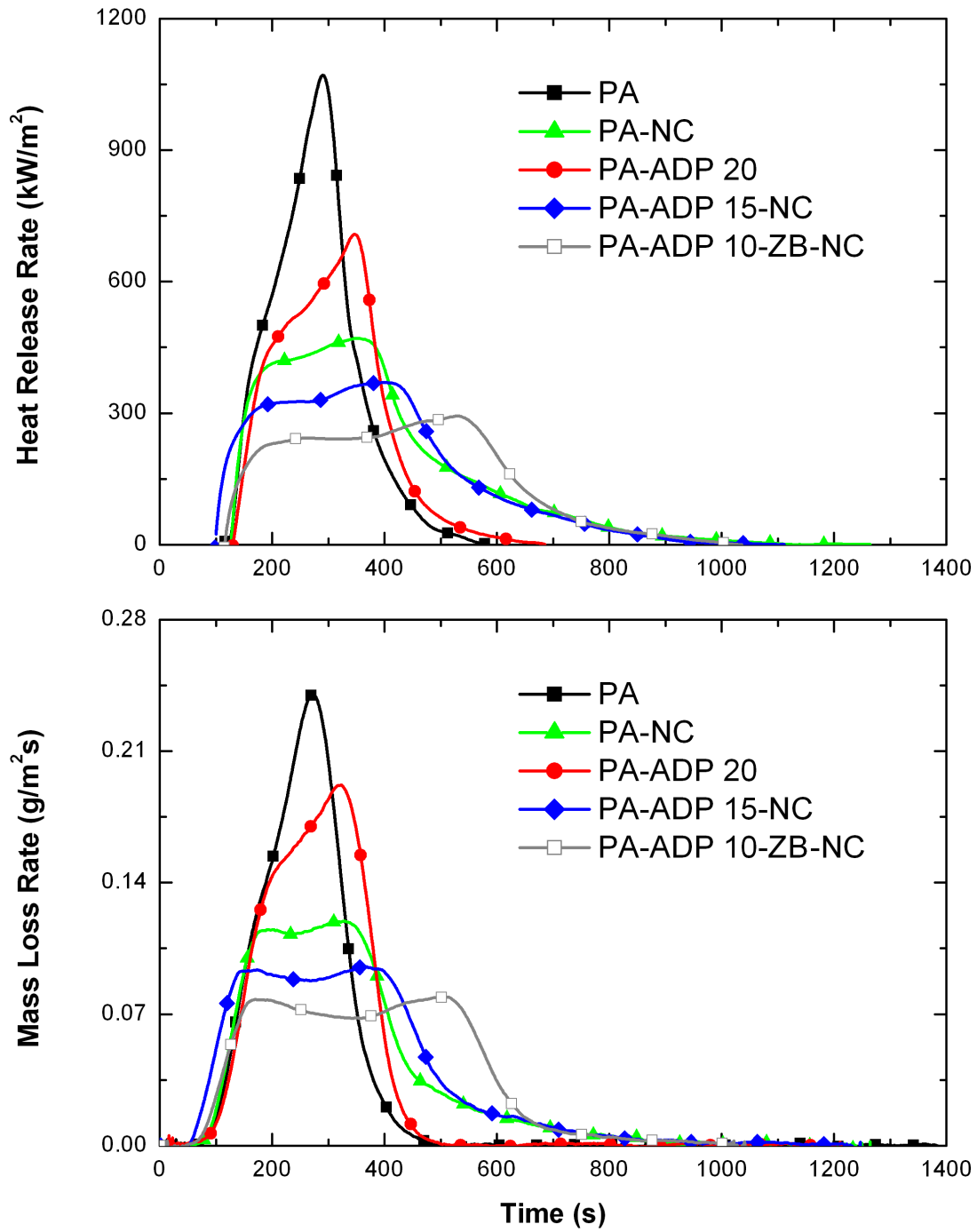


**Figure 3.37** Heat Release Rate and Mass Loss Rate Curves for the PA Based Materials

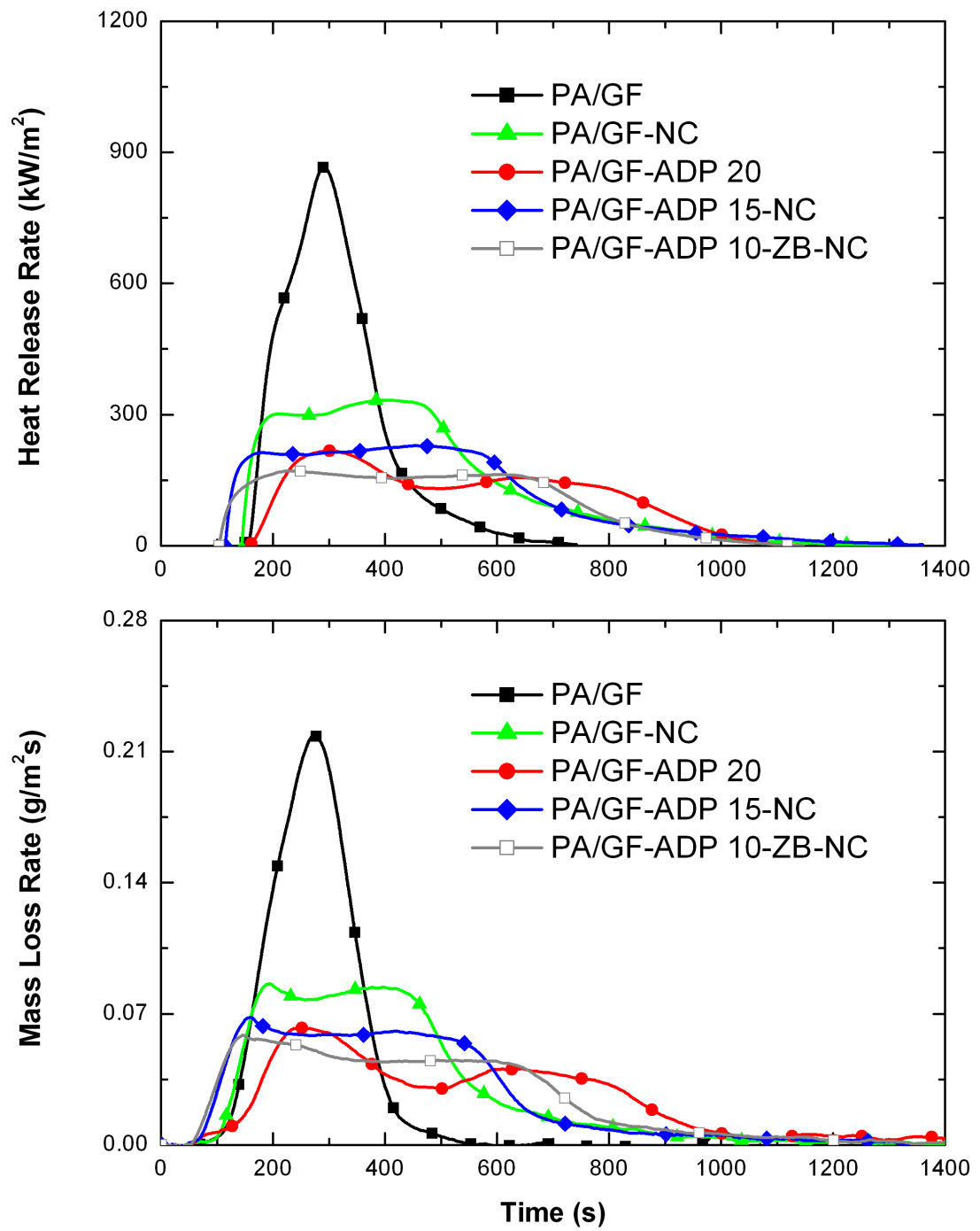


**Figure 3.38** Heat Release Rate and Mass Loss Rate Curves for the PA/GF Based Materials

**Table 3.10** Mass Loss Cone Calorimeter Parameters of the Specimens

Specimens	PHRR <sup>a</sup> (kW/m <sup>2</sup> )	THE <sup>b</sup> (MJ/m <sup>2</sup> )	TTI <sup>c</sup> (s)	TPHRR <sup>d</sup> (s)	TBT <sup>e</sup> (s)	FGI <sup>f</sup> (kW/m <sup>2</sup> .s)	FIGRA <sup>g</sup> (kW/m <sup>2</sup> .s)	THE/TML <sup>h</sup> (MJ/m <sup>2</sup> .g)	Char Yield (%)
PA	1055	171	96	302	437	11.0	3.5	4.2	0.2
PA-NC	473	169	106	358	897	4.5	1.3	4.1	4.6
PA-ADP 20	716	151	108	350	477	6.6	2.0	3.5	2.3
PA-ADP 15-NC	372	147	77	392	882	4.8	1.0	3.6	9.1
PA-ADP 10-ZB-NC	295	139	89	523	958	3.3	0.6	3.6	14.1
PA/GF	868	159	108	291	563	8.0	3.0	4.1	15.0
PA/GF-NC	335	155	126	406	1137	2.7	0.8	4.0	19.5
PA/GF-ADP 20	219	114	112	326	1354	2.0	0.7	3.4	31.3
PA/GF-ADP 15-NC	211	111	95	443	1265	2.2	0.5	6.3	32.5
PA/GF-ADP 10-ZB-NC	172	109	81	231	1310	2.1	0.7	6.7	33.4

<sup>a</sup> PHRR: peak heat release rate

<sup>b</sup> THE: total heat evolved

<sup>c</sup> TTI: time to ignition

<sup>d</sup> TPHRR: time to peak heat release rate

<sup>e</sup> TBT: total burning time

<sup>f</sup> FGI: fire growth index, where FGI=PHRR/TTI

<sup>g</sup> FIGRA: fire growth index rate, where FIGRA=PHRR/TPHRR

<sup>h</sup> THE/TML: ratio of total heat evolved/total mass loss

### 3.3.5 Flame Retardancy Mechanisms

As investigated by various studies [41,42,44,45,47-50,55], the main flame retardancy mechanism of nanoclays is the “condense phase action”, that is, formation of an “insulative barrier” preventing the underlying polymeric material from heat and mass transfer during fire. When NC silicate layers were very-well intercalated and/or exfoliated in the polymeric matrix, then physical barrier formation mechanism would be more effective. Diffusion of volatile species generated during fire would be restricted by the “tortuous pathway” formed via intercalated/exfoliated NC layers, which is also called “labyrinth effect”. In this study, when NC was added alone, Table 3.10 indicated that there were very significant suppressions in the values of PHRR, due to the insulative barriers of NC layers with tortuous pathway.

It was indicated in Section 3.1.4 that as the primary mechanism, ADP acts in the “gaseous” phase, while its secondary mechanism could be in the “condensed” phase. When ADP was vaporized during fire, it might get oxidized to  $\text{HPO}_2\bullet$ ,  $\text{PO}\bullet$ ,  $\text{PO}_2\bullet$ , and  $\text{HPO}\bullet$  radicals, which would scavenge very harmful  $\text{H}\bullet$  and  $\text{OH}\bullet$  hot radicals. This gaseous phase action is called “flame inhibition”. When ADP was oxidized to phosphoric acid during fire, it might lead to the formation of two-layer protective barrier; a carbon based char and an inorganic residue layer of aluminum phosphate. This condensed phase action is called “barrier effect”. In this study, due to the very high efficiency of these mechanisms, use of ADP alone resulted in very significant improvements in all flammability parameters including UL-94, LOI, PHRR, etc. values as tabulated in Table 3.9 and 3.10.

When ADP was used together with NC, those mechanisms mentioned above would continue to operate. In this study, the synergistic contribution of NC to ADP would be retardation of gaseous aluminum phosphinate evolution by means of the labyrinth effect of intercalated/exfoliated NC layers leading to the formation of larger amount of aluminum phosphates in the char residue.

The main contribution of ZB when used together with ADP and NC would be in the formation of additional inorganic barriers, i.e. boron phosphate /aluminum phosphate layers as also stated by Braun et.al. [29,34]. Certainly, another contribution to the condensed phase barrier mechanism would take place by the short glass fibers used in the PA/GF based specimens, which would increase the effectiveness of char barriers via reinforcing or stabilizing their structure.

For further clarification of these flame retardancy mechanisms, two additional analyses namely; thermogravimetry and X-ray diffraction were conducted and discussed in the following sections.

### 3.3.6 Thermogravimetric Analysis

Since results of each group were very similar, thermogravimetric (TG) and differential thermogravimetric (DTG) curves are given in Figure 3.39 only for the PA based materials, while the thermal degradation parameters derived from these curves are tabulated in Table 3.11 for both PA and PA/GF based materials.

These curves showed that neat PA decomposes in one step with a maximum mass loss rate at around 460°C, leaving very little organic residue. On the contrary, due to the 15 wt% glass fiber reinforcements, PA/GF specimen formed considerable amount of residue. It is known that during decomposition, polyamide-6 releases water, ammonia, carbon monoxide, carbon dioxide and certain hydrocarbon fragments.

Figure 3.39 shows that when NC was added, TG and DTG curves shift slightly to higher temperatures. Therefore, Table 3.11 reveals that, not only maximum mass loss rate temperatures ( $T_{DTG\text{-peak}}$ ), but also 10 wt% and 50 wt% degradation temperatures ( $T_{10\text{ wt\%}}$  and  $T_{50\text{ wt\%}}$ ) of the PA and PA/GF specimens were increased.

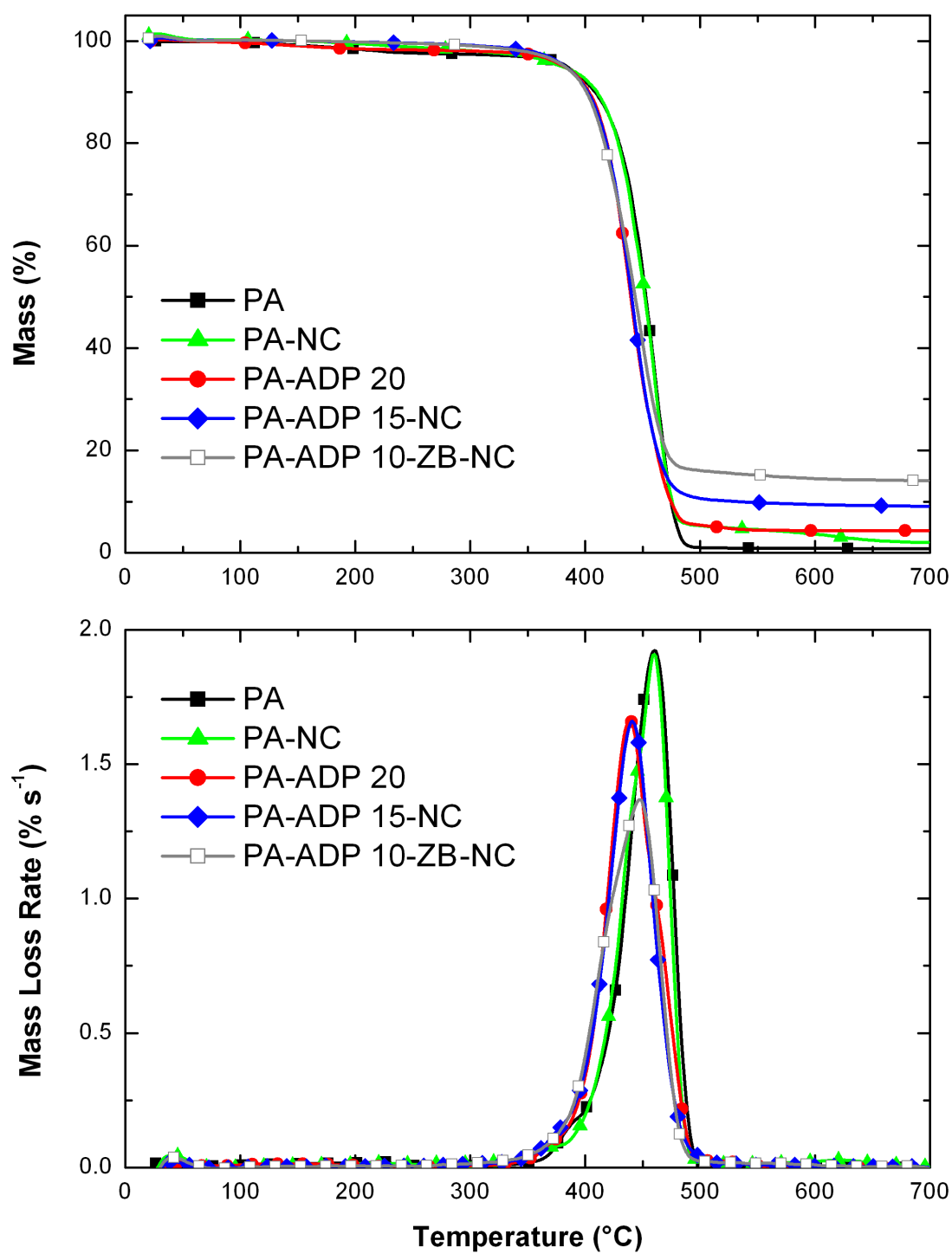


**Figure 3.39** Thermogravimetric (TG) and Differential Thermogravimetric (DTG) Curves for the PA Based Materials

**Table 3.11** Thermal Degradation Parameters of the Specimens Determined from TG and DTG Curves

Specimens	T <sub>DTG-Peak 1</sub> <sup>a</sup> (°C)	T <sub>DTG-Peak 2</sub> <sup>b</sup> (°C)	T <sub>10 wt%</sub> <sup>c</sup> (°C)	T <sub>50 wt%</sub> <sup>d</sup> (°C)	% Residue at 600 °C
ZB	242	415	428	-	85.8
ADP	-	496	459	494	15.8
NC	263	376	326	-	72.7
PA	-	460	408	452	0.9
PA-NC	-	460	411	453	3.7
PA-ADP 20	-	436	404	439	4.4
PA-ADP 15-NC	-	441	405	441	9.4
PA-ADP 10-ZB-NC	-	447	401	443	14.5
PA/GF	-	465	416	455	14.8
PA/GF-NC	-	450	418	456	18.4
PA/GF-ADP 20	-	430	395	436	18.2
PA/GF-ADP 15-NC	-	439	406	446	20.7
PA/GF-ADP 10-ZB-NC	-	448	403	456	31.5

<sup>a</sup> T<sub>DTG-Peak 1</sub>: first peak temperature in DTG curve<sup>b</sup> T<sub>DTG-Peak 2</sub>: second peak temperature in DTG curve<sup>c</sup> T<sub>10 wt%</sub>: thermal degradation temperature for 10% mass loss<sup>d</sup> T<sub>50 wt%</sub>: thermal degradation temperature for 50% mass loss

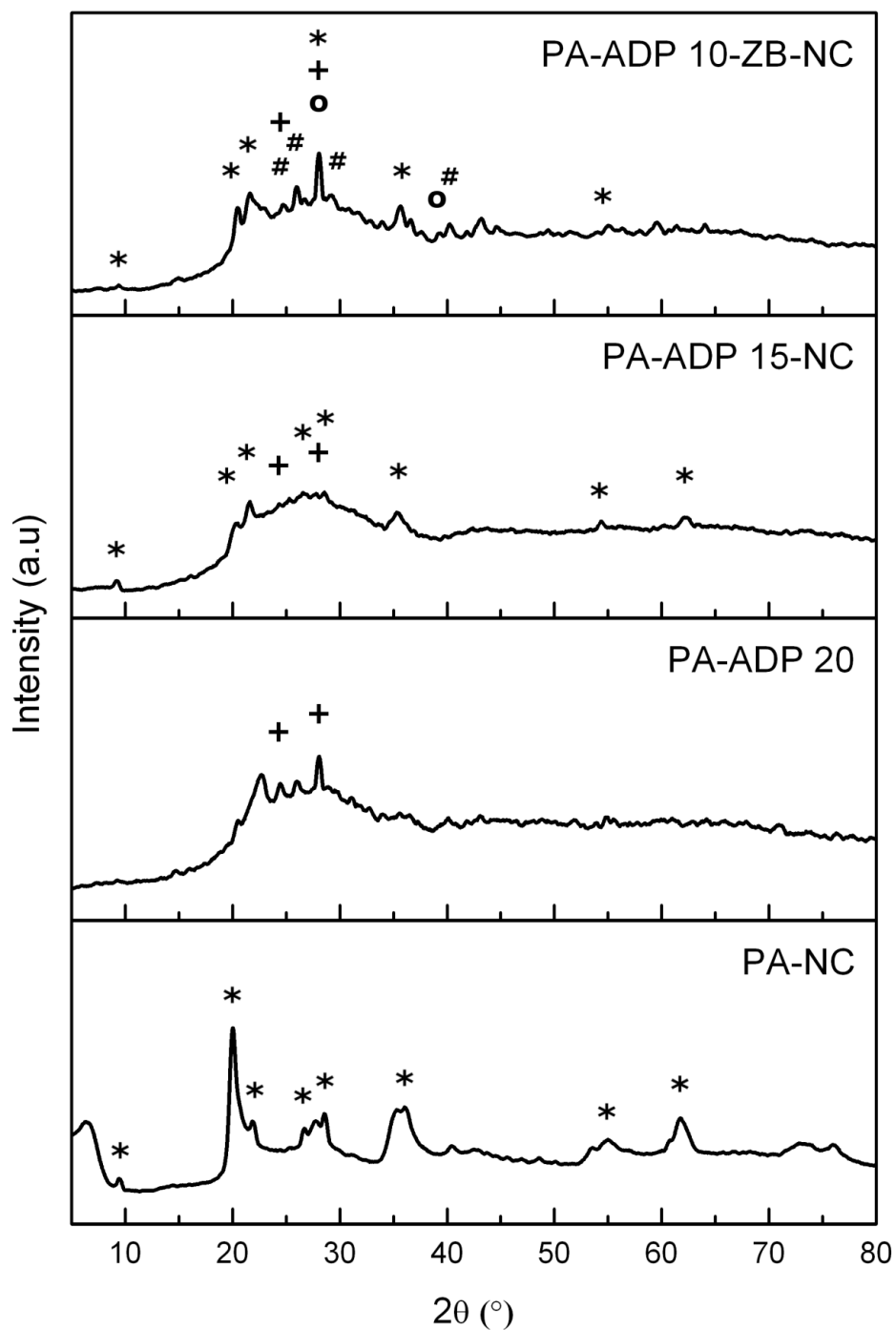
Table 3.11 also indicates that addition of NC in all compositions increases the amount of residue significantly, for instance, use of only 5 wt% NC leads to more than 3.5 wt% residue. It is seen that the use of NC together with ADP and ZB leads to even more significant increases in the amount of residue. Thus, TG analysis supported the physical barrier formation mechanisms of NC, ADP and ZB as discussed in the previous section.

### 3.3.7 XRD Analysis of MLC Residues

To reveal the crystal structure of the phases in the char layers, XRD analyses were conducted on the MLC chars of representative specimens of each group. Since results of each group were very similar, XRD diffractograms are provided in Figure 3.40 only for the PA based materials.

Figure 3.40 shows that when NC was used alone, typical peaks of the crystallographic planes of montmorillonite (MMT) clay mineral were seen. When ADP was used alone, peaks of its main decomposition phase, i.e. peaks of aluminum phosphate ( $\text{AlPO}_4$ ) were seen. When NC and ADP were used together, no additional peaks formed. When NC was used together with ADP and ZB, additional peaks of the decomposition phases of ADP and ZB were also observed, which were boron phosphate ( $\text{BPO}_4$ ) and dehydrated zinc borates ( $\text{Zn}(\text{BO}_2)_2$ ,  $\text{ZnB}_4\text{O}_7$  and  $\text{Zn}_4\text{B}_6\text{O}_{13}$ ).

Thus, it can be stated that, apart from the MMT structure of NC and the expected decomposition byproducts of ADP and ZB, no other phases were formed in the chars of the MLC specimens. This could be interpreted as another confirmation of the physical barrier mechanism of especially NC, ZB, and also partly for ADP.



\* : Montmorillonite (MMT) clay

+ : Aluminum phosphate  $\text{AlPO}_4$ , Card no: 46-0695

# : Boron phosphate  $\text{BPO}_4$ , Card no: 11-0237, 12-0380, 34-0132

o : Dehydrated zinc borate  $\text{ZnB}_4\text{O}_7$ , Card no: 24-1438, or  $\text{Zn}_4\text{B}_6\text{O}_{13}$ , Card no: 27-1487, or  $\text{Zn}(\text{BO}_2)_2$ , Card no: 39-1126

**Figure 3.40** XRD Patterns of the MLC Residues of the PA Based Materials

### 3.3.8 Tensile Testing for Mechanical Properties

To reveal effects of NC alone and together with ADP on the mechanical performance of the specimens studied, a minimum of five samples for each formulation were subjected to tension tests. Figure 3.41 shows tensile stress-strain behavior of the specimens, while Table 3.12 gives determined mechanical properties.

Figure 3.41 and Table 3.12 show that when only 5 wt% NC was added alone to neat PA, its modulus and strength values increased. The increase in Young's modulus was 56%, while that in yield and tensile strengths were 34% and 31%, respectively. These increases were due to the strengthening mechanism of decreased chain mobility of the PA matrix with intercalated/exfoliated silicate layers, and the efficient load transfer to the NC layers having very high aspect ratios. Consequently, the decreased chain mobility by NC layers resulted in significant ductility (i.e. % elongation at break) decrease from 58% down to 7%.

As expected, composite strengthening mechanism of load transfer was also effective when 15 wt% short glass fiber reinforcements were used. Table 3.12 indicates that compared to PA, improvements in the specimen of PA/GF were 64% for Young's modulus, 36% for yield strength, and 34% for tensile strength. However, Table 3.12 also shows that when 5 wt% NC was added to PA/GF specimen, there was no further improvement in the strength values, i.e. strengthening mechanism of NC were obscured by the mechanism of 15 wt% GF.

On the other hand, when 20 wt% ADP was incorporated into PA and PA/GF, except modulus their other mechanical properties decreased. For instance, the decrease in tensile strength was 14% for PA and 20% for PA/GF specimen. These decreases could be basically due to the very coarse size (42.3  $\mu\text{m}$ ) and rather weak organic structure of the ADP particles. However, it is seen that, when 5 wt% of ADP was replaced with NC, then decreased strength values of PA-ADP 20 and PA/GF-ADP 20 increased again. Therefore, it can be concluded that 5 wt% of ADP

replacement with NC not only improves many flame retardancy parameters of PA-ADP 20 and PA/GF-ADP 20; but, NC also compensates their decreased strength values.

SEM examination was also conducted to the fracture surfaces of the tensile test specimens in order to reveal morphology of the fracture surfaces and distribution of ADP, ZB and GF. Figures 3.42 and 3.43 show that very smooth fracture surfaces of PA and PA/GF specimens transformed into very rough morphology when ADP and ZB were incorporated. It can be also observed that ADP, ZB and GF were all distributed rather uniformly having certain level of interfacial bonding with the PA matrix. Due to their nano-range size, it was not possible to observe the distribution of NC layers via SEM.

**Table 3.12** Tensile Mechanical Properties of the Specimens

<b>Specimens</b>	<b>Young's Modulus (GPa)</b>	<b>Yield Strength (MPa)</b>	<b>Tensile Strength (MPa)</b>	<b>Elongation at break (%)</b>
PA	1.96 ± 0.08	40.3 ± 3.4	54.2 ± 0.7	58.3 ± 3.5
PA-NC	3.06 ± 0.05	53.9 ± 1.3	70.8 ± 1.4	7.1 ± 1.9
PA-ADP 20	2.43 ± 0.17	33.3 ± 3.9	46.6 ± 0.3	9.0 ± 0.4
PA-ADP 15-NC	3.40 ± 0.05	49.6 ± 0.9	56.2 ± 0.3	5.1 ± 0.3
PA-ADP 10-ZB-NC	3.27 ± 0.08	48.7 ± 1.2	55.1 ± 0.5	5.6 ± 0.7
PA/GF	3.22 ± 0.04	54.8 ± 2.9	72.5 ± 0.6	8.8 ± 0.4
PA/GF-NC	3.65 ± 0.08	51.6 ± 1.1	63.4 ± 0.4	5.7 ± 0.9
PA/GF-ADP 20	3.46 ± 0.08	42.8 ± 3.4	57.7 ± 0.3	5.1 ± 0.1
PA/GF-ADP 15-NC	4.59 ± 0.05	51.5 ± 0.9	56.5 ± 0.8	3.3 ± 0.2
PA/GF-ADP 10-ZB-NC	4.48 ± 0.16	47.5 ± 2.7	51.1 ± 1.8	2.9 ± 0.4

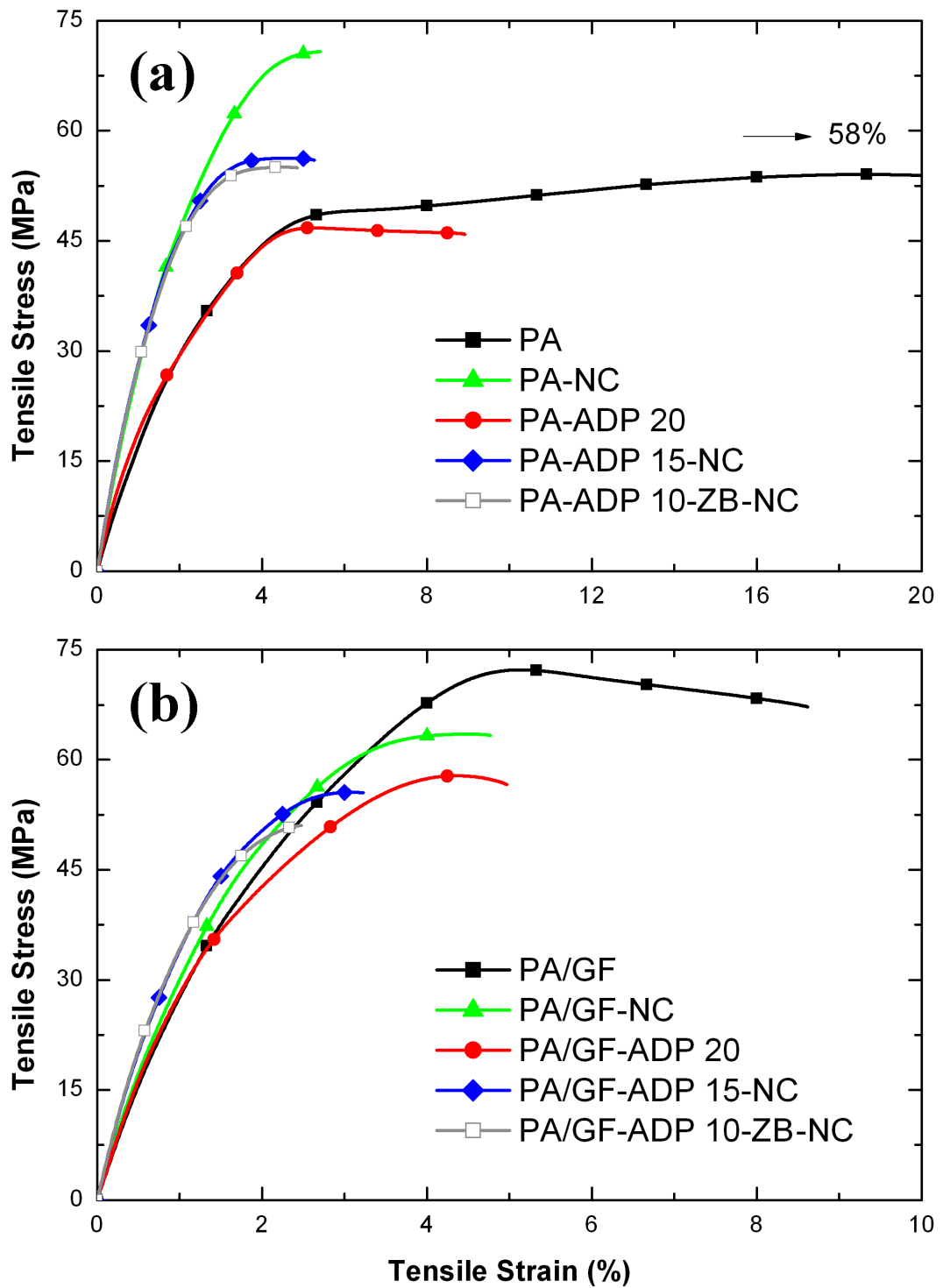


**Figure 3.41** Tensile Stress-strain Curves of the (a) PA and (b) PA/GF Based Materials

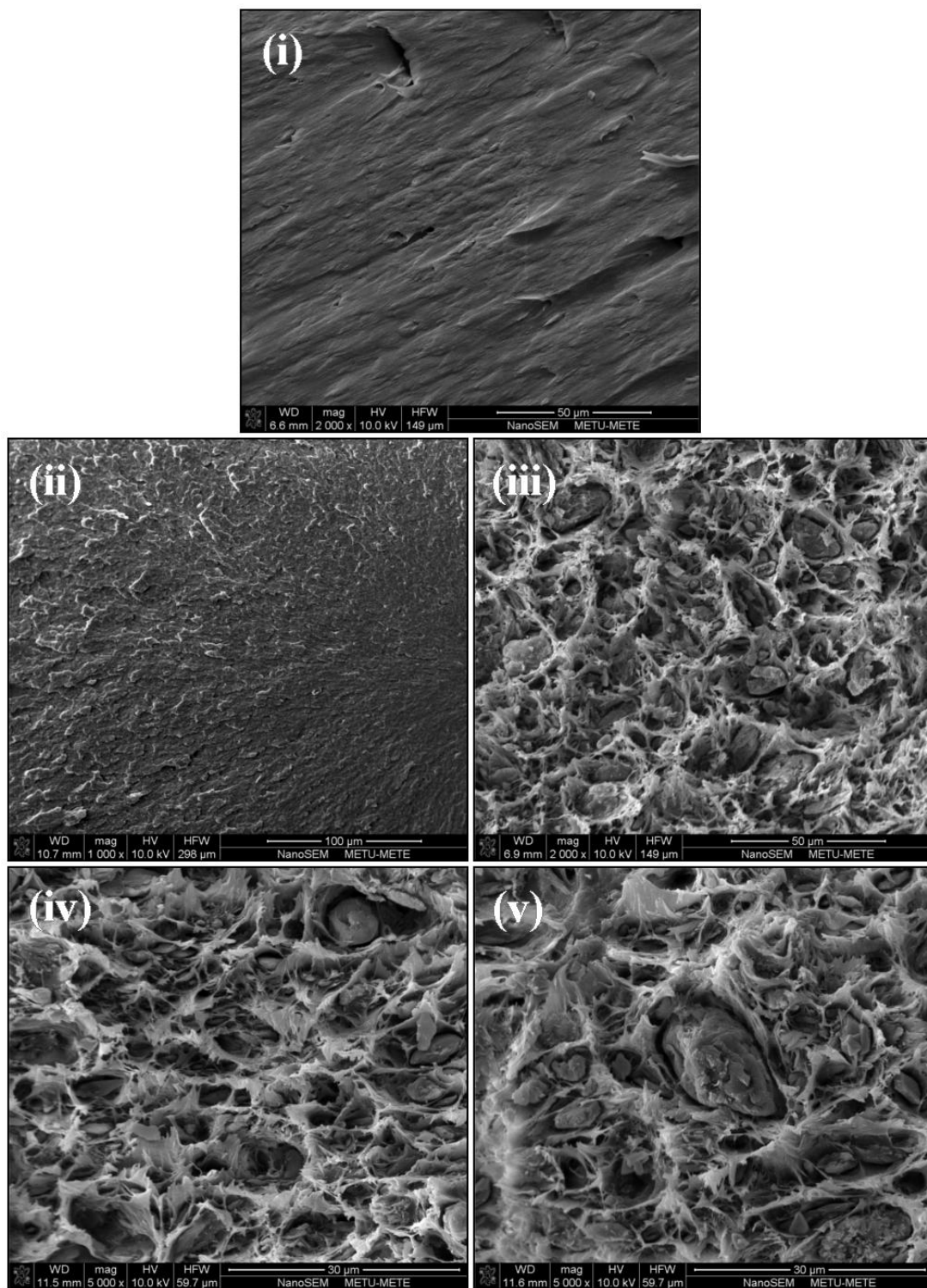


**Figure 3.42** SEM Fractographs of the PA Based Materials:  
(i) PA, (ii) PA-NC, (iii) PA-ADP 20, (iv) PA-ADP 15-NC,  
(v) PA-ADP 10-ZB-NC

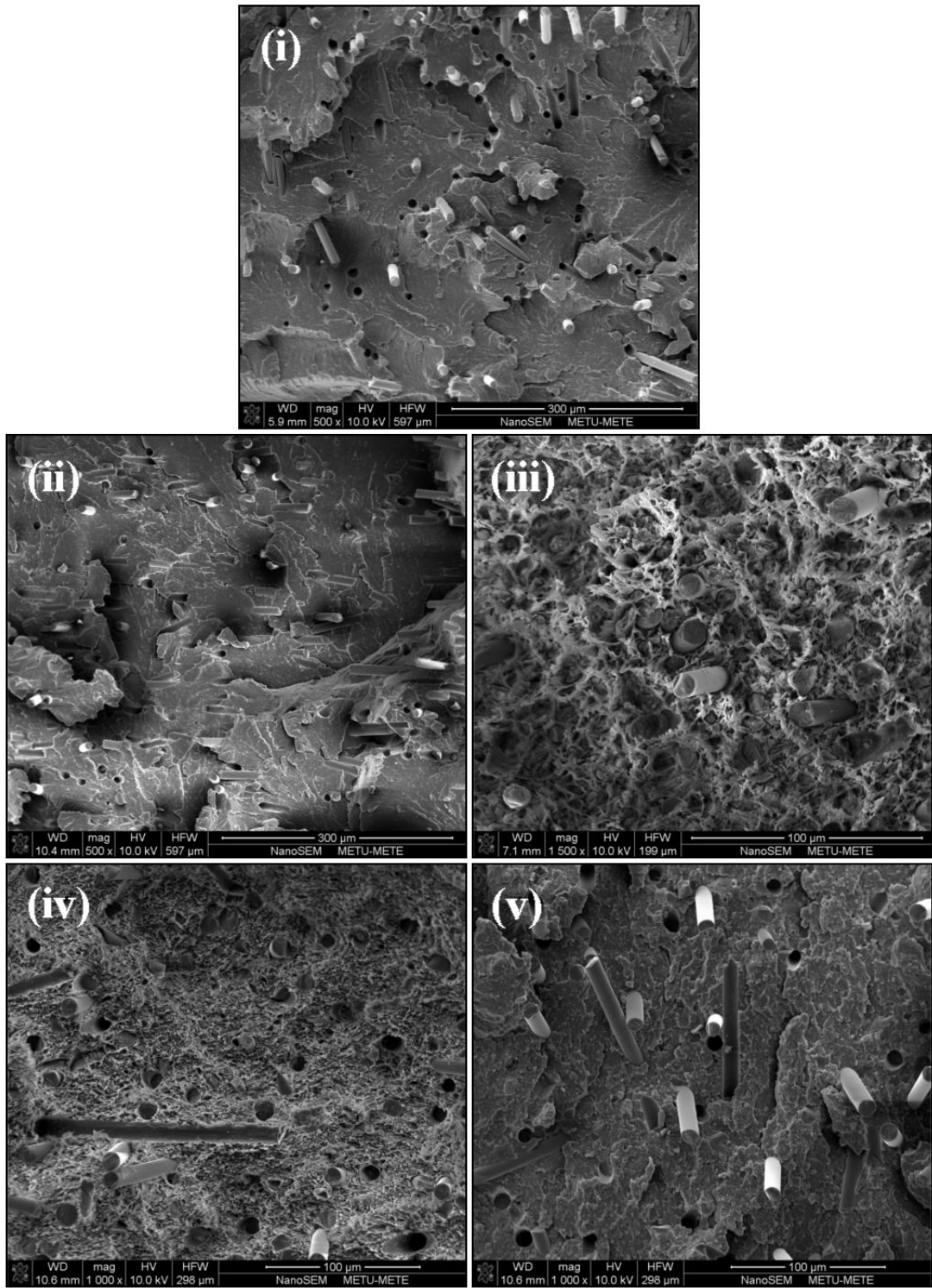


**Figure 3.43** SEM Fractographs of the PA/GF Based Materials:  
 (i) PA/GF, (ii) PA/GF-NC, (iii) PA/GF-ADP 20,  
 (iv) PA/GF-ADP 15-NC, (v) PA/GF-ADP 10-ZB-NC



## CHAPTER 4

### CONCLUSIONS

The main conclusions drawn from the three different parts of this dissertation can be summarized as follows:

#### *(i) Effects of Zinc Borate*

- UL-94 vertical burning and LOI tests indicated that both in PA and PA/GF based materials replacement of ADP with 1, 3, 5, 7 wt% ZB kept not only the best UL-94 V-0 rating, but also resulted in slight increases in LOI values. The highest increase in LOI value was achieved with 3 wt% ZB replacement.
- MLC analyses revealed that use of ZB together with ADP resulted in significant improvements in many cone calorimetry parameters such as PHRR, THE, TBT, FGI, FIGRA, Char Yield, etc. For instance, when 15 wt% ADP and 5 wt% ZB were used together, the suppression in PHRR (peak heat release rate) value of polyamide-6 could be as much as 82%, while this suppression was only 32% when 20 wt% ADP was used alone.
- The main flame retardancy mechanism of ADP is its gaseous phase action called “flame inhibition”, while the secondary mechanism is its condensed phase action called “barrier effect”. The main contribution of ZB to the barrier mechanism of ADP was the formation of additional boron phosphate layers together with aluminum phosphate layers. Certainly, endothermic dehydration of ZB also contributed with an additional fuel dilution

mechanism. These mechanisms were clarified with char examination, TGA, XRD and evolved gas analyses.

- Tensile test indicated that due to its coarse size and weaker organic structure, ADP decreased both yield and tensile strength of the specimens. On the other hand, due to its fine size and stronger inorganic structure, addition of ZB resulted in improvements in the yield and tensile strength of the materials.

#### *(ii) Effects of Boron Oxide and Boric Acid*

- UL-94 vertical burning and LOI tests indicated that when BO or BA were used alone, or when certain amount of ADP was replaced with BO or BA, UL-94 ratings were kept, but there were no further improvements in LOI values.
- MLC analyses revealed that for the PA based materials use of BO or BA together with ADP resulted in significant improvements in many cone calorimetry parameters such as PHRR, THE, TBT, FGI, FIGRA, Char Yield, etc. For instance, when 17 wt% ADP were used together with 3 wt% BO or BA, the suppression in PHRR (peak heat release rate) value of PA could be as much as 84% or 86%, while this suppression was only 32% when 20 wt% ADP was used alone.
- On the other hand, for the PA/GF based materials, due to the high efficiency of glass fiber reinforcements, replacements of certain amount of ADP with BO or BA resulted in no further improvements in many cone calorimetry parameters.
- The main contribution of BO and BA to the barrier mechanism of ADP was the formation of additional glassy boron oxide layers. Moreover, BA also has

the ability of formation of another additional barrier layer, i.e. boron phosphate layers together with aluminum phosphate layers of ADP. Certainly, endothermic dehydration reactions of BA also contributed with an additional fuel dilution mechanism. These mechanisms were clarified with char examination, TGA, XRD and evolved gas analyses.

- Tensile tests indicated that due to the decreased chain mobility of the PA matrix by BO, BA or ADP, elastic modulus of the specimens increased significantly when these flame retardant were used alone or together. However, they all resulted in substantial decreases in the tensile strength values, especially due to the lowered efficiency of load transfer mechanism from the matrix to these non-surface treated particles, having very low aspect ratio, either.

### *(iii) Effects of Nanoclays*

- XRD and TEM analyses revealed that mainly intercalated and partially exfoliated NC silicate layers can be homogeneously distributed in the PA and PA/GF matrices.
- UL-94 vertical burning and LOI tests indicated that both in PA and PA/GF based materials, addition of 5 wt% NC alone led to no enhancements, however, when 5 wt% of ADP was replaced with NC, then each specimen not only kept the best UL-94 rating of V-0, but their LOI values increased by 3 %O<sub>2</sub> further.
- MLC analyses revealed that use of only 5 wt% NC alone, resulted in significant improvements in many cone calorimetry parameters such as PHRR, THE, TBT, FGI, FIGRA, Char Yield, etc. For instance, the suppression in PHRR values of PA and PA/GF were 55% and 61%,

respectively. These suppressions were 32% and 75% when 20 wt% ADP alone was used.

- Contribution of NC silicate layers were much more significant when 5 wt% of ADP was replaced with NC. In this case, PHRR suppressions were as much as 65% in PA and 76% in PA/GF based materials.
- Various analyses to reveal the flame retardancy mechanism of NC indicated the formation of insulative barrier via tortuous pathway of intercalated/exfoliated silicate layers preventing the underlying polymer from heat and mass transfer during fire.
- Tensile tests indicated that increases in the modulus and strength values of PA by adding only 5 wt% NC were as good as by adding 15 wt% GF. It was also seen that, all the mechanical properties lost due to the use of 20 wt% ADP could be compensated when 15 wt% ADP was used together with 5 wt% NC.

## REFERENCES

- [1] Kroschwitz JI. "Kirk-Othmer concise encyclopedia of chemical technology". *Wiley, New York* 1999.
- [2] Holland BJ, Hay JN. "Thermal degradation of nylon polymers". *Polymer International* 2000; (49): 943-948.
- [3] Cho JW, Paul DR. "Nylon 6 nanocomposites by melt compounding". *Polymer* 2001; (42): 1083-1094.
- [4] Kawasumi M. "The discovery of polymer-clay hybrids". *Journal of Polymer Science Part a-Polymer Chemistry* 2004; (42): 819-824.
- [5] Mouritz AP, Gibson AG. "Fire properties of polymer composite materials". *Springer, Dordrecht* 2006.
- [6] Laoutid F, Bonnaud L, Alexandre M, Lopez-Cuesta JM, Dubois P. "New prospects in flame retardant polymer materials: From fundamentals to nanocomposites". *Materials Science & Engineering R-Reports* 2009; (63): 100-125.
- [7] Yang YM, Shi XC, Zhao RR. "Flame retardancy behavior of zinc borate". *Journal of Fire Sciences* 1999; (17): 355-361.
- [8] Wilkie CA, Morgan AB. "Fire retardancy of polymeric materials". *CRC Press, Boca Raton* 2010.
- [9] Gilleo KB. "Nylon flammability - effects of thiourea, ammonium sulfamate, and halogen compounds". *Industrial & Engineering Chemistry Product Research and Development* 1974; (13): 139-143.
- [10] Mailhoslefievre V, Sallet D, Martel B. "Thermal-degradation of pure and flame-retarded polyamide-11 and polyamide-12". *Polymer Degradation and Stability* 1989; (23): 327-336.

- [11] Levchik SV, Weil ED. "Combustion and fire retardancy of aliphatic nylons". *Polymer International* 2000; (49): 1033-1073.
- [12] Sallet D, Mailhoslefievre V, Martel B. "Flame retardancy of polyamide 11 with a decabromodiphenyl-antimony trioxide mixture - a bromine-antimony-nitrogen synergism". *Polymer Degradation and Stability* 1990; (30): 29-39.
- [13] Fei GX, Wang Q, Liu YA. "Synthesis of novolac-based char former: Silicon-containing phenolic resin and its synergistic action with magnesium hydroxide in polyamide-6". *Fire and Materials* 2010; (34): 407-419.
- [14] Fei GX, Liu Y, Wang Q. "Synergistic effects of novolac-based char former with magnesium hydroxide in flame retardant polyamide-6". *Polymer Degradation and Stability* 2008; (93): 1351-1356.
- [15] Braun U, Scharrel B. "Flame retardant mechanisms of red phosphorus and magnesium hydroxide in high impact polystyrene". *Macromolecular Chemistry and Physics* 2004; (205): 2185-2196.
- [16] Dogan M, Yilmaz A, Bayramli E. "Effect of boron containing materials on flammability and thermal degradation of polyamide-6 composites containing melamine cyanurate". *Polymers for Advanced Technologies* 2011; (22): 560-566.
- [17] Chen YH, Wang Q, Yan W, Tang HM. "Preparation of flame retardant polyamide 6 composite with melamine cyanurate nanoparticles in situ formed in extrusion process". *Polymer Degradation and Stability* 2006; (91): 2632-2643.
- [18] Liu Y, Wang Q, Fei GX, Chen YH. "Preparation of polyamide resin-encapsulated melamine cyanurate/melamine phosphate composite flame retardants and the fire-resistance to glass fiber-reinforced polyamide 6". *Journal of Applied Polymer Science* 2006; (102): 1773-1779.
- [19] Levchik SV, Levchik GF, Balabanovich AI, Camino G, Costa L. "Mechanistic study of combustion performance and thermal decomposition behaviour of nylon 6 with added halogen-free fire retardants". *Polymer Degradation and Stability* 1996; (54): 217-222.
- [20] Weil ED, Choudhary V. "Flame-retarding plastics and elastomers with melamine". *Journal of Fire Sciences* 1995; (13): 104-126.

- [21] Gijssman P, Steenbakkers R, Furst C, Kersjes J. "Differences in the flame retardant mechanism of melamine cyanurate in polyamide 6 and polyamide 66". *Polymer Degradation and Stability* 2002; (78): 219-224.
- [22] Levchik SV, Costa L, Camino G. "Effect of the fire-retardant, ammonium polyphosphate, on the thermal-decomposition of aliphatic polyamides: part II polyamide 6". *Polymer Degradation and Stability* 1992; (36): 229-237.
- [23] Levchik SV, Levchik GF, Camino G, Costa L. "Mechanism of action of phosphorus-based flame retardants in nylon 6. II. Ammonium polyphosphate/talc". *Journal of Fire Sciences* 1995; (13): 43-58.
- [24] Siat C, Bourbigot S, Le Bras M. "Thermal behaviour of polyamide-6-based intumescent formulations - a kinetic study". *Polymer Degradation and Stability* 1997; (58): 303-313.
- [25] Levchik GF, Vorobyova SA, Gorbarenko VV, Levchik SV, Weil ED. "Some mechanistic aspects of the fire retardant action of red phosphorus in aliphatic nylons". *Journal of Fire Sciences* 2000; (18): 172-182.
- [26] Chen YH, Wang Q. "Preparation, properties and characterizations of halogen-free nitrogen-phosphorous flame-retarded glass fiber reinforced polyamide 6 composite". *Polymer Degradation and Stability* 2006; (91): 2003-2013.
- [27] Balabanovich AI, Levchik GF, Levchik SV, Schnabel W. "Fire retardance in polyamide-6. The effects of red phosphorus and radiation-induced cross-links". *Fire and Materials* 2001; (25): 179-184.
- [28] Scharrel B, Kunze R, Neubert D. "Red phosphorus-control led decomposition for fire retardant PA 66". *Journal of Applied Polymer Science* 2002; (83): 2060-2071.
- [29] Braun U, Scharrel B, Fichera MA, Jager C. "Flame retardancy mechanisms of aluminium phosphinate in combination with melamine polyphosphate and zinc borate in glass-fibre reinforced polyamide 6,6". *Polymer Degradation and Stability* 2007; (92): 1528-1545.
- [30] Braun U, Bahr H, Scharrel B. "Fire retardancy effect of aluminium phosphinate and melamine polyphosphate in glass fibre reinforced polyamide 6". *E-Polymers* 2010.

- [31] Hu Z, Lin GP, Chen L, Wang YZ. "Flame retardation of glass-fiber-reinforced polyamide 6 by combination of aluminum phenylphosphinate with melamine pyrophosphate". *Polymers for Advanced Technologies* 2011; (22): 1166-1173.
- [32] Zhao B, Chen L, Long JW, Chen HB, Wang YZ. "Aluminum hypophosphite versus alkyl-substituted phosphinate in polyamide 6: Flame retardance, thermal degradation, and pyrolysis behavior". *Industrial & Engineering Chemistry Research* 2013; (52): 2875-2886.
- [33] Isitman NA, Gunduz HO, Kaynak C. "Halogen-free flame retardants that outperform halogenated counterparts in glass fiber reinforced polyamides". *Journal of Fire Sciences* 2010; (28): 87-100.
- [34] Braun U, Scharfel B. "Flame retardancy mechanisms of aluminium phosphinate in combination with melamine cyanurate in glass-fibre-reinforced poly(1,4-butylene terephthalate)". *Macromolecular Materials and Engineering* 2008; (293): 206-217.
- [35] Gao M, Nyu JC, Yang RJ. "Synergism of GUP and boric acid characterized by cone calorimetry and thermogravimetry". *Journal of Fire Sciences* 2006; (24): 499-511.
- [36] Nyambo C, Kandare E, Wilkie CA. "Thermal stability and flammability characteristics of ethylene vinyl acetate (EVA) composites blended with a phenyl phosphonate-intercalated layered double hydroxide (LDH), melamine polyphosphate and/or boric acid". *Polymer Degradation and Stability* 2009; (94): 513-520.
- [37] Demirel M, Pamuk V, Dilsiz N. "Investigation of flame retardancy and physical-mechanical properties of zinc borate/boric acid polyester composites". *Journal of Applied Polymer Science* 2010; (115): 2550-2555.
- [38] Xie KL, Gao AQ, Zhang YS. "Flame retardant finishing of cotton fabric based on synergistic compounds containing boron and nitrogen". *Carbohydrate Polymers* 2013; (98): 706-710.
- [39] Mulazim Y, Kizilkaya C, Kahraman MV. "Thermal and neutron shielding properties of (B<sub>2</sub>O<sub>3</sub>)-B-10/polyimide hybrid materials". *Polymer Bulletin* 2011; (67): 1741-1750.

- [40] Ibibikcan E, Kaynak C. "Usability of three boron compounds for enhancement of flame retardancy in polyethylene-based cable insulation materials". *Journal of Fire Sciences* 2014; (32): 99-120.
- [41] Manias E, Touny A, Wu L, Strawhecker K, Lu B, Chung TC. "Polypropylene/montmorillonite nanocomposites. Review of the synthetic routes and materials properties". *Chemistry of Materials* 2001; (13): 3516-3523.
- [42] Morgan AB. "Flame retarded polymer layered silicate nanocomposites: A review of commercial and open literature systems". *Polymers for Advanced Technologies* 2006; (17): 206-217.
- [43] Zhu J, Start P, Mauritz KA, Wilkie CA. "Thermal stability and flame retardancy of poly(methyl methacrylate)-clay nanocomposites". *Polymer Degradation and Stability* 2002; (77): 253-258.
- [44] Ahmadi SJ, Huang YD, Li W. "Synthetic routes, properties and future applications of polymer-layered silicate nanocomposites". *Journal of Materials Science* 2004; (39): 1919-1925.
- [45] Qin HL, Su QS, Zhang SM, Zhao B, Yang MS. "Thermal stability and flammability of polyamide 66/montmorillonite nanocomposites". *Polymer* 2003; (44): 7533-7538.
- [46] Devaux E, Rochery M, Bourbigot S. "Polyurethane/clay and polyurethane/POSS nanocomposites as flame retarded coating for polyester and cotton fabrics". *Fire and Materials* 2002; (26): 149-154.
- [47] Camino G, Tartaglione G, Frache A, Manfredi C, Costa G. "Thermal and combustion behaviour of layered silicate-epoxy nanocomposites". *Polymer Degradation and Stability* 2005; (90): 354-362.
- [48] Shi Y, Kashiwagi T, Walters RN, Gilman JW, Lyon RE, Sogah DY. "Ethylene vinyl acetate/layered silicate nanocomposites prepared by a surfactant-free method: Enhanced flame retardant and mechanical properties". *Polymer* 2009; (50): 3478-3487.
- [49] Zhang HF, Wang YQ, Wu YP, Zhang LQ, Yang J. "Study on flammability of montmorillonite/styrene-butadiene rubber (SBR) nanocomposites". *Journal of Applied Polymer Science* 2005; (97): 844-849.

- [50] Pereira CMC, Herrero M, Labajos FM, Marques AT, Rives V. "Preparation and properties of new flame retardant unsaturated polyester nanocomposites based on layered double hydroxides". *Polymer Degradation and Stability* 2009; (94): 939-946.
- [51] Kashiwagi T, Harris RH, Zhang X, Briber RM, Cipriano BH, Raghavan SR, Awad WH, Shields JR. "Flame retardant mechanism of polyamide 6-clay nanocomposites". *Polymer* 2004; (45): 881-891.
- [52] Shanmuganathan K, Deodhar S, Dembsey N, Fan QG, Calvert PD, Warner SB, Patra PK. "Flame retardancy and char microstructure of nylon-6/layered silicate nanocomposites". *Journal of Applied Polymer Science* 2007; (104): 1540-1550.
- [53] Samyn F, Bourbigot S, Jama C, Bellayer S. "Fire retardancy of polymer clay nanocomposites: Is there an influence of the nanomorphology?". *Polymer Degradation and Stability* 2008; (93): 2019-2024.
- [54] Jang BN, Wilkie CA. "The effect of clay on the thermal degradation of polyamide 6 in polyamide 6/clay nanocomposites". *Polymer* 2005; (46): 3264-3274.
- [55] Bourbigot S, Samyn F, Turf T, Duquesne S. "Nanomorphology and reaction to fire of polyurethane and polyamide nanocomposites containing flame retardants". *Polymer Degradation and Stability* 2010; (95): 320-326.
- [56] Beyer G. "Flame retardant properties of EVA-nanocomposites and improvements by combination of nanofillers with aluminium trihydrate". *Fire and Materials* 2001; (25): 193-197.
- [57] Yen YY, Wang HT, Guo WJ. "Synergistic flame retardant effect of metal hydroxide and nanoclay in EVA composites". *Polymer Degradation and Stability* 2012; (97): 863-869.
- [58] Kaynak C, Ibibikcan E. "Contribution of nanoclays to the flame retardancy of polyethylene-based cable insulation materials with aluminum hydroxide and zinc borate". *Journal of Fire Sciences* 2014; (32): 121-144.
- [59] Isitman NA, Sipahioglu BM, Kaynak C. "Nanomorphology and fire behavior of polystyrene/organoclay nanocomposites containing brominated epoxy and antimony oxide". *Polymers for Advanced Technologies* 2012; (23): 984-991.

- [60] Chang LN, Jaafar M, Chow WS. "Thermal behavior and flammability of epoxy/glass fiber composites containing clay and decabromodiphenyl oxide". *Journal of Thermal Analysis and Calorimetry* 2013; (112): 1157-1164.
- [61] Ma HY, Tong LF, Xu ZB, Fang ZP. "Intumescent flame retardant-montmorillonite synergism in ABS nanocomposites". *Applied Clay Science* 2008; (42): 238-245.
- [62] Zhang J, Lewin M, Pearce E, Zammarano M, Gilman JW. "Flame retarding polyamide 6 with melamine cyanurate and layered silicates". *Polymers for Advanced Technologies* 2008; (19): 928-936.
- [63] Yang W, Kan YC, Song L, Hu Y, Lu HD, Yuen RKK. "Effect of organo-modified montmorillonite on flame retardant poly(1,4-butylene terephthalate) composites". *Polymers for Advanced Technologies* 2011; (22): 2564-2570.
- [64] Lei S, Yuan H, Lin ZH, Xuan SY, Wang SF, Chen ZY, Fan WC. "Preparation and properties of halogen-free flame-retarded polyamide 6/organoclay nanocomposite". *Polymer Degradation and Stability* 2004; (86): 535-540.
- [65] Fang KY, Li JA, Ke CH, Hu QL, Tao K, Zhu J, Yan Q. "Intumescent flame retardation of melamine-modified montmorillonite on polyamide 6: Enhancement of condense phase and flame retardance". *Polymer Engineering and Science* 2011; (51): 377-385.
- [66] Tai QL, Yuen RKK, Yang W, Qiao ZH, Song L, Hu Y. "Iron-montmorillonite and zinc borate as synergistic agents in flame-retardant glass fiber reinforced polyamide 6 composites in combination with melamine polyphosphate". *Composites Part a-Applied Science and Manufacturing* 2012; (43): 415-422.
- [67] Bourbigot S, Duquesne S, Fontaine G, Bellayer S, Turf T, Samyn F. "Characterization and reaction to fire of polymer nanocomposites with and without conventional flame retardants". *Molecular Crystals and Liquid Crystals* 2008; (486): 1367-1381.
- [68] Isitman NA, Gunduz HO, Kaynak C. "Nanoclay synergy in flame retarded/glass fibre reinforced polyamide 6". *Polymer Degradation and Stability* 2009; (94): 2241-2250.

[69] Dahiya JB, Rathi S, Bockhorn H, Haussmann M, Kandola BK. "The combined effect of organic phosphinate/ammonium polyphosphate and pentaerythritol on thermal and fire properties of polyamide 6-clay nanocomposites". *Polymer Degradation and Stability* 2012; (97): 1458-1465.

[70] Dogan M, Bayramli E. "The flame retardant effect of aluminum phosphinate in combination with zinc borate, borophosphate, and nanoclay in polyamide-6". *Fire and Materials* 2014; (38): 92-99.

## CURRICULUM VITAE

### Osman POLAT

Ankara / Turkey

E-mail: polatosm@gmail.com or polato@hotmail.com

#### EDUCATION

- 2008-2014 Ph.D. Polymer Science and Technology,  
Middle East Technical University  
Thesis title: *“Contribution Of Boron Compounds And Nanoclays  
On The Flame Retardancy Of Aluminium Diethylphosphinate In  
Neat And Fiber Reinforced Polyamide-6”*  
Thesis advisor: Prof. Dr. Cevdet KAYNAK
- 2004-2007 MBA  
İstanbul Bilgi University  
*“Risk Management in Manufacturing : An Analysis of Managing the  
Investment Projects”*  
Thesis advisor: Dr. Murat YÜCELEN
- 1996-1999 M.Sc. Polymer Science and Technology,  
Middle East Technical University  
Thesis title: *“Flame Retardant and Water Dispersed Polyurethane  
Paints”*  
Thesis advisor: Prof. Dr. Leyla ARAS, Prof. Dr. Güngör GÜNDÜZ
- 1986-1992 B.S. Chemical Engineering,  
Hacettepe University

## EXPERIENCES

- 2012-2013      Quality Manager  
Pakpen A.Ş.
- 2009-2011      Project Assistant  
“*Widespread Utilization of Turkish Boron Compounds as Flame Retardant Additives in Plastic and Composites*”  
National Boron Research Institute (Boren) and  
Middle East Technical University Research Project  
(Proje No : 2009-Ç-0236)
- 2007-2008      World Class Manufacturing (WCM) Department Responsible  
Saint-Gobain Rigips
- 2000-2005      Specialist Researcher and Process Engineer at R&D  
Aksa Akrilik Kimya San. A.Ş.

## PUBLICATIONS

### (a) SCI Articles

1. Polat O. and Kaynak C., “Effects of zinc borate on the flame retardancy performance of aluminum diethylphosphinate in polyamide-6 and its fiber reinforced composite”, *Fire Safety Journal*, (2014 , under review).
2. Polat O. and Kaynak C., “Use of boron oxide and boric acid to improve flame retardancy of an organophosphorus compound in neat and fiber reinforced polyamide-6”, *Journal of Vinyl and Additive Technology*, (accepted in August 2014, available online, DOI: 10.1002/vnl.21445).

3. Kaynak C. and Polat O. “Influences of nanoclays on the flame retardancy of fiber filled and unfilled polyamide-6 with and without aluminum diethylphosphinate”, *Journal of Fire Sciences*, (accepted in September 2014, available online, DOI: 10.1177/0734904114555961).

4. Çelebi F., Polat O., Aras L., Gündüz G., and Akhmedov İ.M., “Synthesis and characterization of water-dispersed flame-retardant polyurethane resin using phosphorous-containing chain extender,” *Journal of Applied Polymer Science*, 2004 (91), 1314-1321.

**(b) Conference Proceeding**

1. Polat O., Kaynak C., “Synergistic Effects of Boron Compounds on the Flammability of Polyamide 6 with Organic Phosphorous Flame Retardant”, *17 th International Symposium on Boron, Borides and Related Materials*, Sep. 11-17, 2011, İstanbul, pp.131.

2. Polat O., Aras L., Gündüz G. and Mecidoğlu İ., “Flame-retardant water dispersed polyurethane paint production”, *Proceeds of 3 th International Paint, Varnish, Ink, and Auxiliary Products Industry Conference and Exhibit*, Nov. 11-13, 1999, İstanbul, pp.153-167.

3. Polat O., Aras L., Gündüz G. and Mecidoğlu İ., “Flame Retardant Paint-Synthesis and Characterization”. *SCI Fire Chemistry Discussion Group*, 1, 1999, pp.40.